Precise U-Pb Zircon Ages and Geochemistry of Jurassic Granites, Ellsworth-Whitmore Terrane, Central Antarctica

John P. Craddock, Geology Department, Macalester College, St. Paul, MN 55105 USA

Mark D. Schmitz , James L. Crowley, & Jeremiah Larocque, Dept. of Geosciences, Boise State University, Boise, ID, USA

Robert J. Pankhurst, Visiting Research Associate, British Geological Survey, Nottingham NG12 5GG, UK

Natalie Juda# and Alexandros Konstantinou*, Geology Department, Macalester College, St. Paul, MN 55105 USA

Bryan Storey, University of Canterbury, Private Bag 4800, Christchurch, NZ

[#-Now at U.S. Geological Survey, Reston, VA, USA
*- Now at Cyprus Hydrocarbons Company, Nicosia, Cyprus].

Abstract

The Ellsworth-Whitmore Mountain terrane (EWT) of central Antarctica was part of the early Paleozoic amalgamation of Gondwana, including a 13,000 m section of Cambrian-Permian sediments in the Ellsworth Mountains deposited on Grenville-age crust. The Jurassic break-up of Gondwana involved a regional, bi-modal magmatic event with the EWT being intruded by intraplate granites before translation of the terrane to its present location in central Antarctica. Five widely-separated granitic plutons in the EWT were analyzed for their whole-rock geochemistries (XRF), Sr, Nd and Pb isotopic compositions and U-Pb zircon ages to infer the origins of the EWT magmas and their relationships to mafic magmatism of the 182 Ma Karoo-Ferrar large igneous province (LIP). We report high-precision (±0.1 Ma) ID-TIMS U-Pb zircon ages from granitic rocks from the Whitmore Mountains (208.0 Ma), Nash Hills (177.4 to 177.3 Ma), Linck Nunatak (175.3 Ma), Pagano Nunatak (174.8 Ma) and Pirrit Hills (174.3 to 173.9 Ma) and U-Pb SHRIMP ages from the Whitmore Mountains (200 ± 5 Ma), Linck Nunatak (180 ± 4 Ma), Pagano Nunataks (174 ± 4 Ma), and the Pirrit Hills (168 ± 4 Ma). These results are compared with existing K-Ar ages and Nd model ages. Initial Sr, Nd and Pb isotope ratios, combined with xenocrystic zircon U-Pb inheritance, are used to infer characteristics of the source(s) of the parent magmas. We conclude that the Jurassic plutons were not derived exclusively from crustal melts, but rather are hybridized magmas with convecting mantle, subcontinental lithospheric mantle, and lower continental crustal contributions. The mantle contributions to the granites share isotopic similarities to the sources of other Jurassic LIP mafic magmas, including radiogenic ($^{87}Sr/^{86}Sr$; 0.706-0.708), unradiogenic $^{143}Nd/^{144}Nd$ [$\varepsilon Nd < -5$] and Pb isotopes consistent with a low-μ source. Isotopes and zircon xenocrysts point toward a crustal end-member of predominantly Proterozoic provenance (0.5 to 1.0 Ga; Grenville crust), extending the trends illustrated by Ferrar mafic intrusives, but contrasting with the inferred Archean crustal and/or lithospheric mantle contributions to some basalts of the Karoo sector of the LIP. The EWT granites are the result of mafic rocks underplating hydrous crust causing crustal melting,

hybridization and fractionation to produce granitic magmas that were eventually emplaced as post-Ferrar, within-plate melts at higher crustal levels as the EWT terrane rifted off Gondwana (47°S) before migrating to its current position (82°S) in central Antarctica.

Introduction

Central Antarctica, the 720,000 km^2 region between the Ellsworth and Transantarctic mountains, is characterized by the exposure of a few widely-separated nunataks within the West Antarctic ice sheet (Fig. 1). It has frequently been referred to as the “problem child” of Antarctic and Gondwana tectonics (Dalziel and Elliot, 1982; Grunow et al., 1987; Storey et al., 1988a,b, 1999). This largely reflects the fact that, although the folded Lower Paleozoic stratigraphic succession of the Ellsworth Mountains (Anderson et al., 1962; Webers et al., 1992; Curtis, 2001) is analogous to those of the Transantarctic Mountains, its present trend is orthogonal to theirs. This led to the idea that it represents a rotated Gondwana fragment, known as the Ellsworth-Whitmore block or terrane (EWT) – one of four individual geological terranes that constitute West Antarctica (Dalziel et al., 1987; Storey et al. 1988a). Its boundaries are not well defined but seismic profiles (Bentley et al., 1960) confirm one as the margin of Archean-Proterozoic cratonic East Antarctica (e.g., Harley and Kelley, 2007; Goodge and Fanning, 2010); the other is thought to lie to the present north of the Ellsworth Mountains, since aeromagnetic surveying shows a similar basement signature as far as Haag Nunataks (Maslanyj & Storey, 1990; Fig. 1).

Because of its remoteness and lack of continuous exposure, this area has rarely been visited by geologists: U.S. geological parties worked there in the years 1959-1965 and a joint US-UK expedition visited the area in the mid-1980s. It is characterized by the sparse exposure of widely-separated granite nunataks dated as Jurassic (K-Ar whole rock radiometric ages by Craddock, 1972, 1977; Rb-Sr whole rock isochrons by Millar and Pankhurst, 1987). The structural discontinuity between (Permian) Gondwana-orogen rocks in the Ellsworth Mountains and the Pensacola Mountains (on the nearby margin of East Antarctica) helped define the EWT in central Antarctica, thereby posing a tectonic mystery: what is the age of the crust into which these granitic magmas intruded, what plate boundaries bordered the EWT, and how does this crustal fragment fit into Gondwana and older reconstructions?

In the Transantarctic Mountains along the western margin of cratonic East Antarctica there are widespread Jurassic mafic intrusions, e.g., the Dufek gabbroic massif and equivalent extrusive and hypabyssal rocks - the Ferrar dolerite. Riley and Knight (2001) summarized geochronological data for these in the range 180–183 Ma, whereas Burgess et al. (2015) report highly precise U-Pb CA-ID-TIMS data indicating a very short period of emplacement at 182.78 ± 0.03 Ma. These, as well as other igneous rocks in South Africa, Tasmania, the Antarctic Peninsula and Patagonia appear to be broadly contemporaneous or slightly older than the granites in the EWT. The Ferrar-Karoo-Tasman mafic igneous suite represents a divergent rifting phase as Gondwana fragmented separating the EWT continental crust from cratonic Antarctica (Grunow, 1993; Elliot and Fleming, 2000; König and Jokat, 2006). Early Jurassic silicic volcanism in Patagonia and the Antarctic Peninsula has also been interpreted as due to the break-up and dispersal of SW Gondwana (Pankhurst et al., 2000). The geochemistry of the EWT granites was studied by Storey et al. (1988b) who interpreted them as resulting from to differentiation of mantle-derived Ferrar-type magma with varying amounts of crustal contamination. Granite ages (K-Ar) were first reported on the geologic map of Antarctica (Craddock, 1972), results supported by Rb-Sr methods (Millar and Pankhurst, 1987; Pankhurst et al., 1991). Zircons from nine samples from the collections of U.S. field geologists in 1959-1965 were analysed by separating U and Pb chemically and determining their concentrations and isotopic compositions by isotope dilution and thermal ionisation mass-spectrometry (ID-TIMS; Table 1). Zircon was also separated from four samples from subsequent 1983-84 U.S.-U.K. fieldwork (Dalziel & Pankhurst, 1984) and analysed directly by Sensitive High Resolution Microprobe (SHRIMP; Table 1). Our goals were to: 1) use the precise U-Pb TIMS zircon ages to refine the less precise K-Ar and Rb-Sr granite intrusion ages, thereby testing the proposed links between the Jurassic mafic (i.e., Ferrar suite) and felsic magmatism, 2) to see if the zircon histories (zircon SHRIMP ages) would provide a constraint on the ages of the basement rocks from which the granites may have been derived, and, 3) to use additional geochemical (XRF) and isotopic (Sr, Nd, Pb) data to augment the sparse data set from the EWT granites to further constrain the magmatic sources and test the Storey et al. (1988b) tectonomagmatic hypothesis regarding Gondwana dispersal.

Regional Setting

The geology of Antarctica was first pieced together with the compilation of the Antarctic Folio series maps (Craddock, 1969) and the geologic map of the continent (Craddock, 1972). The EWT sits between the Weddell Sea in the east and the Ross Sea in the west, where the nature of the crust is poorly known and seemingly little-deformed (Huebscher et al., 1996) despite the 90° counter-clockwise rotation of the EWT block out of Gondwana (see below). The Ross Sea is thought to be the location of active divergence, namely the Terror rift system (LeMausier, 1990; Salvini et al., 1997; Paulsen et al. 2014), and is the location of on-going drilling projects. To the north of the EWT is the Antarctic Peninsula (see Burton-Johnson and Riley, 2015), to the northwest the Thurston Island terrane (see Pankhurst et al., 1993) and to the west is Marie Byrd Land (see Pankhurst et al., 1998). The EWT boundary is tectonically stationary and aseismic; the POLENET GPS array has been in place since 2009 and may better resolve the plate velocities, if any, in central Antarctica (Dalziel, 2008) and help define the boundaries of the west Antarctic terranes.

Haag Nunataks (Millar and Pankhurst, 1987; Storey et al., 1994) to the northeast of the Ellsworth Mountains are composed of Grenville-age gneisses dated at 990–1260 Ma by Rb-Sr and K-Ar methods and confirmed by unpublished U-Pb SHRIMP zircon data. These are the oldest rocks in West Antarctica. Nd model ages (T_{DM}) here and elsewhere in the EWT (Storey et al., 1994; Curtis et al., 1999) and the presence of Grenville-age detrital zircons in the Ellsworth Mountains Paleozoic section, suggest that much of the EWT is underlain by Grenville crust (Flowerdew et al., 2007; Craddock et al., 2008). The Ellsworth Mountains are the highest peaks in Antarctica (up to 4892 m) and contain an essentially continuous Cambrian-Permian section of 13,000 m (Webers et al., 1992; Flowerdew et al. 2007; Elliot et al. 2014) that was deformed as part of the Permo-Triassic Gondwanide orogeny (Craddock and Webers, 1964; Craddock et al., 1965; Craddock 1966; Curtis, 1997, 2001). As Gondwana dispersed in the early Mesozoic, counterclockwise rotation of the Ellsworth Mountains (Watts and Bramall, 1981; Grunow et al., 1987; Randall and Mac Niocaill, 2004) was broadly contemporaneous with intrusion of granites in central Antarctica, the mafic suite of the Ferrar-Karoo-Tasman LIP and much of the silicic volcanism of southern Patagonia (Pankhurst et al., 2000). Four kilometres of exhumation in the early Cretaceous (~100 Ma) is documented by fission track studies from the Vinson Massif (4892 m) profile in the Ellsworth Mountains (Fitzgerald and Stump, 1991).

Our contribution is based on geologic maps and field descriptions of many of the remote mountains and nunataks within the EWT (Appendices 1-4) and detailed whole-rock geochemistry, isotope studies (Sr, Pb and Nd) and U-Pb zircon geochronology of the granites to further improve understanding of the geology and tectonic history of the EWT.

Methods

Detailed procedures are given in Appendix 1 and are only briefly summarised here.

Whole-rock powders were prepared at Macalester College. Geochemical analyses were performed by X-ray fluorescence spectrometry (Phillips PW-2400 spectrometer with a Rh target) at Macalester College following the methods of Vervoort et al. (2007). Major elements were determined after lithium metaborate/tetraborate fusion and trace elements on pressed powder pellets.

Rb-Sr and Sm-Nd isotope analyses were performed by mass-spectrometric isotope dilution following HCl–HNO_3 dissolution and cation exchange chromatography, using an Isoprobe-T spectrometer in the Boise State University Isotope Geology Laboratory. Pb isotope compositions were determined on K-feldspar sequentially leached with HF following the method of Housh and Bowring (1991) - the least radiogenic isotopic composition being taken as representative of the magmatic Pb. Reproducibility data for isotope analyses are given in the Tables.

Zircons for precise mass-spectrometry chronology were separated using standard techniques at Carleton College, MN, mounted in epoxy resin and imaged by cathodo-luminescence in a scanning electron microscope. Only simple igneous-zoned grains were extracted for U-Pb zircon chronology at Boise State University Isotope Geology Laboratory following modified chemical abrasion (Mattinson, 2005). U and Pb isotopic measurements were made on an IsotopX GV Isoprobe-T multicollector thermal ionization mass spectrometer equipped with an ion-counting Daly detector. Internal errors on analyses of single grains are at 2σ and errors on weighted mean dates are at the 95% confidence interval: internal 2σ errors expanded by the square root of the MSWD (Mean Square of Weighted Deviates) and the Student's T multiplier of n-1 degrees of freedom.

Earlier U-Pb dating reported here was carried out using Sensitive High Resolution Ion Microprobe (SHRIMP) instruments at The Australian National University (Williams, 1998) on zircon concentrates prepared at the NERC Isotope Geosciences Laboratory (BGS, Keyworth, UK). Cathodo-luminescence was used to select igneous-zoned areas for dating, and a few older cores were also analysed in the case of the Linck Nunataks sample. The age uncertainties reported in Table 1 are 95% confidence-limit estimates including counting statistics, the reproducibility of the standard (SL13: 572 Ma) during the analytical session and an additional 1% (1σ) to make allowance for fact that this standard was subsequently found not to be ideally homogeneous in composition (see Ireland et al., 2008).

Calculations for all U-Pb data were performed using Isoplot 3.0 (Ludwig, 2003), but U-decay constant uncertainties were not taken into account.

Results

Field Relations

The EWT contains a number of separate isolated rock outcrop areas above ice level (Figures 1 and 2). The Ellsworth Mountains and Haag Nunataks are detailed above and we present results for the Pirritt Hills (north), Nash Hills, Martin Hills, Whitmore Mountains, Linck Nunatak, Hart Hills and Pagano Nunatak (south). The outcrops of Mt. Johns, Moreland Nunatak and Mt. Woollard are described by Storey and MacDonald (1987) and do not contain granites.

Geologic maps of some field sites are the unpublished results of the field efforts of Cam Craddock and colleagues (see Acknowledgements) in the 1960s and these materials are included in appendices 2-5.

Geochronology

Sample sites can be found in Figure 1 and are described below. A summary of all radiometric ages is given in Table 1. ID-TIMS results are in Figure 3 and Table 2; SHRIMP results are in Figure 4 and Table 3. Fifty of the fifty five ID-TIMS analyses from five sites yielded concordant $^{206}Pb/^{238}U$ dates that are Triassic-Jurassic in age. Dates older than those used in the weighted mean calculations are thought to have inherited components and one younger one is thought to have suffered Pb loss. SHRIMP analyses of zircons from three sites (Pirrit Hills, Pagano Nunatak and Linck Nunataks) yielded Jurassic crystallization ages and some older, inherited ages.

Pirrit Hills

The Pirrit Hills (81°17'S, 85°21'W, first positioned in 1958 and named for glaciologist John Pirrit) are a range of peaks 14 km in length, ~110 km southwest of the southernmost point of the Ellsworth Mountains (Figure 2a). The range is composed of pink granite that is locally pegmatitic with tourmaline, beryl and muscovite: it is jointed and weakly foliated and there are metasedimentary rocks exposed nearby that are folded and contain a steep foliation (Appendix 2). Craddock (1972) reported a K-Ar age of 176 +/- 6 Ma, Millar and Pankhurst (1987) a Rb-Sr age of 173 +/- 3 Ma, and Storey et al. (1988b) a Nd model age of 1740 Ma (Table 1).

Four of the eight analyzed grains from Pirrit Hills granite sample 60-8-27 yielded ID-TIMS equivalent dates with a weighted mean $^{206}Pb/^{238}U$ age of 174.06 ± 0.16 Ma (MSWD = 3.0). Two other grains are slightly older (175 Ma) and two others are considerably older (178, 243 Ma). Five of the seven analyzed grains from granite sample 60-8 yielded equivalent dates with a weighted mean $^{206}Pb/^{238}U$ age of 174.01 ± 0.14 Ma (MSWD = 2.0). Again, one grain is slightly older (175 Ma) and another is considerably older (181 Ma). Overall, nine grains from the two samples yielded equivalent dates with a weighted mean $^{206}Pb/^{238}U$ age of 174.04 ± 0.08 Ma (MSWD = 2.3; Table 2, Figure 3). Pirrit Hills granite (sample R.2243.4) yielded a SHRIMP age of 168 ± 4 Ma (n= 13, MSWD= 1.3) with evidence of inheritance back to ca. 900 Ma (Table 3, Figure 4). Add a comment here about Lee et al. 2012 (164 Ma)?

Nash-Martin Hills

The Nash Hills (81° 53' S, 89° 23'W, first surveyed in 1958 and named for US naval officer A.R. Nash) are ~110 km southwest of the Pirrit Hills and extend for ~20 km. The smaller outcrop of the Martin Hills (82° 04'S, 88° 01'W, ~30 southeast of the Nash Hills) were named after L.R. Martin, scientific leader of Byrd Station in 1962. Due to the proximity of the two ranges and their similar geology, i.e., granites intruding ~400 m of folded and foliated Nash Hills Formation metasediments (Appendices 3 and 4), they are referred to collectively as the Nash-Martin Hills. Craddock (1972) reported six K-Ar ages on granites and a porphyritic andesite that range in age from 163 to 175 Ma. Millar and Pankhurst (1987) reported a Rb-Sr age of 175 ± 8 Ma and Storey et al. (1988b) a Nd model age of 1270 Ma (Table 1).

Zircon from four samples was analysed for U-Pb by ID-TIMS (Table 2). Four grains from sample 63-C-69 yielded consistent dates with a weighted mean $^{206}Pb/^{238}U$ age of 177.49 ±

0.11 Ma (MSWD = 1.9) and five grains from sample 63-C-67 yielded a weighted mean $^{206}Pb/^{238}U$ age of 177.46 ± 0.05 Ma (MSWD = 1.0). Six of the seven analyzed grains from sample 63-C-68 yielded equivalent dates with a weighted mean $^{206}Pb/^{238}U$ age of 177.42 ± 0.09 Ma (MSWD = 2.5); one grain was strongly discordant and considerably older (with a $^{207}Pb/^{206}Pb$ age of 1409 Ma). Four of the seven analyzed grains from sample 63-C-63 yielded equivalent dates with a weighted mean $^{206}Pb/^{238}U$ age of 177.38 ± 0.12 Ma (MSWD = 1.7). Another grain is slightly older and two others are considerably older. Nineteen grains from the four samples from the Nash Hills yielded equivalent dates with a combined weighted mean $^{206}Pb/^{238}U$ age of 177.44 ± 0.04 Ma (MSWD = 2.1).

Linck Nunataks

Linck Nunataks (82°41'S, 104°12'W, first surveyed in 1959 and named for U.S. Geological Survey Branch Chief M. Kerwin Linck) consists of four small outcrops on the southwest side of the Whitmore Mountains, which are ~220 km west-southwest of the Nash Hills. These outcrops are composed of gray leucogranite that crosscut the Mt. Seelig granite (see below); many dikes of the Linck granite contain xenoliths of the older Mt. Seelig granite (Webers et al. 1982). Pankhurst et al (1991) reported a Rb-Sr age of 176 ± 5 Ma and Storey et al. (1988b) a Nd model age of 1541 Ma (Table 1).

Three of the five analyzed zircon grains from Linck sample 65-W-80 yielded equivalent ID-TIMS dates with a weighted mean $^{206}Pb/^{238}U$ age of 174.82 ± 0.26 Ma (MSWD = 2.6). Two other grains are discordant and considerably older (Table 2, Figure 3). Zircons recovered from a granite dike yield a U-Pb SHRIMP age of 180 ± 4 Ma (4 youngest grains only, MSWD= 1.1). The older apparent ages are interpreted as reflecting inherited zircon (Table 3 and Figure 4).

They show a clear Triassic component (220, 230 Ma), as well as ca. 300 Ma and older inheritance (ca. 380-600 Ma and ca.1040 Ma). This is not a comprehensive study of zircon provenance as the main thrust of the work was to date crystallization, but gives a brief impression of the crustal origin of magma components, not their relative importance. The 300-600 Ma ages should be treated with caution due to the paucity and, in some cases, discordance of the data.

Pagano Nunatak

Pagano Nunatak (83°41'24"S, 87°37'0"W, Figure 2b) is an isolated, high-relief (1830 m) pillar of granite first observed by Ed Thiel (1959-60) and named for US naval officer Gerald Pagano. It consists of a pink-gray granite crosscut by leucogranite dikes, both of which preserve two joint sets. A geologic map is provided in Webers et al. (1983). Millar and Pankhurst (1987) reported a Rb-Sr age of 175 +/- 8 Ma and Storey et al. (1988b) a Nd model age of 1410 Ma.

Four of the five analyzed grains yielded equivalent dates with a weighted mean $^{206}Pb/^{238}U$ age of 174.62 ± 0.16 Ma (MSWD = 2.0; Table 2, Figure 3). Another grain is slightly younger. The Pagano Nunatak granite (R.2215.4) SHRIMP age is 174 ± 4 Ma (n= 13, MSWD= 1.3) Two grains had inherited ages (ca. 420, 580 Ma) and there is evidence of Pb-loss to 160 Ma (Table 3, Figure 4).

Hart Hills

The Hart Hills (83° 43’S, 89° 05’W, first observed from the air in 1959 and named for Pembroke Hart, a geophysicist involved in IGY exploration of Antarctica and are a series of low hills ~ 13 km west of Pagano Nunatak, ~210 m above the ice level and ~14 km^2 in extent. The stratigraphic section includes ~400 m of cleaved metasediments intruded by a 100 m thick undated quartz gabbro (Webers et al. 1983). The gabbro has geochemical affinities to the Jurassic Ferrar dolerite (Vennum and Storey, 1987). A geologic map is provided in Appendix 5.

Whitmore Mountains

Webers et al. (1982) have described the exploration history of this small range (82° 35’S, 104° 30’W) as well as its general geologic, geochemical and geochronologic relations. The range is named for U.S. Geological Survey topographic engineer George D. Whitmore after being surveyed in 1959. The Mt. Seelig (3022 m) granite is a coarse-grained intrusion with a K-Ar age between 174 +/- 4 and 190 +/- 8 Ma (Craddock, 1972) and an Rb-Sr whole-rock age of 203 +/-8 Ma (Pankhurst et al., 1991). It intrudes a metasedimentary sequence of unknown age (Storey and MacDonald, 1987). The Mt. Seelig granite has a poorly-developed micaceous lineation and is crosscut by the fine-grained Linck Nunataks granite (see above).

Four of the seven analyzed grains from Mt. Seelig granite sample 65-W-44 yielded ID-TIMS equivalent dates with a weighted mean $^{206}Pb/^{238}U$ age of 207.96 ± 0.06 Ma (MSWD = 1.1). Two other grains are slightly older and another is considerably older (Table 2, Figure 3). Sample R.2226.1 yielded a SHRIMP age of 194 ± 2 Ma (n=15, MSWD= 1.6) with a bimodal age suite (190 Ma and 200 Ma) and Pb-loss to ~180 Ma. (Table 3 or Figure 4). Thirty-nine zircon analyses using SHRIMP gave ages in the range 176–210 Ma (ignoring one very high-U grain). The pattern is clearly bimodal (Fig. 4) and is thought to reflect disturbance due to a major mid-

Jurassic thermal event (see below); the 22 oldest ages give a weighted mean of 200 ± 4 Ma (MSWD = 1.2), confirmed by the Sambridge & Compston (1994) unmixing algorithm.

X-Ray Fluorescence Geochemistry

The new major and trace element data obtained in this study were added to the geochemical dataset presented in Storey et al. (1988b) and data from Lee et al. (2012) from the Pirrit Hills. Overall the Jurassic EWT granitic suite ranges from metaluminous granodioritic to peraluminous granitic intrusions (A/CNK = 0.74-1.27); but it is predominantly medium to coarse-grained leucocratic biotite±muscovite granite. Most samples of the EWT have enrichments in LILE (large ion lithophile elements) and HFSE (high field strength elements), with large Eu/Eu*. These characteristics indicate strong fractionation trends where feldspar is the dominant stable aluminous phase. Depletion of HFSE in the most evolved granitic samples can be attributed to fractionation of minor phases (zircon, sphene, apatite and allanite), thus limiting source and genetic interpretations based on the HFSE alone. The Nb+Y versus Rb plot for the combined dataset (Figure 5) shows simple trace element mixing models (Pearce et al. 1984), between the crystallization pathway for the Pirrit Hills granite (dashed line) from a "crustal end-member" in a rifting environment. Most of the geochemical data from the Nash Hills, Pagano Nunatak and Linck Nunatak suites can be explained by 40-60% mixing of an end-member from the evolving petrogenetic pathway for the Pirrit Hills and a 60-40% deep crustal source (do we want to say this after we took the 40-60% mixing lines off Fig. 5?). The Jurassic geochemical data plot in the WPG field (Martin Hills) and on the border of the synCOLG and WPG fields and the data fields for each widely-separated field site overlap. The Mt. Seelig granite, which is 30 Ma older, plots entirely in the WPG field.

Isotopes (Sr, Nd, Pb)

Our new results for the Jurassic granites exhibit a wide range of radiogenic initial ^{87}Sr/^{86}Sr (0.7096 to 0.7179) and much less varaiable initial εNd (-4.3 to -5.6); these are comparable to and within the slightly broader ranges of 0.7070 to 0.7232 and -4.5 to -5.9 for these parameters found by Millar and Pankhurst (1987) and Storey et al. (1988b); they show the same differences between the individual outcrops (Table 1). The initial ^{87}Sr/^{86}Sr of the Whitmore Mountains granite (0.7094) is comparable to that of the Pirrit Hills granite and the initial εNd of -2.4 agrees with one of the previously published values. The Sr and Nd isotope compositions are correlated, resulting in a subhorizontal array stretching from isotopic compositions similar to those of the enriched-mantle sources of ocean island basalts (OIB) toward a highly enriched (time integrated high-Rb/Sr, low Sm/Nd) reservoir characteristic of Proterozoic continental crust (Fig. 6). This trend is essentially the same as that shown by Storey et al. (1988b). The greater variation in initial ^{87}Sr/^{86}Sr relative to ^{143}Nd/^{144}Nd appears to be a robust signal in these granitoids, given that it is consistently shown by initial ^{87}Sr/^{86}Sr ratios from Rb-Sr isochrons and low Rb/Sr apatite analyses. The low ^{87}Sr/^{86}Sr end of the array overlaps with the fields of a variety of Jurassic mafic rocks of the Karoo-Ferrar and Parana large igneous provinces (LIPs), including low-Ti Parana basalts, Tasmanian dolerites and Ferrar andesitic basalts (Mortimer *et. al*. 1995; Antonini *et. al*. 1999; Peate *et. al*. 1999, Hawkesworth *et. al*. 1986, Petrini *et. al*. 1987).

In Sr-Pb space (Fig. 6) the moderately elevated ^{206}Pb/^{204}Pb (>18.47) of the EWT granitoids highlights their similarity to Ferrar mafic rocks and low-Ti Parana basalts, but distinguish them from those of most Karoo magmas. The subvertical array defined by the EWT granites trends toward an isotopically enriched source with time-integrated high Rb/Sr and moderate U/Pb, typical of continental crust. In detail the EWT granitoids define a short linear array in Pb isotope space (Fig. 6); the end-members of this array can be reproduced with a variety of three-stage Pb isotope evolution models that vary the third-stage μ ($^{238}U/^{204}Pb$) between 9.6 and 13.6 at *ca* 1 Ga. The radiogenic end of this array trends toward and past the EMII ocean island basalt end-member, toward compositions again typical of continental crust. The unradiogenic end of this array is remarkably similar to the Pb isotope compositions of both Tasmanian dolerites and Ferrar basaltic andesites (Hergt *et al.*, 1988; Mortimer *et. al.*, 1995; Antonini *et. al*. 1999), and somewhat similar to low-Ti Parana basalts, although the Parana field extends to less radiogenic Pb (Peate *et. al*. 1999, Hawkesworth *et. al*. 1986, Petrini *et. al*. 1987).

The EWT Jurassic granite suite has fairly uniform Nd isotope signatures with εNd at 175 Ma ranging ~ -4.3 to -5.9 (Table 1), although Pankhurst et al. (1991) reported two more negative values of -7.9 (Pirrit Hills) and -7.1 (Linck Nunataks). The Mount Seelig granite sample analysed here has an εNd at 208 Ma of -2.4. Negative values of εNd imply an old crustal contribution to the magmas. Model ages projecting the measured Sm/Nd ratios back in time before Jurassic crystallization (Fig. 7) give widespread model ages of ~0.6 to 1.9 Ga for separation from a chondritic source and ~1.4 to 3.2 Ma for a depleted mantle source. However, Nd model ages calculated by assuming a more uniform crustal source composition (De Paolo et al., 1991) are consistently Mesoproterozoic (almost entirely in the range 1.33–1.40 Ga for the Pirrit and Nash-Martin Hills and Pagano Nunatak).

Discussion

The age of EWT granite magmatism

The U-Pb geochronological data obtained on separated zircon in this study provide robust support for earlier K-Ar and Rb-Sr ages for the emplacement of the EWT granites (Table 1). The new ID-TIMS ages of 174.04 ± 0.08 Ma (Pirrit Hills), 177.44 ± 0.04 Ma (Nash-Martin Hills), 174.62 ± 0.16 Ma (Pagano Nunatak) and 174.82 ± 0.26 Ma (Linck Nunataks) are the most precise yet and may be taken as the best estimates for the ages of crystallization of the individual granite bodies. They overlap within errors with all previous Rb-Sr isochron ages, and mostly with the U-Pb SHRIMP ages presented here. The main exception in this group is the slightly low SHRIMP age for the Pirrit Hills granite (168 ± 4 Ma), where we surmise that zircon may have suffered from small amounts of Pb-loss during the emplacement of pegmatites. The very high U contents of most of these zircon grains make them prone to radiation damage, which facilitates Pb-loss, whereas the chemical leaching process used in the ID-TIMS analysis should effectively remove material affected in this way. A similar explanation may be suggested for the 165 ± 2 Ma SHRIMP age of Lee et al. (2012) for Pirrit Hills zircons, although in addition our recalculation of the data in Table 2 of that paper suggests an older result of c. 172 Ma, which would be compatible with both our TIMS age and the published Rb-Sr age.The SHRIMP age for the Linck Nunataks granite may be distorted by the abundance of inherited zircon apparent in the analysis. Our conclusion is that these granites were all emplaced within a rather short period between 174 and 177 Ma ago. This corresponds to topmost Early Jurassic, essentially late Toarcian (http://www.stratigraphy.org/ICSchart/ChronostratChart2016-04.pdf).

The Whitmore Mountains granites present a more complex chronology. The new ID-TIMS age of 207.96 ± 0.06 Ma is within uncertainty of the Rb-Sr errorchron age (Table 1). They are taken as establishing a latest Triassic episode of EWT granite magmatism, although it is unknown whether this is more widely spread, either in space or time. It is clearly older than the 174, 176 and 190 Ma K-Ar ages presented by Craddock (1972) and the U-Pb SHRIMP age of 200 ± 2 Ma, albeit consistent within error with the Rb-Sr isochron age. The K-Ar ages imply that Jurassic magmatism of ca. 175 Ma may have occurred here 30 Ma after the Triassic event. Twelve of the individual grain SHRIMP dates for the Mount Seelig granite are younger than 190 Ma, and this could indicate that zircon in this sample was affected by Pb-loss associated with this later magmatism.

Magma Genesis and Regional Implications

The Ellsworth-Whitmore terrane is presumed to be mostly Grenville-age crust exposed at Haag Nunataks (Pankhurst and Millar, 1987), with Grenville-age detrital zircons found in overlying Paleozoic sediments (Flowerdew et al. 2007; Craddock et al. 2008) and the evidence for Grenville-age inheritance found by SHRIMP analyses of Mesozoic zircons in the granites reported in this study. The EWT is also characterized by the presence of Jurassic granites, exposed as widely-separated nunataks, that have the same U-Pb zircon crystallization ages, and related bulk geochemistry (within-plate granites) and isotopic (Sr, Pb, Nd) signatures. The EWT is also surrounded by crustal fragments and terranes that do not contain Grenville-orogen affinities (Fig. 1; Dalziel and Elliot, 1982; Storey et al. 1988a). ~~Our study confirms the model of granite petrogenesis and crystallization ages reported by Craddock (1972; K-Ar) and Storey et al. (1988; Rb-Sr) but also allow additional interpretations about the Mesozoic crustal melting that contributed to the break-up of Gondwana and the ultimate migration of the EWT to its position in central Antarctica. (I didn't delete this as I thought you might want to keep it??)~~

Collectively the geochemical data and modeling of the EWT suite can be interpreted to reflect a complex generation of crustal melts that are genetically related to the more mafic Ferrar suite (Storey et al. 1988b; Figure 5). The Ferrar magmas have been interpreted to indicate differentiation of a mantle-derived source that may have incorporated variable amounts of enriched sub-continental mantle lithosphere. When the Ferrar "parental" magma is fully fractionated it would produce compositions similar to the Pirrit Hills granite (Fig. 5; Storey et al., 1988b). Variable mixing of magmas along the fractionation trend of the Ferrar suite with crustal melts can produce the magmatic compositions observed in the Nash Hills, Pagano Nunatak and Linck Nunatak suites. Thus, our data supports the initial interpretation of Storey et al. (1988b), that the EWT suite is part of a larger Middle Jurassic igneous province in West Antarctica that includes the EWT and the Ferrar suite and represents a deep-seated thermal event that is driven by mantle-derived magmatism within the continental crust. This thermal disturbance played a fundamental role as a heating and triggering mechanism for crustal extension and the break-up of Gondwanaland. It is worth noting that similar petrogenetic trends driven by input of enriched mantle-derived magmas and deep crustal melting, have been proposed to explain Eocene-Oligocene magmatism in Cordilleran core complexes, where the thermal disturbance is intimately related to the high-temperature attenuation fabrics observed in metamorphic core complexes (e.g., Konstantinou et al., 2013). (I think you highlighted this…but maybe I did? But parts of this are on page 21-22 so let's see what to do).

Temporal relations with the Karoo-Ferrar LIP

The timing and tempo of magmatism associated with the Karoo-Ferrar LIP has been recently summarized by (Kyle et al. 1981; Pankhurst et al. 1993, 1998, 2000; Elliot and Fleming, 2000; Rapela et al. 2005; Burgess et al. 2015). The four regional episodes of igneous activity resolved in this study effectively bracket the timing of Karoo-Ferrar LIP magmatism. The granites of the Whitmore Mountains (Mt. Seelig) appear to be significantly older than the main array in the EWT by >30 Ma and are thus interpreted as a separate magmatic event with a syn-collisional petrogenesis (Fig. 5 [But Mt. Seelig plots in WPG??]). The Triassic igneous rocks in western Antarctica have been previously interpreted to reflect arc magmas related to Andean-style subduction along the southern South American and West Antarctic corridor (e.g., Meneilly et al., 1987; Pankhurst 1990; Millar et al. 2001; Appendix 6). We support this early interpretation and propose that subduction along the western margin of the West Antarctic Peninsula may have been responsible for modifying and enriching the sub-continental lithosphere beneath the EWT with subduction fluids. This enriched sub-continental lithosphere is consistent with the trace element and isotopic data of the younger (Jurassic) magmatic array of the EWT, indicating that melting of such a potential enriched sub-continental lithospheric mantle source may have been responsible (at least in part) for the excess generation of mafic magmas during the Karoo LIP event.

Our new isotopic major and trace element data support the inferences of Storey et al. (1988b) regarding complex generation via assimilation of crustal and mantle sources during the petrogenesis of the Jurassic EWT granites, and serve to refine the character of the mixing end members. The Ferrar magmas have been interpreted to indicate differentiation of a mantle-derived source that may have incorporated variable amounts of enriched sub-continental mantle lithosphere. Thus, the Ferrar magmas can be used as a proxy for a mantle-derived "parental" magma that, when fully fractionated, would produce compositions similar to the Pirrit Hills granite (Fig. 5; Storey et al., 1988b). The crustal end member is highly radiogenic with respect to

$^{87}Sr/^{86}Sr$ and moderately unradiogenic with respect to ε-Nd, with radiogenic $^{207}Pb/^{204}Pb$ at moderate $^{206}Pb/^{204}Pb$. The aforementioned subhorizontal array in ε-Nd versus $^{87}Sr/^{86}Sr$ data points toward a Proterozoic crustal assimilant, based on the moderately unradiogenic ε-Nd (~-2.4 to -5.6). This inference is consistent with ages of inherited xenocrystic zircon cores in the granites, as well as three-stage Pb isotope evolution models, whereby the minimum age of crustal reservoir segregation, e.g. increase in μ required to produce the elevated $^{207}Pb/^{204}Pb$ at moderate $^{206}Pb/^{204}Pb$, was found to be approximately 1.0 Ga (Grenville crust). The colinearity of the Sr-Nd and Pb-Pb isotope arrays suggests that the isotope systematics are dominated by two-component mixing, however a more diverse suite of enriched sources is suggested by the weaker correlation between Pb and Sr isotopes. The additional enrichment sources could be deeply buried Paleozoic sediments as in the Ellsworth Mountains, remelted synCOLG crust or Grenville crust. This is not surprising given that zircon xenocrysts attest to *ca* 2.5 to 0.5 Ga crustal contributions.

On the whole, the isotopic characteristics and inferred Proterozoic crustal reservoir ages for the EWT are in contrast to the inferred lithospheric contaminants for Karoo lavas, which are clearly distinguished by unradiogenic Sr, Nd and Pb. The latter are consistent with the nature of the Archean lithosphere through which the Karoo lavas were emplaced, in contrast with the dominantly Proterozoic basement of the Ellsworth Mountains (Pankhurst and Millar, 1987; Flowerdew et al. 2007).

The colinearity of the Pb-Pb isotope systematics is noteworthy in that it is consistent with a range of Pb isotope evolution models that produce the end members of the array through Mesoproterozoic fractionation of mμ. This could be taken to suggest a common origin of the radiogenic (high-μ) and unradiogenic (low-μ) reservoirs, for example their identities as complementary enriched crust and depleted subcontinental mantle portions of a lithospheric column formed during *ca* 1 Ga tectonomagmatism.

In summary, based on simple isotopic and trace-element mixing models (Figures 5 and 6) between magmas along the fractionation trend of the Ferrar suite with crustal melts can produce the magmatic compositions observed in the Nash Hills, Pagano Nunatak and Linck Nunataks suites. Thus, our data supports the initial interpretation of Storey et al. (1988b), that the EWT suite is part of a larger Middle Jurassic igneous province in West Antarctica that includes the EWT and the Ferrar suite and represents a deep-seated thermal event that is driven by mantle-derived magmatism within the continental crust (WPG) in the absence of any regional collisional tectonic scenario.

Tectonic Implications

The results of this study provide evidence of the continuation of the Triassic West Antarctic magmatic arc based in the ID-TIMS U-Pb zircon age of 208 Ma in the Whitmore Mountains granite and Rb-Sr ages in the Deseado Massif (Pankhurst et al. 1993; Figure 8). The dynamics of the plate separation and widespread Karoo-Ferrar mafic event at 182 Ma was a brief event (Burgess et al. 2015) associated with dispersal of the EWT from Gondwana and initiation of the thermal and kinematic conditions that gave rise to the Subcordilleran batholith of western Patagonia (181-185 Ma; Rapela et al. 2005), the more widespread Jurassic andesite–rhyolite volcanism of Patagonia and the Antarctic Peninsula (188-153 Ma; Pankhurst et al. 2000) and the within-plate granites in the EWT at 174-177 Ma. The Jurassic magmas in the EWT indicate that during this event, the sub-continental lithosphere was thermally eroded and the whole lithospheric column was probably weakened. While the geochemical data from the Jurassic EWT granites can be interpreted to reflect a regional back-arc extensional event, the intrusion of large volumes of basalt associated with the Karoo-Ferrar LIP lead to a more plausible interpretation of a convective mantle-driven (plume or hot-spot) event that was associated with a brief, well-dated thermal anomaly in the mantle (Burgess et al. 2015). The primitive magmas associated with such a mantle-driven thermal event would have been significantly altered/contaminated in geochemistry by melting of the sub-continental lithosphere and the lower crust. Thus at a lithospheric scale, this thermal disturbance played a fundamental role in thermally eroding/melting the lithospheric column and was the triggering mechanism for crustal extension and the break-up of Gondwanaland. Similarly, Bryan et al. (2002) have proposed that a MASH (mixing-assimilation-storage-hybridization) type model would easily explain the slightly younger ages of the EWT granites relative to the mafic Ferrar suite. This process is especially prominent with volatile-rich silicic magmas relative to anhydrous silicic magmas. It is a pattern observed in much younger rocks too, even within single eruptive centers including large volume rhyolites in the Basin and Range province that contain zircons that may be up to 8-10 m.y. older than the eruptive age. The implication is long-term storage of the silicic magmas in the middle-lower crust before emplacement in the upper crust (magma chamber).

Terrane History

The Ellsworth-Whitmore terrane, with its Grenville-age crust was part of Rodinia at ~1 Ga (Moores, 1991; Dalziel, 1992; Dalziel, 1997; Wareham et al. 1998) and may have been in proximity to Laurentia as Keweenawan rift magmatic rocks have been identified in Coats Land (Loewy et al., 2011; U-Pb zircon age of 1112 Ma). Cambrian sedimentation is known, or inferred, across the EWT (Storey and MacDonald, 1988; Webers et al. 1992; Flowerdew et al. 2007) as Gondwana began to amalgamate in the early Paleozoic although Cambrian sedimentation was local and rift-related, in a convergent tectonic setting (Curtis, 1999; Craddock et al. 2008). Sedimentation continued across southern Gondwana in the Paleozoic until the supercontinent formed in conjunction with the Permian Gondwanide orogen (duToit, 1937; Halbich, 1992; DeWit and Ransome, 1992). As Gondwana began to fragment at ~210 Ma (Lawver et al. 1991), the EWT was located in the Natal Embayment and all the now-dispersed portions of the Gondwanide thrust belt were continuous and aligned, including the Ellsworth Mountains (Dalziel and Grunow, 1992; Fig. 8a). Intrusion of the Mt. Seelig granite (203-208 Ma) to form the Whitmore Mountains occurred before the break-up of Gondwana so this intrusion is likely related to arc magmatism associated with Triassic subduction ~1000 km to the west (Rapela et al. 1992, Pankhurst et al. 1993; Fig. 8a). The Karoo-Ferrar LIP province (182 Ma; 1 Ma duration) is related to the robust break-up of Gondwana with a mafic igneous suite that is found along the ~5000 km boundary between East Antarctica and the terranes of West Antarctica and Africa and includes the Weddell and Limpopo triple junctions within the associated hotspot (Elliot and Fleming, 2000; Fig. 8b). Initial rifting is also recorded by the Early Jurassic rhyolites in north-eastern Patagonia (V1 episode of Pankhurst et al. 2000) and the Subcordilleran batholith farther west (Rapela et al. 2005). Paleomagnetic results (Grunow et al. 1987a,b; Dalziel and Grunow, 1992) suggest that the EWT was at 47°S when the bulk of the within-plate granites (177 Ma) were intruded (Storey et al. 1988b; this study) and far from the remains of Gondwana as the Weddell Sea opened (Grunow, 1993). This was also the time of the more widespread Chon Aike volcanism of Patagonia which merges into subduction-related magmatism in the Andean domain (Pankhurst et al. 2000; Riley et al. 2001; Figure 8c). The EWT is now at 82°S but there is no paleomagnetic data to constrain the 35° of latitudinal motion of the EWT between the late Jurassic and present. Outcrops in the EWT are widely separated and include a few nunataks and the highest peaks in the Ellsworth Mountains, the later of which were uplifted ~4 km at 120 Ma (Fitzgerald and Stump, 1991). The cause of this uplift is unknown but the high-standing portions of the EWT are important in stabilizing the ice volumes in central Antarctica (Dalziel, 2007).

Conclusions

We conclude that the Triassic-Jurassic EWT granites are mixtures of crustal and mantle melts, specifically Ferrar-type basalts that have undergone a significant degree of fractional crystallization with concomitant Grenville-aged crustal assimilation, resulting from the deep-seated Limpopo hotspot thermal disturbance linked to the subsequent breakup of Gondwana (Storey *et al.* 1988 a,b; Elliot and Fleming, 2000). Arc-related magmatism produced the Mt. Seelig syn-collisional granites (but plot as WPG in Fig. 5?) that intruded the EWT at 208 Ma, followed by regional Gondwana break-up Karoo-Ferrar (182 Ma) mafic intrusions and extrusions, and finally within-plate granitic intrusions at 174-177 Ma that were intruded after the Ellsworth-Whitmore terrane rotated to its position in central Antarctica. Combined geochemical (XRF, isotopes) and geochronological studies (U-Pb SHRIMP and CA-ID-TIMS ages on zircon) provide multiple insights into the petrogenesis of simple granites (see also Bickford et al. 2006 and Schmitz et al. 2006).

Acknowledgements

This project is a continuation of the early exploration and sample collection of J. Campbell Craddock (1959-60, 1962-3, 1964-5 field seasons; deceased 2006), Ed Thiel (1959-60, 60-61 field seasons; deceased 1961 in an Antarctic plane crash), and Gerald Webers (1964-5 field season; deceased 2008) in central Antarctica. Details of the early exploration of central Antarctica can be found in the preface of Geological Society of America Memoir 170 (Webers et al. 1992). The original mylar (2 x 3 feet) geologic maps in Appendices 2-5 have been archived at the Byrd Polar Institute, Ohio State University. John P. Craddock acquired these samples and materials in 2002. Anne Grunow contributed paleomagnetic cores (separated for zircons) from Pagano Nunatak. John Splettstoesser (deceased 2016), Staci Loewy and an anonymous reviewer greatly improved the clarity of the manuscript.

Figures

Fig. 1: Figure 1: Sub-ice topographic DEM of Antarctica (B) with continental crust terranes identified (EANT: East Antarctic craton; AP: Antarctic Peninsula; TI: Thurston Island; MBL: Marie Byrd Land; EWT: Ellsworth-Whitmore terrane; from Dalziel, 2008) and in (A), a detailed sub-ice DEM of central west Antarctica. Red-orange areas are bedrock exposed above ice whereas yellow areas are sub-ice and blue areas are below sea level.

Fig. 2: Figure 2: Field photos of the Pirrit Hills (A) and Pagano Nunatak (B; 230 m relief) granites.

Fig. 3: ID-TIMS plots (ranked $^{206}Pb/^{238}U$ age plot) illustrating single crystal zircon analyses from 9 granites of the EWT. Error bars are plotted at 2σ. Filled bars represent analyses included in weighted mean age (grey horizontal bar); open bars represent analyses interpreted as inheritance or Pb-loss). See table 2.

Fig. 4: A. Concordia plots of SHRIMP U-Pb ages from cores and rims of zircons from EWT granites. B.relative probability plot of inherited ages (See Tables 1 and 3).

Fig. 5: Rb Vs (Nb+Y) discrimination diagram for EWT granitic suite. Fields and data for 'crust-free' WPG from Pearce et al., (1984). Petrogenetic pathway for Ascension Island from Pearce et al., (1984); Long dashes, petrogenetic pathway for crystallization of Pirrit Hills granite (from Storey et al., 1988b, using parameters therein). Assumed mafic precursor (Pb) to the Pirrit Hills granite (Pa); Pi is intermediate step. Dotted lines indicate mixing lines between two points on the petrogenetic pathway and an assumed crustal end-member approximated by the Thiel Mts. Granite. Ancronyms: WPG, within plate granite; synCOLG, syn-collisional granite; VAG, volcanic arc granite. See Table 4 for data.

Fig. 6a: Tracer Isotopes (Initial epsilon Nd versus $^{87}Sr/^{86}Sr$ isotope correlation diagram, illustrating the isotopic composition of Ellsworth-Whitmore granites (filled triangles) with respect to the compositional fields of various Mesozoic ultramafic to mafic-intermediate magmas from southern Gondwana, and oceanic basalt mantle end-members (gray filled squares). Literature sources for Gondwanan magmas cited in text; mantle end-members back-calculated to 178 Ma using present-day isotopic compositions and parent-daughter ratios from Zindler and Hart, 1986; Eisele et al. 2002; Salters and Stracke, 2004; Stracke et al. 2003, 2005; Workman et al. 2004; Workman and Hart, 2005).

Fig. 6b: Tracer Isotopes ($^{87}Sr/^{86}Sr$ versus $^{206}Pb/^{204}Pb$ isotope correlation diagram, illustrating the isotopic composition of Ellsworth-Whitmore granites. Symbols and data sources as in Figure 3.

Mantle end-members back-calculated to 178 Ma using present-day isotopic compositions and parent-daughter ratios (see citations above).

Fig. 6c: Tracer Isotopes (^{207}Pb/^{204}Pb versus ^{206}Pb/^{204}Pb isotope correlation diagram, illustrating the isotopic composition of Ellsworth-Whitmore granites. Symbols and data sources as in Figure 3. Mantle end-members back-calculated to 178 Ma using present-day isotopic compositions and parent-daughter ratios. Also illustrated are a pair of 3-stage Pb isotope evolution models constructed to reproduce the end-members of the correlated array of Ellsworth-Whitmore granite Pb isotope data.

Fig. 7: Nd model ages for Ellsworth-Whitmore terrane Jurassic granites. See Table 5.

Fig. 8a: Figure 8a: Schematic tectonic recontruction for Gondwana in the late Triassic when the Mt. Seelig granite (pink) was intruded into the Grenville-aged crust (patterned) of the Ellsworth-Whitmore terrane as a within-plate intrusion. The central Patagonia and Deseado monzonite suites (224-200 Ma; Rb-Sr Pankhurst et al. 1993) are similar intrusions. Symbols: AP: Antarctic Peninsula; TI: Thurston Island; MBL: Marie Byrd Land; CL: Coats Land.

Fig. 8b: Schematic tectonic reconstruction for Gondwana in the middle Jurassic when the Weddell triple junction began the divergence of Gondwana coeval with the eruption of Karoo-Ferrar mafic extrusions (182 Ma) and the Marifil Group silicic rocks (188 Ma; see Rapela et al. 2005). These mafic melts are only observed on the east and north side of the rifting margin.

Symbols: AP: Antarctic Peninsula; TI: Thurston Island; MBL: Marie Byrd Land; CL: Coats Land.

Fig. 8c: Figure 8c: Schematic tectonic reconstruction for Gondwana in the middle Jurassic when the Weddell triple junction began the opening of the Weddell Sea and the divergence of Gondwana coeval with the intrusion of the granites now exposed in the EWT (174-177 Ma; yellow dots) and the regional extrapolation of the Chon Aike province (Bryan et al. 2002). Symbols: AP: Antarctic Peninsula; TI: Thurston Island; MBL: Marie Byrd Land; CL: Coats Land.

Tables

Table 1: Summary of Radiometric Ages

Table 2: TIMS U-Pb Zircon Results

Table 3: SHRIMP U-Pb Zircon Results

Table 4: XRF Geochemistry

Table 5: Isotopic Data (Sr, Pb, Nd)

Appendices

Appendix 1: Detailed Methods

Appendix 2: Geologic map, Pirritt Hills.

Appendix 3: Geologic map, Martin Hills.

Appendix 4: Geologic map, Nash Hills.

Appendix 5: Geologic map, Hart Hills.

Appendix 6: West Antarctic granite geochemistry (non-EWT).

References

Anderson, J.J., Bastien, T.W., Craddock, C., Schmidt, P.G., and Spletttoesser, J.F., 1962, Antarctica: geology of the Ellsworth Mountains: Science, v. 138, no. 3542, p. 824-825.

Antonini, P., Piccirillo, E.M., Petrini, R., Civetta, L., D'Antonio, M., and Orsi G. 1999, Enriched mantle – Dupal signature in the genesis of the Jurassic Ferrar tholeiites from Prince Albert Mountains (Victoria Land, Antarctica): Contributions to Mineralogy and Petrology, v. 136, p. 1-19.

Behrendt, J.C., Drewry, D.J., Jankowski, E.J., and Grim, M.S., 1981, Aeromagnetic and radio echo ice-sounding measurements over the Dufek Intrusion, Antarctica: J. Geophys. Res., v. 86, p. 3014–3020.

Bell, R E., Brozena,J., Haxby, W., and LaBrecque, J.L., 1990, Continental margins of the western Weddell Sea: Insights from airborne gravity and GEOSAT derived gravity, in Contributions to Antarctic Research I, Antarct. Res. Ser., vol. 50, edited by D. E. Hayes, pp. 91 – 102, AGU, Washington, D. C.

Bentley, C.R., Crary, A.P., Ostenso, N.A., and Thiel, E.C., 1960, Structure of West Antarctic: Science, v. 131, p. 131-136.

Bickford, M.E., Wooden, J.L., and Bauer, R.L., 2006, SHRIMP study of zircon grains from Early Archean rocks in the Minnesota River Valley: implications for the tectonic history of the Superior Province: Geol. Soc. Am. Bull., v. 118, p. 94–108.

Bryan, S.E., Riley T.R., Jerram, D.A., Stephens, D.J., and Leat, P.T., 2002, Silicic volcanism: An undervalued component of large igneous provinces and volcanic rifted margins: Geological Society of America Special Paper 362, p. 99-120.

Burgess, S.D., Bowring, S.A., Fleming, T.H., and Elliot, D.H., 2015, High-precision geochronology links Ferrar large igneous province with early Jurassic ocean anoxia and biotic crisis: Earth and Planetary Science Letters, v. 415, p. 90-99.

Burton-Johnson, A., and Riley, T.R., 2015, Autochthonous vs. accreted terrane development of continental margins: A new in situ tectonic history of the Antarctic Peninsula: Journal of the Geological Society, London, v. 172, p. 832-835.

Comin-Chiaramonti, P., Cundari, A., Piccirillo, E.M., Gomes, C.B., Castorina, F., Censi, P., De Min, A., Marzoli, A., Speziale, S., and Velazquez, V.F., 1997, Potassic and Sodic Igneous Rocks from Easter Paraguay: their Origin from the Lithospheric Mantle and Genetic Relationships with the Associated Parana Flood Tholeiites: Journal of Petrology, v. 38, p. 495-528.

Curtis, M.L., 1997, Gondwanian age dextral transpression and spatial kinematic partitioning within the Heritage Range, Ellsworth Mountains, West Antarctica: Tectonics, v. 16, p. 172–181.

Curtis, M.L., 1998a, Development of kinematic partitioning in a pure-shear dominated dextral transpression zone: the southern Ellsworth Mountains, Antarctica, in Holdsworth, R.E., et al., eds., Continental transpressional and transtensional tectonics: Geological Society, London, Special Publication 135, p. 289–306.

Curtis, M.L., 1998b, Evidence for Cambrian deformation in the Ellsworth-Whitmore Mountains terrane, Antarctica: Stratigraphic and tectonic implications: Comment: Geology, v. 26, p. 1054–1055.

Curtis, M.L., 2001, Tectonic history of the Ellsworth Mountains, West Antarctica: Reconciling a Gondwana enigma: Geological Society of America Bulletin, v. 113, p. 939–958, doi: 10.1130/0016-7606(2001)113<0939: THOTEM>2.0.CO;2.

Curtis, M.L., Leat, P.T., Riley, T.R., Storey, B.C., Millar, I.L., and Randall, D.E., 1999, Middle Cambrian volcanism in the Ellsworth Mountains: Implications for paleo-Pacific margin tectonics: Tectonophysics, v. 304, p. 275–299.

Craddock, C., and Webers, G. F., 1964, Fossils from the Ellsworth Mountains, Antarctica: Nature, v. 201, no. 4915, p. 174-175.

Craddock, C., Bastien, T.W., Rutford, R.H., and Anderson, J.J., 1965, Glossopteris discovered in West Antarctica: Science, v. 148, no. 3670, p. 634-637.

Craddock, C., 1966, "Ellsworth Mountains fold belt; a link between east and west Antarctica": Geological Society of America, Special Paper 87, p. 37-38.

Craddock, C., 1969, Geology of the Ellsworth Mountains: Geog. Soc. Antarctic Map Folio Series, Folio.

Craddock, C., 1972, Geological Map of Antarctica: American Geographical Society, 1:5,000,000.

Craddock, J.P., Konstantinou, A., Nereson, A., Webers, G.F., Ojakangas, R.W., Fitzgerald, P., and Gehrels, G., 2008, Detrital Zircon and Heavy Mineral Provenance of the Ellsworth Mountains, Antarctica and Gondwana-wide Carboniferous Tillite: Gondwana 13 (Dali, China), p. 35.

Craddock, J.P., Fitzgerald, P., Thomas, R., Konstantinou ,A., and Nereson, A., in review, Detrital zircon provenance of Paleozoic strata, Ellsworth Mountains, West Antarctica: Gondwana Research.

Crowley, J.L., Schoene, B., Bowring, S.A., 2007, U-Pb dating of zircon in the Bishop Tuff at the millennial scale: Geology v., 35, p. 1123-1126.

Dalziel, I.W.D, 2008, The Ellsworth Mountains: Critical and enduringly enigmatic: U.S. Geological Survey and The National Academies: USGS OF-2007-1047, Short Research Paper 004.

Dalziel, I.W.D., and Elliot, D.H., 1982, West Antarctica: Problem child of Gondwanaland: Tectonics, v. 1, p. 3–19.

Dalziel, I.W.D., and Grunow, A.M., 1992, Late Gondwanide tectonic rotations within Gondwanaland: Tectonics, v. 11, p. 603–606.

Dalziel, I.W.D., and Pankhurst, R.J., 1984, West Antarctica: its tectonics and relationship to East Antarctica: Antarctic Journal of the United States, v. 19, no. 5, p. 35-36.

Dalziel, I.W.D., Storey, B.C., Garret, S.W., Grunow, A.M., Herrold, D.B., and Pankhurst, R.J., 1987, Extensional tectonics and the fragmentation of Gondwanaland, In: Coward MP, Dewey JF, Hancock PL. Jurassic Granites in West Antarctica 1007 (eds) Continental Extensional Tectonics: Special Publication of the Geological Society, London, 28, p. 433-41.

Davydov, V.I., Crowley, J.L., Schmitz, M.D., and Poletaev, V.I., 2010, High-precision U-Pb zircon age calibration of the global Carboniferous time scale and Milankovitch-band cyclicity in the Donets Basin, eastern Ukraine: Geochemistry, Geophysics, Geosystems - G3, 10.1029/2009GC002736.

DePaolo, D.J., Linn, A.M., and Schubert, G., 1991, The continental crustal age distribution: Methods of determining mantle separation ages from Sm-Nd isotopic data and application to the southwestern United States: Journal of Geophysical Research, Solid Earth, v. 96, Issue B2, p. 2071–2088, doi: 10.1029/90JB02219.

DeWit, M.J., and Ransome, I.G., 1992, Regional inversion tectonics along the southern margin of Gondwana. Inversion tectonics of the Cape Fold Belt, Karoo and Cretaceous basins of southern Africa, 15-21.

DuToit, A.L., 1937, Our Wandering Continents: Edinburgh, Scotland, Oliver & Boyd, 355 pp.

Eisele, J., Sharma, M., Galer, S.J.G., Blichert-Toft, J., Devey, C.W., and Hofmann, A.W., 2002, The role of sediment recycling in EM-1 inferred from Os, Pb, Hf, Nd, Sr isotope and trace element systematics of the Pitcairn hotspot: Earth and Planetary Science Letters, v. 196, p. 197-212.

Elliot, D.H., Fleming, T.H., Kyle, P.R., and Foland, K.A., 1999, Long-distance transport of magmas in the Jurassic Ferrar Large Igneous Province, Antarctica: Earth and Planetary Science Letters, v. 167, p. 89-104.

Elliot, D.H., and Fleming, T.H., 2000, Weddell triple junction: The principal focus of Ferrar and Karoo magmatism during initial breakup of Gondwana: Geology, v. 28, p. 539-542.

Elliot, D.H., Fanning M. and T.S. Laudon, 2014, The Gondwana Plate margin in the Weddell Sea sector: zircon geochronology of the upper Paleozoic (mainly Permian) strata of the Ellsworth Mountains and eastern Ellsworth Land, Antarctic: Gondwana Research, http://dx.doi.org/10.1016/j.gr.2014.12.001

Faure, G., and Mensing, T.M., 2005. Isotopes. Principles and Applications. 3rd Ed. Hoboken, New Jersey: John Wiley & Sons.

Fitzgerald, P.G., and Stump, E., 1991, Early Cretaceous uplift in the Ellsworth Mountains of West Antarctica: Science, v. 254, no. 5028, p. 92-94.

Flowerdew, M.J., Millar, I.L., Curtis, M.L., Vaughan, A.P.M., Horstwood, M.S.A., Whitehouse, M.J., and Fanning, C.M., 2007, Combined U-Pb geochronology and Hf isotope geochemistry of detrital zircons from early Paleozoic sedimentary rocks, Ellsworth-Whitmore Mountains block, Antarctica: Geological Society of America Bulletin, v. 119, p. 275-288.

Gerstenberger, H., and Haase, G., 1997, A highly effective emitter substance for mass spectrometric Pb isotope ratio determinations: Chemical Geology, v. 136, p.309-312.

Goodge , J.W., and Fanning, C.M., 2010, Composition and age of the East Antarctic Shield in eastern Wilkes Land determined by proxy from Oligocene-Pleistocene glaciomarine sediment and Beacon Supergroup sandstone, Antarctica: Geological Society of America Bulletin, v. 122, p. 1135-1159.

Goodge, J. W., Fanning, C.M., Brecke, D.M., Licht, K.J., and Palmer, E.F., 2010, Continuation of the Laurentian Grenville province in western East Antarctica: Journal of Geology, v. 118, p. 601-619.

Grunow, A.M., Dalziel, I.W.D., and Kent, D.V., 1987, Ellsworth-Whitmore mountains crustal block, western Antarctica; new paleomagnetic results and their tectonic significance; Gondwana Six; Structure, tectonics, and geophysics: American geophysical Union, Geophysical Monograph 40, p. 161-171.

Grunow, A.M., 1993, Creation and destruction of Weddell Sea floor in the Jurassic: Geology, v. 21, p. 647-650.

Halbich, I.W., 1992, The Cape fold belt orogeny: state of the art 1970s-1980s: in Inversion Tectonics of the Cape Fold Belt, Karoo and Cretaceous Basins of Southern Africa (Rotterdam), p. 141-158.

Harley, S.L., and Kelley, N.M., 2007, Ancient Antarctica: The Archean of the East Antarctic Shield, In, Earth's Oldest Rocks: Developments in Precambrian Geology , v. 15, p. 149-186.

Hawkesworth, C.J., Mantovani, M.S.M., Taylor, P.N., and Palacz, Z., 1986, Evidence from the Parana of south Brazil for a continental contribution to Dupal basalts: Nature, v. 322, p. 356-359.

Hergt, J.M., Chappell, B.W., McCulloch, M., McDougall, I., and Chivas, A.R., 1989, Geochemical and Isotopic Constraints on the Origin of the Jurassic Dolerites of Tasmania: Journal of Petrology, v. 30, p. 841-883.

Housh, T., and Bowring, S.A., 1991, Lead isotopic heterogeneities within alkali feldspars: implications for the determination of initial lead isotopic compositions: Geochemica at Cosmoshemica Acta, v. 55, p. 2309-2316.

Huebscher, C., Jokat, W., and Miller, H., 1996, Crustal structure of the Antarctic continental margin in the eastern Weddell Sea, In Weddell Sea Tectonic and Gondwana Break-up: Geological Society Special Publication 108, p. 165-74.

Ireland, T.R., Clement, S., Compston, W., Foster, J.J., Holden, P, Jenkins, B., Lanc, P., Schram, N., and Williams, I.S., 2008, Development of SHRIMP: Australian Journal of Earth Sciences, v. 55, p. 937-954.

Jaffey, A.H., Flynn, K.F., Glendenin, L.E., Bentley, W.C., and Essling, A.M., 1971, Precision measurements of half-lives and specific activities of ^{235}U and ^{238}U: Physical Review, v. C 4, p. 1889-1906.

Jourdan, F., Bertrand, H., Scharar, U., Blichert-Toft, J., Feraud, G., and Kampunzu, A.B., 2007, Major and Trace Element and Sr, Nd, Hf, and Pb Isotope Compositons of the Karoo Large Igneous Province, Botswana-Zimbabwe: Lithosphere vs Mantle Plume Contribution: Journal of Petrology, v. 48, p. 1043-1077.

König, M., and Jokat, W., 2006, The Mesozoic breakup of the Weddell Sea: J. Geophys. Res., 111, B12102, doi:10.1029/2005JB004035.

Konstantinou, A., Wirth, K.R., Vervoort, J.D., Davidson, C., Malone, D.H., and Craddock, J.P., 2014, Detrital zircon geochronology of Early Paleozoic Midcontinent region, supermature quartz arenites: Implications for paleogeography, erosion and sedimentation patterns: Journal of Geology, v. 122, p. 201-216.

Krogh, T.E., 1973, A low contamination method for hydrothermal decomposition of zircon and extraction of U and Pb for isotopic age determination: Geochimica et Cosmochimica Acta, v. 37, p. 485-494.

Kyle, P.R., 1980, Development of heterogeneities in the subcontinental mantle: evidence from the Ferrar group, Antarctica: Contrib. Mineral. and Petrology, v. 73, p. 89-104.

LaBreque, J.L., and Barker, P., 1981, The age of the Weddell Basin: Nature, v. 290, p. 489-492.

Lawver , L.A., Sandwell, D.A., Royer, J.-Y., and Scotese, C.R., 1991, Evolution of the Antarctic continental margins, In: Thomson, M.R.A., Crame, J.A., Thomson, J.W. (Eds.), Geological Evolution of Antarctica, Cambridge Univ. Press, p. 533-540.

Leat, P.T., Riley, T.R., Storey, B.C., Kelley, S.P., and Millar, I.L., 2000, Middle Jurassic ultramafic lamprophyre dyke within the Ferrar magmatic province, Pensacola Mountains, Antarctica: Mineralogical Magazine, v. 64, p. 95-111.

Lee, H.M, Lee, J.I., Lee, M.J., Kim, J. and S.W Choi, 2012, The A-type Pirrit Hills granite, West Antarctica: an example of magmatism associated with the break-up of the Gondwana supercontinent: Geosciences Journal 16, p. 421-433.

Leowy, S.L., Dalziel, I.W.D., Pisarevsky, S., Connelly, J.N., Tait, J., Hanson, R.E., and Bullen, D., 2011, Coats Land crustal block, East Antarctica: a tectonic tracer for Laurentia?: Geology, v. 39, p. 859-62.

Le Masurier, W.E., 1990, Late Cenozoic volcanism on the Antarctic Plate: An overview, in Volcanoes of the Antarctic Plate and Southern Oceans, Antarct. Res. Ser., vol 48, edited by W.E. Le Masurier and J.W. Thomson, pp. 1-19, AGU, Washington, D.C.

Ludwig, K.R., 2003, User’s Manual for Isoplot 3.00. Berkeley Geochronology Center, Berkeley, CA, 70 pp.

Maslanyj, M.P., and Storey, B.C., 1990, Regional aeromagnetic anomalies in Ellsworth Land; crustal structure and Mesozoic microplate boundaries within West Antarctica: Tectonics, v. 9, no. 6, p. 1515-1532.

Mata, J., Kerrich, R., MacRae, N.D., and Wu, T.W., 1998, Elemental and isotopic (Sr, Nd, and Pb) characteristics of Madiera Island basalts: evidence for a composite HIMU – EM I plume fertilizing lithosphere: Canadian Journal of Earth Sciences, v. 35, p. 980-997

Mattinson, J.M., 2005, Zircon U-Pb chemical abrasion ("CA-TIMS") method: combined annealing and multi-step partial dissolution analysis for improved precision and accuracy of zircon ages: Chemical Geology, v. 220, p. 47-66.

Meneilly, A.W., Harrison, S.M., Piercy B.A., and Storey, B.C., 1987, Structural evolution of the magmatic arc in northern Palmer Land, Antarctica Peninsula: Gondwana Six: Structure, Tectonics and Geophysics, American Geophysical Union, Geophysical Monograph 40, p. 34-56.

Millar, I.L., and Pankhurst, R.J., 1987, "Rb-Sr geochronology of the region between the Antarctic Peninsula and the Transantarctic Mountains; Haag Nunataks and Mesozoic granitoids; Gondwana Six; Structure, tectonics, and geophysics", American Geophysical Union, Geophysical Monograph 40, p. 151-160.

Millar, I.L., Willan, C.R.R., Wareham, C.D., and A.J. Boyce, 2011, The role of crustal and mantle sources in the genesis of granitoids of the Antarctic Peninsula and adjacent crustal blocks: Journal of the Geological Society, London 158, p, 855-867.

Minor, D., and Mukasa, S.B., 1997, Zircon U–Pb and hornblende 40Ar/39Ar ages for the Dufek layered mafic intrusion, Antarctica: implications for the age of the Ferrar large igneous province: Geochim. Cosmochim. Acta, v. 61, p, 2497–2504.

Mortimer, D., Parkinson, D., Raine, J.I., Adams, C.J., Graham, I.J., Oliver, P.J., and Palmer, K., 1995, Ferrar magmatic province rocks discovered in New Zealand: Implications for Mesozoic Gondwana geology: Geology, v. 35, p. 185-188.

Naish, T., Powell, R., Levy, R., Wilson, G., Scherer, R., Talarico, F., Krissek, L., Niessen, F., Pompilio, M., Wilson, T., Carter, L., DeConto, R., Huybers, P., McKay, R., Pollard, D., Ross, J., Winter, D., Barrett, P., Browne, G., Cody, R., Cowan, E., Crampton, J., Dunbar, G., Dunbar, N., Florindo, F., Gebhardt, C., Graham, I., Hannah, M., Hansaraj, D., Harwood, D., Helling, D., Henrys, S., Hinnov, L., Kuhn, G., Kyle, P., Läufer, A., Maffioli, P., Magens, D., Mandernack, K., McIntosh, W., Millan, C., Morin, R., Ohneiser, C. , Paulsen, T., Persico, D., Raine, I., Reed, J., Riesselman, C., Sagnotti, L., Schmitt, D., Sjunneskog, P., Strong, C., Taviani, M., Vogel, S., Wilch, T., and Williams, T., 2009, Obliquity-paced Pliocene West Antarctic ice sheet oscillations: Nature, v. 458, p. 322-328.

Pankhurst, R.J., Storey, B.C., and Millar, I.L., 1991, agmatism related to the break-up of Gondwanaland. In: Thomson, M.R.A., Crame, J.A., and Thomson, J.W. (eds) Geological Evolution of Antarctica. Cambridge University Press, p. 573-579.

Pankhurst, R.J., Rapela, C.W., and Márquez, M.J., 1993, Geocronología y petrogénesis de los granitoides jurásicos del noreste del Macizo Deseado: Actas del XII Congreso Geológico Argentino, Mendoza, Alcira Vergara Oroño, Buenos Aires, Tomo IV, p. 134-141.

Pankhurst, R.J., and Rapela, C.W., 1998, The proto-Andean margin of Gondwawa: an introduction: Geological Society, London, Special Publications 142, p. 1-9.

Pankhurst, R.J., Riley, T.R., Fanning, C.M., and Kelley, S.P., 2000, Episodic silicic volcanism in Patagonia and the Antarctic Peninsula: chronology of magmatism associated with the break-up of Gondwana: Journal of Petrology, v. 41, p. 605-625.

Paulsen, T., Wilson, T.J., Demosthenous, C., Millan, C., Jarrard, R.,and Laufer, A., 2014, Kinematics of the Neogene Terror Rift: Constraints from calcite twinning strain in ANDRILL-1B core, McMurdo Ice Shelf, Victoria Land Basin, Antarctica: Geosphere.

Pearce, J.A., Harris, N.B.W., and Tindle, A.G., 1984, Trace Element discrimination diagrams for the tectonic interpretation of granitic rocks: Journal of Petrology, v. 25, p. 956-983.

Peate, D.W., Hawkesworth, C.J., Mantovani, M.M.S., Rogers, N.W., and Turner, S.P., 1999, Petrogenesis and Stratigraphy of the High-Ti/Y Urubici Magma type in the Parana Flood

Basalt Province and Implications for Dupal type Magma in the South Atlantic Region: Journal of Petrology, v. 40, p. 451-473

Petrini, R., Civetta, L., Piccirillo, E.M., Gelleini, G., Comin-Chiaramonti, P., Marques, L.S., and Melfi, A.J., 1987, Mantle Heterogeneity and Crustal Contamination in the Genesis of Low-Ti Continental Flood Basalts from the Parana Plateau (Brazil): Sr-Nd Isotope and Geochemical Evidence: Journal of Petrology, v. 28, p. 701-726

Prestvik, T., Goldberg, S., Goles, G.G., 1999, Petrogenesis of the volcanic suite of Bouvetoya (Bouvet Island), South Atlantic: Norsk Geologisk Tidssk Rift, v. 79, p. 205-218.

Randall, D.E., and Mac Niocaill, C., 2004, Cambrian palaeomagnetic data confirm a Natal location for the Ellsworth-Whitmore Mountains, Antarctica, in Gondwana reconstructions: Geophysical Journal International, v. 157, p. 105–116, doi: 10.1111/j.1365-246X.2004.02192.x.

Rapela, C.W., Pankhurst, R.J., and Harrison, S.M., 1992, Triassic "Gondwana" granites of the Gastre District, North Patagonian Massif: Transactions of the Royal Society of Edinburgh: Earth Sciences, v. 83, p. 291-304.

Rapela, C.W., Pankhurst, R.J., Fanning, C.M., and Hervé, F., 2005, Pacific subduction coeval with the Karoo mantle plume: the Early Jurassic Subcordilleran belt of northwestern Patagonia. In: Vaughan, A.P.M., Leat, P.T., and Pankhurst, R.J. (eds) Terrane Processes at the Margins of Gondwana, Geological Society, London, Special Publication 246, p. 217-240.

Riley, T.R., and Knight, K.B., 2001, Age of Pre-Break-up of Gondwana Magmatism: Antarctic Science, v. 13, p. 99-110.

Riley, T.R., Leat, P.T., Pankhurst, R.J., and Harris, C., 2001, Origins of large-volume rhyolite volcanism in the Antarctic Peninsula and Patagonia by crustal melting: Journal of Petrology, v. 42, p. 1043-1065.

Riley, T.R., Leat, P.T., Storey, B.C., Parkinson, I.J., and Millar, I.L., 2003, Ultramafic lamprophyres of the Ferrar large igneous province: evidence for a HIMU mantle component: Lithos, v. 66, p. 63-76

Riley, T.R., Curtis, M.L., Leat, P.T., and Millar, I.L., 2009, The geochemistry of Middle Jurassic dykes associated with the Straumsvola –Tvora alkaline plutons, Dronning Maud Land, Antarctica and their association with the Karoo large igneous province: Mineralogical Magazine, v. 73, p. 205-226.

Salters, V.J.M., and Stracke, A., 2004, Composition of the depleted mantle: Geochemistry, Geophysics, Geosystems (G3), v. 5, p. 05004.

Salvini, F., Brancolini, G., Busetti, M., Storti, F., Mazzarini, F., and Coren, F., 1997, Cenozoic Geodynamics Of The Ross Sea Region, Antarctica: Crustal Extension, Intraplate Strike-Slip Faulting, And Tectonic Inheritance: Journal of Geophysical Research, v. 102, Bll, p. 24,669-24,696.

Schmitz, M.D., Southwick, D.L., Bowring, S.A., Boerboom, T.R., and Wirth, K.R., 2006, High-precision UPb geochronology in the Minnesota River Valley subprovince and its bearing on the Neoarchean to Paleoproterozoic evolution of the southern Superior Province: Geol. Soc. Am. Bull. v. 118, p. 82–93.

Schmitz, M.D., and Schoene, B., 2007, Derivation of isotope ratios, errors and error correlations for U-Pb geochronology using 205Pb-235U-(233U)-spiked isotope dilution thermal ionization mass spectrometric data: Geochemistry, Geophysics, Geosystems (G3) 8, Q08006, doi:10.1029/2006GC001492.

Stacey, J.S., and Kramers, J.D., 1975, Approximation of terrestrial lead isotope evolution by a two-stage model: Earth and Planetary Science Letters, v. 26, p. 207-221.

Steiger, R.H., and Jager, E., 1977, Subcommission on geochronology: convention on the use of decay constants in geo- and cosmochronology: Earth and Planetary Science Letters, v. 36, p. 359-362.

Storey, B.C., Pankhurst, R.J., and Johnson, A.C., 1994, The Grenville province within Antarctica: a test of the SWEAT hypothesis: Journal of the Geological Society, v. 151, p. 1-4.

Storey, B.C., and MacDonald, D.I.M., 1987, Sedimentary rocks of the Ellsworth-Thiel mountains ridge and their regional equivalents: British Antarctic Survey Bulletin, v. 76, pp. 21-49.

Storey, B.C., Dalziel, I.W.D., Garrett, S.W., Grunow, A.M., Pankhurst, R.J., and Vennum, W.R., 1988a, West Antarctica in Gondwanaland: Crustal blocks, reconstruction and breakup processes: Tectonophysics, v. 155, p. 381–390, doi: 10.1016/0040-1951(88)90276-4.

Storey, B.C., Hole, M.J., Pankhurst, R.J., Millar, I.L., and Vennum, W., 1988b, Middle Jurassic within-plate granites in West Antarctica and their bearing on the break-up of Gondwanaland: Journal of the Geological Society, London, v. 145, p. 999–1007.

Stracke A., Bizimis, M., and Salters, V.J.M., 2003, Recycling ocean crust: Quantitative constraints: Geochemistry, Geophysics, Geosystems (G3), v. 4, p. Q8003.

Stracke, A., Hofmann, A.W., and Hart, S.R., 2005, FOZO, HIMU, and the rest of the mantle zoo: Geochemistry, Geophysics, Geosystems (G3), v. 6, p. Q05007.

Vennum, W.R., and Storey, B.C., 1987, "Petrology, geochemistry, and tectonic setting of granitic rocks from the Ellsworth-Whitmore mountains crustal block and Thiel Mountains, West Antarctica; Gondwana Six; Structure, Tectonics, and Geophysics", American Geophysical Union, Geophysical Monograph 40, p. 139-150.

Vervoort, J. D., Wirth, K., Kennedy, B., Sandland, T., and Harpp, K. S., 2007, The magmatic evolution of the Midcontinent Rift: new geochronologic and geochemical evidence from felsic magmatism: Precambrian Res., v. 157, p. 235–268.

Wareham, C.D., Pankhurst, R.J., Thomas, R.J., Storey, B.C., Grantham, G.H., Jacobs, J., and Eglington, B.M., 1998, Pb, Nd, and Sr Isotope Mapping of Grenville - Age Crustal Provinces in Rodinia: Journal of Geology, v. 106, p. 647-660.

Watts, D.R., and Bramall, A.M., 1981, Paleomagnetic evidence for a displaced terrain in western Antarctica: Nature (London), v. 293, no. 5834, p. 638-641.

Webers, G.F., Craddock, C., Rogers, M.A., and Anderson, J.J., 1982, Geology of the Whitmore Mountains: In Antarctic Geoscience, International Union of Geological Sciences, Series B, v. 4, p. 841-847.

Williams, I.S., 1998, U–Th–Pb geochronology by ion microprobe. In: McKibben, M.A., Shanks, W.C. III, Ridley, W.I., (eds.), Applications of Microanalytical Techniques to Understanding Mineralizing Processes: Reviews of Economic Geology, v. 7, p. 1–35.

Wilson, M., 1991, Igneous Petrogenesis: London, Harper Collins Academic.

Workman, R.K., and Hart, S.R., 2005, Major and trace element composition of the depleted MORB mantle (DMM): Earth and Planetary Science Letters, v. 231, p. 53-72.

Workman, R.K., Hart, S.R., Jackson, M., Regelous, M., Farley, K.A., Blusztajn, J., Kurz, M., and Staudigel, H., 2004, Recycled metasomatized lithosphere as the origin of the enriched mantle II (EM2) end-member: Evidence from the Samoan Volcanic Chain: Geochemistry, Geophysics, Geosystems (G3), v. 5, p. Q04008.

Zindler, A., and Hart, S.R., 1986, Chemical dynamics: Annual Review of Earth and Planetary Science, v. 14, p. 493-571.

Table 1: Ellsworth-Whitmore Granite Geochemisty and Radiometric Ages and Isotope Data

Sample ID	Rock ID	XRF[1,2]	K-Ar Age (Ma)[3]	Rb-Sr Age (Ma)[4]	U-Pb SHRIMP Age (Ma)1,8	U-Pb ID-TIMS Age (Ma)[1]	$^{87}Sr/^{86}Sr_t$ [1,4,5]	eNd_t [1,2,5]	T_{DM} (Ga)[1,5,6]	T_{DM}* (Ga)[7]
Pirrit Hills										
various	granite	x		173 ± 3	168 ± 4, 164 ±2		0.7070 ± 16	-4.7 to -7.8		1.37 to 1.59
60-8	granite	x				174.01 ± 0.14	0.7096	-4.32	3.16	1.33
60-8-17	granite		176 ± 6							
60-8-27	granite					174.06 ± 0.16	0.7178	-4.36	2.58	1.34
Nash-Martin Hills										
various	granite			175 ± 8			0.7122 ± 8	-4.5 to -5.0	1.3 to 3.5	1.35 to 1.38
63-C-63	granite	x	172 ± 6			177.38 ± 0.12	0.7140	-4.29	1.42	1.33
63-C-67	Porph. andesite	x	174 ± 6			177.46 ± 0.05	0.7144	-5.63	1.65	1.43
63-C-68	granite	x	175 ± 5			177.42 ± 0.09	0.7179	-4.43	1.43	1.34
63-C-69	granite	x				177.49 ± 0.11	0.7170	-4.72	1.43	1.37
63-C-76	granite	x	166 ± 8							
63-C-77	granite	x	163 ± 4							
63-C-80	granite	x	167 ± 5							
Linck Nunataks										
various	granite			176 ± 5	180 ± 4		0.7232 ± 8	-6.9	1.68	1.53
65-W-80	granite	x				174.8 2± 0.26	0.7168	-5.13	1.73	1.21
Pagano Nunatak										
various	granite, aplite			175 ± 8	174 ± 4		0.7157 ± 14	-5.0 to -5.9	1.42 to 1.52	1.39 to 1.45
PRR-7184	aplite	x				174.62 ± 0.16	0.7163	-4.94	1.89	1.38
PRR-7186	granite									
PRR-7187	aplite									
PRR-7188	granite									
Whitmore Mtns (Mt Seelig)										
various	granite			203 ± 8	200 ± 4		0.7068 ± 7	-12, -1.5		1.9, 1.1
65-W-4	granite	x	174 ± 4							
65-W-14	granite	x								
65-W-25	granite	x								
65-W-44	granite-gneiss					207.96 ± 0.06	0.7094	-2.38	1.86	
65-W-45	granite		190 ± 8							
65-W-76	granite		176 ± 5							
Lewis Nunatak										
various	dolerite	x		(183)			0.7104-0.7112	-5.2	1.53	1.4

Data Sources:

1. this study; 2. Storey et al. (1988b); 3. Craddock (1972); 4. Millar & Pankhurst (1987); 5. Pankhurst et al. (1991, summarized)

NB: 6. Nd model age according to DePaolo (1981); 7. according to DePaolo et al. (1991); 8. Lee et al. (2012)

Table 2. U-Pb Isotopic Data, Ellsworth-Whitmore Granites

							Radiogenic Isotope Ratios								Radiogenic Isotope Dates					
Grain	Th/U	^{206}Pb* x10^{-13} mol	mol % ^{206}Pb*	Pb*/Pbc	Pbc (pg)	^{206}Pb/^{204}Pb	^{208}Pb/^{206}Pb	^{207}Pb/^{206}Pb	% err	^{207}Pb/^{235}U	% err	^{206}Pb/^{238}U	% err	corr. coef.	^{207}Pb/^{206}Pb	±	^{207}Pb/^{235}U	±	^{206}Pb/^{238}U	±
(a)	(b)	(c)	(c)	(c)	(c)	(d)	(e)	(e)	(f)	(e)	(f)	(e)	(f)		(g)	(f)	(g)	(f)	(g)	(f)
60-8-27 Pirrit Hills																				
z1	0.674	1.4889	99.13%	36	1.07	2118	0.221	0.053095	0.389	0.281727	0.435	0.038484	0.086	0.606	332.8	8.8	252.0	1.0	243.43	0.21
z6	0.589	3.8818	99.87%	235	0.42	13963	0.189	0.049947	0.101	0.192609	0.160	0.027968	0.080	0.855	192.5	2.3	178.9	0.3	177.82	0.14
z4	0.387	2.0039	99.69%	93	0.52	5828	0.123	0.049642	0.182	0.188441	0.228	0.027531	0.077	0.705	178.3	4.3	175.3	0.4	175.08	0.13
z7	0.532	1.7321	99.21%	38	1.14	2312	0.169	0.049451	0.451	0.187262	0.484	0.027465	0.096	0.428	169.3	10.5	174.3	0.8	174.66	0.17
z8	0.717	0.9289	98.03%	16	1.54	933	0.229	0.049602	0.691	0.187332	0.744	0.027392	0.094	0.612	176.4	16.1	174.4	1.2	**174.20**	**0.16**
z2	0.439	4.0532	99.75%	121	0.83	7451	0.140	0.049647	0.141	0.187266	0.192	0.027357	0.080	0.759	178.5	3.3	174.3	0.3	**173.98**	**0.14**
z3	0.506	3.8065	99.72%	109	0.87	6631	0.161	0.049615	0.153	0.187126	0.205	0.027354	0.086	0.732	177.0	3.6	174.2	0.3	**173.97**	**0.15**
z5	0.407	16.4310	99.95%	543	0.74	33806	0.130	0.049670	0.069	0.187287	0.135	0.027347	0.076	0.935	179.6	1.6	174.3	0.2	**173.92**	**0.13**
60-8 Pirrit Hills																				
z1	0.584	1.9271	99.43%	55	0.90	3244	0.189	0.050584	0.291	0.198195	0.332	0.028417	0.074	0.640	221.9	6.7	183.6	0.6	180.63	0.13
z5	0.774	0.6083	99.21%	41	0.40	2310	0.247	0.049639	0.430	0.188453	0.477	0.027534	0.080	0.638	178.1	10.0	175.3	0.8	175.10	0.14
z4	0.755	2.1882	99.68%	101	0.58	5740	0.240	0.049448	0.179	0.186656	0.257	0.027377	0.143	0.739	169.1	4.2	173.8	0.4	**174.11**	**0.25**
z2	0.781	1.0195	98.49%	21	1.29	1218	0.249	0.049679	0.600	0.187430	0.679	0.027363	0.205	0.513	180.0	14.0	174.4	1.1	**174.02**	**0.35**
z7	0.751	2.3188	99.48%	61	1.00	3516	0.239	0.049436	0.344	0.186498	0.376	0.027361	0.088	0.466	168.5	8.0	173.6	0.6	**174.01**	**0.15**
z6	0.522	21.0677	99.93%	453	1.17	27357	0.166	0.049548	0.080	0.186809	0.138	0.027345	0.073	0.898	173.8	1.9	173.9	0.2	**173.91**	**0.13**
z8	0.666	0.4087	97.27%	11	0.94	673	0.211	0.049279	1.574	0.185592	1.665	0.027315	0.172	0.565	161.1	36.8	172.9	2.6	**173.72**	**0.30**
63-C-69 Nash Hills																				
z4	0.476	4.9423	99.83%	178	0.69	10905	0.152	0.049654	0.120	0.191125	0.172	0.027916	0.076	0.804	178.84	2.8	177.59	0.28	**177.49**	**0.13**
z1	0.362	4.4091	99.77%	128	0.83	8091	0.115	0.049611	0.134	0.190944	0.184	0.027914	0.076	0.774	176.82	3.1	177.43	0.30	**177.48**	**0.13**
z3	0.645	2.3349	99.83%	186	0.32	10896	0.205	0.049590	0.118	0.190784	0.171	0.027903	0.073	0.825	175.83	2.8	177.30	0.28	**177.41**	**0.13**
z2	0.658	1.5463	99.18%	38	1.06	2226	0.210	0.049666	0.395	0.191017	0.438	0.027894	0.075	0.629	179.41	9.2	177.50	0.71	**177.35**	**0.13**
63-C-67 Nash Hills																				
z3	0.573	5.5704	99.72%	109	1.30	6496	0.182	0.049601	0.132	0.190907	0.182	0.027914	0.074	0.785	176.35	3.1	177.40	0.30	**177.48**	**0.13**
z2	0.416	3.4366	99.59%	72	1.17	4482	0.132	0.049632	0.192	0.190943	0.236	0.027903	0.074	0.693	177.78	4.5	177.43	0.38	**177.41**	**0.13**
z1	0.470	3.3850	99.44%	54	1.57	3295	0.150	0.049711	0.196	0.191206	0.249	0.027896	0.099	0.679	181.50	4.6	177.66	0.41	**177.37**	**0.17**
z4	0.411	8.0976	99.93%	395	0.50	24584	0.131	0.049630	0.075	0.190884	0.136	0.027895	0.071	0.930	177.70	1.8	177.38	0.22	**177.36**	**0.12**
z5	0.303	14.9591	99.95%	629	0.56	40293	0.096	0.049648	0.068	0.190928	0.145	0.027891	0.093	0.926	178.57	1.6	177.42	0.24	**177.33**	**0.16**
63-C-68 Nash Hills																				
z1	0.207	2.7947	99.03%	30	2.26	1891	0.106	0.089218	0.143	0.489736	0.206	0.039812	0.096	0.793	1408.8	42.7	404.73	0.69	251.66	0.24
z4	0.562	2.9851	99.67%	94	0.80	5641	0.179	0.049619	0.188	0.190989	0.233	0.027917	0.077	0.693	177.17	4.4	177.47	0.38	**177.50**	**0.14**
z5	0.422	3.4559	99.76%	121	0.70	7495	0.134	0.049590	0.148	0.190769	0.197	0.027901	0.076	0.751	175.81	3.5	177.28	0.32	**177.40**	**0.13**
z2	0.530	0.9500	98.74%	24	1.00	1453	0.168	0.049543	0.651	0.190562	0.709	0.027897	0.115	0.567	173.61	15.2	177.11	1.15	**177.37**	**0.20**
z3	0.529	2.2210	99.80%	156	0.36	9388	0.168	0.049605	0.127	0.190787	0.178	0.027895	0.073	0.804	176.51	3.0	177.30	0.29	**177.36**	**0.13**
z6	0.515	3.7718	99.84%	193	0.49	11670	0.164	0.049639	0.105	0.190834	0.160	0.027882	0.073	0.851	178.14	2.4	177.34	0.26	**177.28**	**0.13**
z7	0.762	1.2258	99.54%	70	0.47	3999	0.242	0.049535	0.258	0.190419	0.302	0.027880	0.074	0.672	173.24	6.0	176.99	0.49	**177.27**	**0.13**
63-C-63 Nash Hills																				
z2	0.022	10.6650	99.88%	217	1.07	15079	0.007	0.050294	0.086	0.226113	0.145	0.032607	0.073	0.893	208.61	2.0	206.98	0.27	206.84	0.15
z1	0.497	4.1458	99.65%	87	1.18	5319	0.160	0.050271	0.161	0.197758	0.206	0.028531	0.070	0.743	207.53	3.7	183.23	0.34	181.35	0.12

z7	0.388	9.8526	99.88%	236	1.01	14810	0.123	0.049556	0.091	0.190868	0.148	0.027934	0.074	0.877	174.24	2.1	177.37	0.24	177.60	0.13
z8	0.390	8.0758	99.89%	263	0.74	16444	0.124	0.049518	0.088	0.190494	0.146	0.027901	0.072	0.888	172.44	2.1	177.05	0.24	**177.40**	**0.13**
z6	0.517	2.7256	99.79%	144	0.47	8706	0.164	0.049601	0.132	0.190744	0.224	0.027891	0.150	0.823	176.35	3.1	177.26	0.37	**177.33**	**0.26**
z3	0.494	2.6219	98.97%	29	2.24	1793	0.157	0.049690	0.247	0.191021	0.290	0.027881	0.076	0.664	180.52	5.7	177.50	0.47	**177.27**	**0.13**
z5	0.443	2.9230	99.75%	121	0.59	7468	0.141	0.049580	0.166	0.190578	0.213	0.027878	0.078	0.719	175.33	3.9	177.12	0.35	**177.26**	**0.14**
65-W-44 Whitmore Mountains																				
z2	0.143	2.0745	99.35%	42	1.11	2843	0.046	0.055916	0.283	0.468348	0.345	0.060748	0.137	0.614	449.0	6.3	390.0	1.1	380.17	0.51
z4	0.388	5.2580	99.91%	316	0.40	19753	0.123	0.050304	0.084	0.228113	0.144	0.032889	0.073	0.904	209.1	1.9	208.6	0.3	208.60	0.15
z8	0.332	1.7906	99.77%	126	0.34	8013	0.106	0.050266	0.160	0.227361	0.206	0.032805	0.073	0.739	207.3	3.7	208.0	0.4	**208.08**	**0.15**
z6	0.259	4.5630	99.79%	138	0.77	8950	0.082	0.050206	0.131	0.226971	0.181	0.032788	0.074	0.784	204.5	3.0	207.7	0.3	**207.97**	**0.15**
z7	0.321	2.4119	99.79%	136	0.42	8676	0.102	0.050297	0.132	0.227261	0.182	0.032770	0.070	0.810	208.8	3.1	207.9	0.3	**207.86**	**0.14**
z5	0.254	3.3239	99.89%	248	0.31	16117	0.081	0.050244	0.094	0.226996	0.151	0.032766	0.072	0.882	206.3	2.2	207.7	0.3	**207.84**	**0.15**
z3	0.337	2.6377	99.57%	67	0.94	4258	0.107	0.050247	0.243	0.227002	0.287	0.032766	0.084	0.631	206.4	5.6	207.7	0.5	**207.84**	**0.17**
65-W-80 Linck Nunatak																				
z8	0.514	0.4489	98.21%	17	0.68	1023	0.169	0.051728	0.909	0.215532	0.977	0.030219	0.106	0.670	273.41	20.84	198.18	1.76	191.92	0.20
z6	0.448	0.6938	99.42%	51	0.34	3148	0.143	0.049688	0.360	0.192691	0.407	0.028126	0.090	0.600	180.42	8.38	178.92	0.67	178.81	0.16
z5	0.518	0.9429	99.36%	47	0.50	2876	0.165	0.049622	0.421	0.188117	0.467	0.027495	0.083	0.608	177.33	9.82	175.02	0.75	**174.85**	**0.14**
z10	0.399	0.3438	98.42%	18	0.45	1163	0.127	0.049524	0.850	0.187618	0.917	0.027476	0.099	0.710	172.70	19.82	174.59	1.47	**174.73**	**0.17**
z7	0.535	1.0836	98.61%	22	1.26	1318	0.170	0.049567	0.632	0.187701	0.677	0.027464	0.099	0.515	174.76	14.74	174.67	1.09	**174.66**	**0.17**
Pagano Nunatak																				
z5	0.402	0.5704	98.54%	20	0.70	1258	0.126	0.048638	0.748	0.184175	0.809	0.027463	0.088	0.725	130.4	17.6	171.6	1.3	**174.65**	**0.15**
z3	0.526	0.2339	98.92%	28	0.21	1702	0.168	0.049610	0.567	0.187781	0.624	0.027453	0.098	0.634	176.7	13.2	174.7	1.0	**174.59**	**0.17**
z8	0.381	0.3913	97.26%	10	0.91	670	0.121	0.049443	1.469	0.187126	1.563	0.027449	0.140	0.697	168.9	34.3	174.2	2.5	**174.56**	**0.24**
z7	0.474	0.2964	97.56%	12	0.61	751	0.150	0.049435	1.321	0.186948	1.406	0.027428	0.132	0.675	168.5	30.8	174.0	2.2	**174.43**	**0.23**
z4	0.361	0.3193	97.64%	12	0.64	778	0.114	0.049129	1.231	0.185135	1.320	0.027331	0.120	0.762	154.0	28.8	172.5	2.1	173.82	0.21

Notes:

(a) z1, z2, etc. are labels for individual analyzed zircon grains treated by annealing and chemical abrasion [*Mattinson*, 2005]; bold labels denote analyses used in the weighted mean age calculations.

(b) Model Th/U ratio calculated from radiogenic $^{208}Pb/^{206}Pb$ ratio and $^{207}Pb/^{235}U$ date.

(c) Pb* and Pbc are radiogenic and common Pb, respectively. mol % $^{206}Pb*$ is with respect to radiogenic, blank and initial common Pb.

(d) Measured ratio corrected for spike contribution and instrumental fractionation only. Fractionation correction is 0.18 ± 0.03 (1σ) %/atomic mass unit, based on analysis of NBS-981 and NBS-982.

(e) Ratios corrected for fractionation, spike contribution, common Pb, and initial disequilibrium in $^{230}Th/^{238}U$. All common Pb is assigned to procedural blank with a composition of $^{206}Pb/^{204}Pb$ = 18.60 ± 0.80%; $^{207}Pb/^{204}Pb$ = 15.69 ± 0.32%; $^{208}Pb/^{204}Pb$ = 38.51 ± 0.74% (1σ). $^{206}Pb/^{238}U$ and $^{207}Pb/^{206}Pb$ ratios and dates are corrected for initial disequilibrium in $^{230}Th/^{238}U$ using a melt Th/U = 3.

(f) Errors are 2σ, propagated using algorithms of [*Schmitz and Schoene*, 2007].

(g) Calculations based on the decay constants of [*Jaffey et al.*, 1971].

Table 3: Summary of SHRIMP U-Pb zircon results for Ellsworth-Whitmore granites

Grain. spot	U (ppm)	Th (ppm)	Th/U	$^{206}Pb^*$ (ppm)	$^{204}Pb/^{206}Pb$	f_{206} %	Total $^{238}U/^{206}Pb$	±	Total $^{207}Pb/^{206}Pb$	±	Radiogenic $^{206}Pb/^{238}U$	±	Age (Ma) $^{206}Pb/^{238}U$	±
R.2243.4 Pirrit Hills (81°15'S, 85°24'W)														
*1.1	125	130	1.04	3	-	0.42	38.963	0.653	0.0526	0.0018	0.0256	0.0004	162.7	2.7
*2.1	671	43	0.06	44	0.00004	0.47	13.114	0.216	0.0603	0.0008	0.0759	0.0013	471.6	7.6
2.2	281	183	0.65	6	-	0.06	37.528	0.496	0.0499	0.0011	0.0266	0.0004	169.4	2.2
3.1	1647	668	0.41	38	0.00025	0.59	37.138	0.426	0.0541	0.0005	0.0268	0.0003	170.3	1.9
*4.1	335	73	0.22	27	0.00020	0.01	10.648	0.453	0.0594	0.0027	0.0939	0.0041	578.6	24.1
5.1	947	478	0.51	22	0.00054	1.24	36.846	0.425	0.0594	0.0007	0.0268	0.0003	170.5	2.0
6.1	911	616	0.68	21	0.00070	1.01	37.313	0.428	0.0575	0.0010	0.0265	0.0003	168.8	1.9
7.1	1063	652	0.61	25	0.00007	0.08	36.734	0.407	0.0502	0.0006	0.0272	0.0003	173.0	1.9
8.1	591	260	0.44	13	0.00024	0.52	38.373	0.443	0.0535	0.0010	0.0259	0.0003	165.0	1.9
*9.1	694	206	0.30	79	0.00323	9.35	7.525	0.107	0.1408	0.0110	0.1205	0.0025	733.2	14.6
*10.1	159	153	0.96	12	0.00010	1.78	11.551	0.181	0.0724	0.0011	0.0850	0.0014	526.1	8.1
11.1	89	73	0.83	2	-	0.34	37.382	0.663	0.0522	0.0020	0.0267	0.0005	169.6	3.0
12.1	100	116	1.16	2	0.00104	1.65	37.791	0.640	0.0626	0.0021	0.0260	0.0004	165.6	2.8
13.1	1620	526	0.32	37	0.00009	0.27	37.412	0.399	0.0516	0.0005	0.0267	0.0003	169.6	1.8
*14.1	8781	402	0.05	216	0.00007	0.19	34.970	0.368	0.0512	0.0002	0.0285	0.0003	181.4	1.9
15.1	457	367	0.80	10	0.00001	0.34	38.185	0.457	0.0521	0.0009	0.0261	0.0003	166.1	2.0
16.1	815	512	0.63	19	0.00176	2.85	36.387	0.403	0.0722	0.0007	0.0267	0.0003	169.9	1.9
*17.1	149	136	0.91	23	0.03742	72.49	5.462	0.230	0.6400	0.0034	0.0504	0.0034	316.7	20.6
*18.1	226	161	0.71	29	0.00018	1.04	6.607	0.076	0.0777	0.0006	0.1498	0.0018	899.8	10.0
*18.2	1105	315	0.29	26	0.00019	0.47	36.595	0.406	0.0533	0.0006	0.0272	0.0003	173.0	1.9
19.1	343	201	0.59	8	0.00002	0.28	37.518	0.468	0.0516	0.0010	0.0266	0.0003	169.1	2.1
*20.1	332	122	0.37	17	0.00009	0.27	16.991	0.231	0.0561	0.0007	0.0587	0.0008	367.7	4.9
20.2	571	396	0.69	13	0.00018	0.32	38.175	0.457	0.0519	0.0008	0.0261	0.0003	166.2	2.0
21.1	108	123	1.14	3	0.00407	5.17	36.307	0.633	0.0906	0.0026	0.0261	0.0005	166.2	2.9
*22.1	777	248	0.32	26	0.00031	0.85	25.675	0.309	0.0579	0.0006	0.0386	0.0005	244.3	2.9
*23.1	326	127	0.39	30	0.00004	1.93	9.197	0.152	0.0773	0.0073	0.1066	0.0021	653.1	12.0
23.2	658	424	0.64	15	0.00045	0.50	37.974	0.663	0.0534	0.0007	0.0262	0.0005	166.7	2.9
**24.1	664	360	0.54	15	0.00030	0.05	38.336	0.430	0.0497	0.0006	0.0261	0.0003	165.9	1.9
	** Analysed on SHRIMP RG					**Weighted mean Age**		**168.4**	**± 3.6**		**MSWD= 1.3**			
R.2246.2 Linck Nunatak (82°41'S, 104°12'W)														
1.1	1263	550	0.44	31	0.00008	0.12	34.972	0.381	0.0507	0.0005	0.0286	0.0003	182	2
1.2	1559	880	0.56	39	0.00046	0.78	34.767	0.368	0.0560	0.0005	0.0285	0.0003	181	2
2.1	178	138	0.78	4	0.00082	0.99	35.241	0.495	0.0575	0.0014	0.0281	0.0004	179	3
*3.1	4717	971	0.21	198	0.00122	2.49	20.516	0.209	0.0723	0.0016	0.0475	0.0005	299	3
*4.1	195	61	0.31	29	0.00006	0.10	5.694	0.067	0.0751	0.0008	0.1754	0.0021	1042	11
*5.1	4876	206	0.04	150	0.00214	4.58	27.927	0.303	0.0871	0.0011	0.0342	0.0004	217	2
*6.1	1473	117	0.08	47	0.00003	0.20	27.108	0.286	0.0525	0.0004	0.0368	0.0004	233	2
*7.1	1173	489	0.42	34	0.00066	1.37	29.547	0.317	0.0613	0.0005	0.0334	0.0004	212	2
*8.1	625	248	0.40	19	0.00075	1.53	28.443	0.322	0.0627	0.0015	0.0346	0.0004	219	2
*9.1	2331	408	0.17	81	0.00287	4.96	24.678	0.259	0.0907	0.0029	0.0385	0.0004	244	3
*10.1	544	192	0.35	31	0.00014	0.60	14.857	0.167	0.0600	0.0006	0.0669	0.0008	417	5
*11.1	764	158	0.21	64	0.00003	0.46	10.270	0.118	0.0636	0.0004	0.0969	0.0011	596	7
*12.1	237	206	0.87	14	0.00709	12.89	14.133	0.227	0.1584	0.0128	0.0616	0.0015	386	9
*13.1	788	629	0.80	49	0.00010	0.41	13.959	0.150	0.0591	0.0004	0.0713	0.0008	444	5
*14.1	1136	170	0.15	152	0.00009	0.15	6.420	0.067	0.0768	0.0003	0.1555	0.0016	932	9
15.1	657	258	0.39	16	0.00082	1.48	35.376	0.406	0.0614	0.0022	0.0278	0.0003	177	2
*16.1	390	140	0.36	27	0.00048	1.31	12.414	0.143	0.0676	0.0014	0.0795	0.0009	493	6
*17.1	70	70	1.00	11	0.00049	0.83	5.670	0.082	0.0921	0.0019	0.1749	0.0026	1039	14
*18.1	13730	1827	0.13	428	0.00069	1.30	27.539	0.279	0.0611	0.0002	0.0358	0.0004	227	2
*19.1	239	110	0.46	19	0.00060	2.38	10.851	0.162	0.0781	0.0012	0.0900	0.0014	555	8
						Weighted mean Age		**179.9**	**± 4.1 Ma**		**MSWD= 1.1**			
R.2215.4 Pagano nunatak (83°41'24"S, 87°37'0"W)														
*1.1	979	246	0.25	80	0.00003	0.21	10.453	0.109	0.0613	0.0003	0.0955	0.0010	587.8	6.0
2.1	126	100	0.80	3	0.00020	0.33	35.918	0.558	0.0522	0.0016	0.0277	0.0004	176.4	2.7
3.1	92	65	0.71	2	0.00069	0.86	36.946	0.640	0.0563	0.0021	0.0268	0.0005	170.7	3.0

4.1	136	102	0.75	3	-	0.62	37.473	0.840	0.0544	0.0018	0.0265	0.0006	168.7	3.8
5.1	307	166	0.54	7	0.00009	0.24	36.507	0.463	0.0514	0.0010	0.0273	0.0003	173.8	2.2
6.1	240	160	0.67	6	0.00015	0.23	37.171	0.494	0.0513	0.0012	0.0268	0.0004	170.7	2.3
7.1	225	132	0.59	5	-	<0.01	36.432	0.492	0.0493	0.0012	0.0275	0.0004	174.6	2.4
8.1	138	130	0.94	3	0.00065	0.25	36.744	0.834	0.0516	0.0015	0.0271	0.0006	172.7	3.9
9.1	600	93	0.15	14	0.00030	0.26	36.002	0.424	0.0517	0.0007	0.0277	0.0003	176.2	2.1
10.1	300	145	0.48	7	0.00042	0.83	36.043	0.460	0.0562	0.0011	0.0275	0.0004	175.0	2.2
*11.1	1519	171	0.11	88	0.00049	1.43	14.750	0.154	0.0667	0.0003	0.0668	0.0007	417.0	4.3
*12.1	278	150	0.54	6	0.00029	0.65	39.119	0.539	0.0545	0.0013	0.0254	0.0004	161.7	2.2
*13.1	2594	1260	0.49	61	0.00220	4.60	36.564	0.380	0.0860	0.0004	0.0261	0.0003	166.0	1.7
14.1	134	99	0.74	3	0.00082	1.14	37.616	0.579	0.0585	0.0017	0.0263	0.0004	167.2	2.6
15.1	110	69	0.63	3	0.00287	5.34	34.751	0.565	0.0921	0.0060	0.0272	0.0005	173.3	3.1
16.1	1898	324	0.17	48	0.00303	5.63	34.023	0.358	0.0945	0.0011	0.0277	0.0003	176.4	1.9
17.1	176	59	0.34	4	0.00080	0.49	36.740	0.821	0.0534	0.0015	0.0271	0.0006	172.3	3.8
					Weighted mean Age			**173.6**	**± 3.9 Ma**		**MSWD= 1.3**			
R.2226.1 Mount Seelig														
*1.1	555	208	0.38	15	0.00030	0.38	35.921	0.479	0.0528	0.0012	0.0277	0.0004	176.3	2.3
*2.1	405	186	0.46	12	0.00038	0.89	34.119	0.453	0.0569	0.0015	0.0291	0.0004	184.6	2.4
2.2	5618	98	0.02	190	0.00005	0.17	31.641	0.329	0.0512	0.0005	0.0316	0.0003	200.3	2.1
3.1	108	47	0.43	4	0.00040	1.09	30.721	0.640	0.0590	0.0018	0.0322	0.0007	204.3	4.2
3.2	227	93	0.41	9	0.00287	4.74	28.748	0.533	0.0876	0.0022	0.0331	0.0006	210.2	3.9
*4.1	441	234	0.53	13	0.00034	0.14	34.787	0.540	0.0509	0.0012	0.0287	0.0005	182.4	2.8
5.1	86	64	0.74	3	0.00102	1.64	31.084	1.394	0.0634	0.0024	0.0316	0.0014	200.8	8.9
5.2	468	223	0.48	18	0.00190	1.81	30.622	0.445	0.0643	0.0016	0.0321	0.0005	203.5	2.9
*6.1	376	161	0.43	11	0.00031	0.53	34.084	0.514	0.0540	0.0010	0.0292	0.0004	185.4	2.8
*7.1	383	185	0.48	12	0.00034	0.55	33.313	0.448	0.0544	0.0009	0.0299	0.0004	189.6	2.5
*8.1	177	140	0.79	6	0.00054	1.41	34.074	1.006	0.0610	0.0024	0.0289	0.0009	183.9	5.4
9.1	160	77	0.48	5	0.00039	0.74	31.720	0.692	0.0563	0.0018	0.0313	0.0007	198.6	4.3
10.1	100	35	0.35	3	0.00133	2.19	32.035	0.664	0.0675	0.0024	0.0305	0.0006	193.9	4.0
11.1	114	63	0.55	4	0.00058	0.45	30.411	0.708	0.0539	0.0023	0.0327	0.0008	207.7	4.8
*12.1	1794	132	0.07	43	0.00005	0.04	38.775	0.473	0.0501	0.0005	0.0258	0.0003	164.1	2.0
*13.1	424	121	0.29	13	-	0.29	33.152	0.502	0.0523	0.0009	0.0301	0.0005	191.0	2.9
14.1	118	59	0.50	4	0.00117	2.07	31.692	0.782	0.0665	0.0024	0.0309	0.0008	196.2	4.8
*15.1	138	70	0.51	4	0.00055	1.48	33.108	0.638	0.0618	0.0017	0.0298	0.0006	189.0	3.6
16.1	105	40	0.39	3	0.00079	1.09	32.279	0.715	0.0587	0.0028	0.0306	0.0007	194.6	4.3
17.1	65	47	0.72	2	0.00019	2.96	30.502	0.795	0.0740	0.0036	0.0318	0.0008	201.9	5.3
*18.1	286	124	0.43	9	0.00059	0.77	33.051	0.519	0.0562	0.0014	0.0300	0.0005	190.7	3.0
*18.2	417	205	0.49	15	0.00079	1.62	32.686	0.458	0.0628	0.0013	0.0301	0.0004	191.2	2.7
*19.1	459	200	0.44	13	0.00031	0.51	35.668	0.468	0.0538	0.0011	0.0279	0.0004	177.4	2.3
20.1	132	69	0.53	4	0.00038	1.43	31.907	0.837	0.0614	0.0025	0.0309	0.0008	196.1	5.1
21.1	297	212	0.71	10	0.00052	0.72	32.371	0.523	0.0557	0.0015	0.0307	0.0005	194.7	3.1
21.2	566	202	0.36	21	0.00047	0.58	31.062	0.426	0.0545	0.0014	0.0320	0.0004	203.1	2.8
*22.1	60	40	0.67	2	0.00083	3.33	32.660	1.094	0.0765	0.0030	0.0296	0.0010	188.1	6.3
23.1	251	89	0.36	8	0.00052	0.69	31.659	0.558	0.0558	0.0011	0.0314	0.0006	199.1	3.5
*24.1	437	195	0.45	13	0.00045	0.95	34.856	0.510	0.0573	0.0009	0.0284	0.0004	180.6	2.6
*25.1	379	181	0.48	12	0.00034	0.72	33.269	0.445	0.0558	0.0015	0.0298	0.0004	189.6	2.5
*26.1	388	187	0.48	12	0.00072	0.41	33.015	0.423	0.0532	0.0009	0.0302	0.0004	191.6	2.4
27.2	638	299	0.47	24	0.00057	0.70	31.924	0.403	0.0554	0.0008	0.0311	0.0004	197.5	2.5
28.1	331	165	0.50	13	0.00130	1.92	31.607	0.465	0.0652	0.0013	0.0310	0.0005	197.0	2.9
*29.1	433	212	0.49	16	0.00077	1.38	32.882	0.543	0.0609	0.0016	0.0300	0.0005	190.5	3.1
30.1	422	199	0.47	16	0.00112	1.51	30.782	0.489	0.0619	0.0012	0.0320	0.0005	203.0	3.2
31.1	387	146	0.38	15	0.00109	1.61	30.883	0.439	0.0627	0.0014	0.0319	0.0005	202.2	2.9
32.1	635	266	0.42	24	0.00054	1.02	31.530	0.474	0.0580	0.0008	0.0314	0.0005	199.3	3.0
33.1	360	171	0.48	14	0.00182	2.57	30.682	0.514	0.0703	0.0016	0.0318	0.0005	201.5	3.4
34.1	322	170	0.53	13	0.00169	3.29	30.563	0.481	0.0761	0.0018	0.0316	0.0005	200.8	3.2
	All analysed on SHRIMP I				**Weighted mean Age**			**200.2**	**± 4.3 Ma**		**MSWD= 1.2**			

Notes :
1. Uncertainties on each analysis given at the 1σ level
2. f_{206} % denotes the percentage of ^{206}Pb that is common Pb.
3. Correction for common Pb made using the measured $^{238}U/^{206}Pb$ and $^{207}Pb/^{206}Pb$ ratios following Tera and Wasserburg (1972) as outlined in Williams (1998).
4. Error in SL13 reference zircon calibration was 0.38% for the analytical session
5. a further 1% uncertainty has been allowed (see text)
6. *indicates data not included in age calculation due to assumed Pb-loss or inheritance
7. Uncertainties on calclulated ages are 95% C.L. including calibration errors

Table 4: EWT Granite XRF Data

Un-normalized major element data

Sample	60-8	60-8-27	60-H-57	63-C-63	63-C-67	63-C-68	63-C-69	65-W-44	65-W-80	PAGANO
	Pirrit Hills	Pirrit Hills	Nash Hills	Nash Hills	Nash Hills	Nash Hills	Nash Hills	Nash Hills	Whitmore	Nunatak
SiO2	71.48	63.14	76.77	71.82	73.36	70.41	69.71	65.97	73.91	75.02
TiO2	0.18	0.17	0.07	0.46	0.28	0.47	0.19	0.76	0.27	0.12
Al2O3	14.93	18.3	13.91	13.82	13.71	14.38	15.61	15.35	13.9	13.45
Fe2O3t	1.67	2.57	0.63	2.94	1.92	3.03	1.69	5.09	1.97	1.17
MnO	0.08	1.9	0.05	0.04	0.03	0.04	0.02	0.06	0.04	0.03
MgO	0.17	0.11	0.11	0.78	0.49	0.85	0.17	1	0.4	0.18
CaO	0.88	0.24	0.4	1.36	0.74	1.73	0.3	2.7	1.06	0.49
Na2O	3.61	3.31	3.75	3.08	2.81	3.26	5.63	3.32	3.09	3.55
K2O	6.77	9.96	3.08	5.12	4.95	4.84	4.91	4.91	5.11	4.91
P2O5	0.04	0.04	0.18	0.17	0.26	0.2	0.16	0.26	0.25	0.23
LOI	0.13	1.3	1.01	0.4	1.21	0.72	1.06	0.66	0.72	0.71
Total	***99.81***	***99.74***	***98.95***	***99.59***	***98.55***	***99.21***	***98.39***	***99.42***	***100.0***	***99.15***

Normalized major element data

Sample	60-8	60-8-27	60-H-57	63-C-63	63-C-67	63-C-68	63-C-69	65-W-44	65-W-80	PAGANO
	Pirrit Hills	Pirrit Hills	Nash Hills	Nash Hills	Nash Hills	Nash Hills	Nash Hills	Nash Hills	Whitmore	Nunatak
SiO2	71.62	63.30	77.58	72.12	74.44	70.97	70.85	66.35	73.91	75.66
TiO2	0.18	0.17	0.07	0.46	0.28	0.47	0.19	0.76	0.27	0.12
Al2O3	14.96	18.35	14.06	13.88	13.91	14.49	15.87	15.44	13.90	13.57
Fe2O3t	1.67	2.58	0.64	2.95	1.95	3.05	1.72	5.12	1.97	1.18
MnO	0.08	1.90	0.05	0.04	0.03	0.04	0.02	0.06	0.04	0.03
MgO	0.17	0.11	0.11	0.78	0.50	0.86	0.17	1.01	0.40	0.18
CaO	0.88	0.24	0.40	1.37	0.75	1.74	0.30	2.72	1.06	0.49
Na2O	3.62	3.32	3.79	3.09	2.85	3.29	5.72	3.34	3.09	3.58
K2O	6.78	9.99	3.11	5.14	5.02	4.88	4.99	4.94	5.11	4.95
P2O5	0.04	0.04	0.18	0.17	0.26	0.20	0.16	0.26	0.25	0.23
LOI	0.13	1.3	1.01	0.4	1.21	0.72	1.06	0.66	0.72	0.71

Trace element data

Sample	60-8	60-8-27	60-H-57	63-C-63	63-C-67	63-C-68	63-C-69	65-W-44	65-W-80	PAGANO
Sc	13.6	9.65	6.75	6.9	3.7	6.9	3.7	7.5	5.15	3.65
V	9.8	6.1	4.55	41.75	22	44.35	15.4	54.1	17.85	9.6
Cr	5.6	3.3	4.6	16.15	10.15	17.75	9.25	8.3	7.25	8.3
Co	2.6	3.7	1.6	4.95	4.55	4.35	2.85	10.05	4.6	2.3
Ni	0.7	1000	0.1	7.25	3.9	7.65	5.75	5.45	5.55	3.4
Zn	28.5	128.3	25.1	65.7	58.15	66.9	178.25	106.5	53.65	23.8
Ga	20.8	27.05	22.2	21.9	22.5	23.7	26.25	26.6	19.35	22.4
Rb	496.5	764.75	527.6	321.35	350.45	322.9	232.3	223.65	330.65	399.8
Sr	85.95	186.4	19.25	97.9	65.55	123.1	77	194.1	77.8	41.8
Y	106.5	111.45	7.95	40.4	23.05	40	11.25	71.45	28.75	12.8
Zr	130.75	119.4	17.65	220.2	130.65	228.5	74.65	324.65	111.25	47.35
Nb	62.8	59.3	19	19.95	17.45	21.35	20.75	43	21.8	22.85
Ba	175.55	477.25	75.45	527.65	286.25	513.65	33.45	638.9	218.4	170.4
La	31.05	57.45	3.95	41.8	29.15	45.35	13.2	43.75	19.3	7.25
Ce	78.8	155.1	10	91.4	64.05	101.05	29.35	86.75	43.8	20.85
Pb	38.7	220.55	10.25	34	30.5	31.75	35.95	27.65	32.25	34.15
Th	35.35	26.75	1000	23.05	8.05	21.75	8.2	12.6	3.2	1000
U	14.55	19.5	4.6	6.95	6.15	4.75	21.7	3.05	18.4	16.85

	B	C	D	E	F	G	H	I	J	K
2	**Table 5. Sr-Nd-Pb isotopic data**									
3	**Sample**	[illegible]	[illegible]	[illegible]	[illegible]	[illegible]	[illegible]	[illegible]	[illegible]	[illegible]
4	**Site**	Pirrit Hills	Pirrit Hills	Nash Hills	Nash Hills	Nash Hills	Nash Hills	Linck Nunatak	Whitmore Mtns.	Pagano Nunatak
5	**Age (Ma)**	174	174	177	177	177	177	175	208	175
6	**$^{87}Rb/^{86}Sr$**	0.8094	0.0779	0.2143	0.8943	0.0714	0.0301	0.6727	0.0414	0.5264
7	**$^{87}Sr/^{86}Sr$**	0.711563	0.717971	0.714495	0.716657	0.718085	0.717028	0.718457	0.709479	0.717576
8	**$^{87}Sr/^{86}Sr_i$**	0.709561	0.717778	0.713956	0.714406	0.717905	0.716953	0.716783	0.709357	0.716267
9	**[Sm]**	13.59	16.58	11.04	11.07	6.79	3.04	6.33	13.89	2.38
10	**[Nd]**	46.28	59.45	52.91	53.03	30.80	14.78	27.32	53.28	9.74
11	**$^{147}Sm/^{144}Nd$**	0.1775	0.1686	0.1261	0.1261	0.1333	0.1242	0.1400	0.1575	0.1477
12	**$^{143}Nd/^{144}Nd$**	0.512395	0.512383	0.512336	0.512329	0.512276	0.512312	0.512310	0.512463	0.512329
13	**$f_{Sm/Nd}$**	-0.0977	-0.1429	-0.3589	-0.3587	-0.3225	-0.3686	-0.2884	-0.1992	-0.2493
14	**Epsilon Nd**	-4.75	-4.98	-5.88	-6.02	-7.06	-6.35	-6.40	-3.41	-6.04
15	**Epsilon Nd_i**	-4.32	-4.36	-4.29	-4.43	-5.63	-4.72	-5.13	-2.38	-4.94
16	**t_{DM} (Ga)**	3.16	2.58	1.42	1.43	1.65	1.43	1.73	1.86	1.89
17	**$^{208}Pb/^{204}Pb_i$**	38.286	38.244	38.714	38.604	38.829	38.568	38.418	38.381	38.592
18	**$^{207}Pb/^{204}Pb_i$**	15.617	15.592	15.694	15.687	15.662	15.659	15.655	15.640	15.658
19	**$^{206}Pb/^{204}Pb_i$**	18.472	18.490	18.878	18.782	19.414	18.775	18.712	18.647	18.820
20	**$^{208}Pb/^{206}Pb_i$**	2.0727	2.0683	2.0508	2.0554	2.0000	2.0542	2.0532	2.0583	2.0506
21	**$^{207}Pb/^{206}Pb_i$**	0.8454	0.8432	0.8314	0.8352	0.8068	0.8340	0.8366	0.8387	0.8320
22										
23										
24										
25										

	L	M	N	O	P	Q	R	S	T	U	V	W
2												
3	e vessels at 200°C for 72 hours, dried and dissolved in 5 mL 6M HCl at 150°C for 12 hours. The resulting											
4												
5												
6												
7												
8												
9												
10												
11												
12												
13												
14												
15												
16												
17												
18												
19												
20												
21												
22												
23												
24												
25												

Appendix 1: Analytical Methods

X-Ray Fluorescence Geochemistry

Samples were split with a vise wedge and only pieces lacking weathered or sawmarked edges were used in XRF analyses. Powders were prepared by further splitting the sample and reducing these pieces to a fine powder in a Spex 8510 shatterbox. The use of pre-contaminated bowls (iron for trace element and tungsten carbide for major element powders) reduced the chance of cross contamination between the samples. Pressed powder pellets were prepared for trace element analyses by mixing 10 g of rock powder with 15 drops of 2% polyvinyl alcohol and pressing the mixture into pellets on a stainless steel mold under a pressure of 6 tonnes. Major element concentrations were determined from fused glass beads that were prepared with dried sample powder that was mixed with lithium metaborate/tetraborate flux. The sample pellets and beads were analyzed using a Phillips PW-2400 X-ray fluorescence spectrometer. Elemental concentrations were determined by comparing X-ray intensities for each element in a sample unknown with those from >40 international reference materials. Trace element concentrations were corrected for matrix effects using the Rh tube Compton K alpha scatter peak ratio method. Details of XRF sample preparation, analyses, analytical precision, and detection limits are provided in Vervoort et al. (2007).

Tracer isotopes (Sr, Pb, Nd)

For Sm-Nd isotopic analysis, fifty milligram aliquots of sample powder were spiked with a mixed ^{149}Sm-^{150}Nd tracer, dissolved with 5 mL 29M HF + 15M HNO_3 (3:1) in Parr pressure vessels at 200°C for 72 hours, dried and re-dissolved in 5 mL 6M HCl at 120°C for 24 hours. Total dissolutions were dried and re-dissolved in 5 mL 1M HCl + 0.1M HF at 120°C overnight. Bulk rare earth elements were separated by standard dilute HCl and HNO_3 based cation exchange chemistry (Richard et al., on 6mm i.d. x 20cm columns of AG-50W-X8 resin, (H+ form, 200-400 mesh); Sm and Nd were separated by reverse phase HDEHP chromatography on 4mm i.d. x 10cm columns of Eichrom Ln-spec resin, 50-100 mesh. Sm and Nd isotopes were measured on an IsotopX Isoprobe-T in static and dynamic Faraday modes, respectively. Instrumental mass fractionation of Sm and Nd isotopes was corrected with an exponential law relative to $^{146}Nd/^{144}Nd = 0.7219$ and $^{152}Sm/^{147}Sm = 1.783$. The $^{143}Nd/^{144}Nd$ ratio is reported as spike-stripped and bias-corrected relative to the accepted value of JNdi-1 standard (0.512115; Tanaka et al., 2001).

Comment [RJP1]: Reference missing

For Rb-Sr isotopic analyses, we selected apatite as the preferred phase from which to extract initial Sr isotopic compositions, based upon its relatively low Rb/Sr and lack of secondary alteration. From 1-5 milligrams of apatite were spiked with a mixed ^{87}Rb-^{84}Sr tracer, dissolved with 1 mL 15M HNO_3 in Savillex PFA beakers at 150°C for 60 hours, dried and redissolved in 5 mL 6M HCl at 150°C for 16 hours. The resulting clear solution was dried and redissolved in 1 mL 3.5M HNO_3 at 150°C overnight. Sr was separated via an ion exchange column procedure in 3.5M HNO_3 media using 50 µl of Sr-spec crown ether resin (Eichrom); Rb was collected from the initial washes from this column, and further purified by ion exchange in 0.6M HCl on 6mm i.d. x 10cm columns of AG-50W-X8 resin (H+ form, 200-400 mesh). Rb and Sr were loaded in 0.1N H_3PO_4 along with a tantalum oxide emitter solution (R. Creaser, pers. comm.) on single degassed Re filaments, and their isotope ratios measured on the Isoprobe-T in the Boise State University Isotope Geology Laboratory. The $^{87}Rb/^{85}Rb$ ratio was measured in static Faraday mode; a mass bias correction was estimated by external analysis of natural Rb standards. Sr isotope ratios were analyzed in dynamic mode, fractionation corrected with an exponential law relative to

$^{86}Sr/^{88}Sr = 0.1194$, and are reported as spike-stripped and bias corrected relative to the accepted value of the NBS-987 standard (0.710248).

For Pb isotopic analyses, up to 200 milligrams of potassium feldspar were isolated by selective density separation in lithium polytungstate (Geoliquids), followed by handpicking. Separates were progressively leached following methods modified from Housh and Bowring (1991). All leaching was accomplished in savillex Teflon beakers on a hot plate at 50°C, and each leach step was followed by rinsing with two aliquots of 500 µl high-purity H_2O which was subsequently added to the leachate. After leaching with 500 µl 7 M HNO_3 and 6 M HCl for 15 minutes each, separates were subjected to five sequential treatments of 500 µl of 5% HF for 10 minutes each. All HF leachates were dried and re-dissolved in 0.5 M HBr for separation of Pb by anion exchange chemistry. Total procedural blanks were <20 pg, and thus represent a negligible contribution to the sample Pb.

Purified Pb elutions were dried with 2 µl of 0.05 N H_3PO_4, and then loaded on single degassed Re filaments with 2 µl of a silica-gel/phosphoric acid mixture (Gerstenberger and Haase, 1997). Pb isotope ratios were measured in static Faraday mode for 200 ratios over a restricted and reproducible range in temperature, with ^{208}Pb ion beams ranging from 1 to 4V. Ratios were corrected for instrumental mass fractionation of 0.10 ± 0.03 %/a.m.u., as estimated by repeated analyses of NBS 981 and 982 over the same temperature range. Successive HF leaches yielded progressively less radiogenic isotopic compositions, which usually achieved a plateau by the fourth and fifth leach steps; the least radiogenic isotopic composition for each feldspar separate is reported in Table 2, and is assumed to closely approach the initial isotopic composition of the magma from which the feldspar crystallized.

U-Pb Geochronology Methods (ID-TIMS)

Zircons were extracted from crushed rock samples using standard density and magnetic separation methods, mounted in epoxy, polished until the centers were exposed, and imaged with a scanning electron microscope using a cathodo-luminescence detector (CL) at Carleton College, MN. The CL images were used to guide the selection of grains for dating in the Boise State University Isotope Geology Laboratory. Analyses were exclusively from single grains extracted from the mounts. All imaged grains have sector and oscillatory zoning that is typical of zircon crystallized from granitic magmas; grains with obvious inherited components (as identified by contrasts in CL or zoning truncations) were avoided.

Zircon crystals were subjected to a modified version of the chemical abrasion method of Mattinson (2005), reflecting a preference to prepare and analyze carefully selected single crystals. Zircons extracted from mounts were placed in a muffle furnace at 900°C for 60 hours in quartz beakers, transferred to individual 3 ml Teflon PFA beakers with ultrapure H_2O, and then loaded into 300 µl Teflon PFA dissolution microcapsules. Fifteen microcapsules were placed in a large-capacity Parr vessel, and the crystals partially dissolved in 120 µl of 29 M HF for 10-12 hours at 180°C. The contents of each microcapsule were returned to 3 ml Teflon PFA beakers, the HF removed and the residual grains rinsed in ultrapure H_2O, immersed in 3.5 M HNO_3, ultrasonically cleaned for an hour, and fluxed on a hotplate at 80°C for an hour. The HNO_3 was removed and the grains were rinsed several times with ultrapure H_2O before being reloaded into the same 300 µl Teflon PFA dissolution microcapsules (rinsed and fluxed in 6 M HCl during crystal sonication and washing) and spiked with the Boise State University mixed ^{233}U-^{235}U-^{205}Pb tracer solution (which has been calibrated against EARTHTIME gravimetric standards). The grains were dissolved in

Parr vessels in 120 µl of 29 M HF with a trace of 3.5 M HNO_3 at 220°C for 48 hours, dried to fluorides, and then re-dissolved in 6 M HCl at 180°C overnight. U and Pb were separated from the zircon matrix using an HCl-based anion-exchange chromatographic procedure (Krogh, 1973), eluted together and dried with 2 µl of 0.05 N H_3PO_4.

Pb and U were loaded on a single outgassed Re filament in 2 µl of a silica-gel/phosphoric acid mixture (Gerstenberger and Haase, 1997), and U and Pb isotopic measurements made on an IsotopX GV Isoprobe-T multicollector thermal ionization mass spectrometer equipped with an ion-counting Daly detector. Pb isotopes were measured by peak-jumping all isotopes on the Daly detector for 100 to 150 cycles, and corrected for 0.18 ± 0.04%/a.m.u. (atomic mass unit) mass fractionation. Transitory isobaric interferences due to high-molecular weight organics, particularly on ^{204}Pb and ^{207}Pb, disappeared within approximately 30 cycles, while ionization efficiency averaged 10^4 cps/pg of each Pb isotope. Linearity (to ≥1.4 x 10^6 cps) and the associated dead-time correction of the Daly detector were monitored by repeated analyses of NBS982, and have been constant since installation. Uranium was analyzed as UO_2^+ ions in static Faraday mode with 10^{11} ohm resistors for 150 to 200 cycles, and corrected for isobaric interference of $^{233}U^{18}O^{16}O$ on $^{235}U^{16}O^{16}O$ with an $^{18}O/^{16}O$ of 0.00206. Ionization efficiency averaged 20 mV/ng of each U isotope. U mass fractionation was corrected using the known $^{233}U/^{235}U$ ratio of the BSU tracer solution.

U-Pb dates and uncertainties were calculated using the algorithms of Schmitz and Schoene (2007) and the U decay constants Jaffey et al. (1971). $^{206}Pb/^{238}U$ ratios and dates were corrected for initial ^{230}Th disequilibrium using a Th/U[magma] of 3 ± 1, resulting in a systematic increase in the $^{206}Pb/^{238}U$ dates of ~90 kyr. All common

Pb in analyses was attributed to laboratory blank and subtracted based on the measured laboratory Pb isotopic composition and associated uncertainty. U blanks were <0.1 pg. Over the course of the experiment, isotopic analyses of the TEMORA 2 zircon standard yielded a weighted mean $^{206}Pb/^{238}U$ age of 417.43 ± 0.06 (n = 11, MSWD = 0.8).

U-Pb Geochronology Methods (SHRIMP)

Some reported ages were determined using a Sensitive High Resolution Ion Microprobe (SHRIMP) at The Australian National University (following Williams, 1998). An epoxy resin mount was prepared from a selection of 50–100 grains, ground half-way through, polished and Au-coated. Internal zoning and the characteristics of individual grains were mapped by a combination of microphotography and cathodoluminescence (CL) imaging. Targets were carefully selected so that clean areas, free of cracks, inclusions and radiation damage could be analysed, in order to date specific phases of zircon growth – generally the latest igneous phase with concentric oscillatory zoning, although in the case of the Linck Nunataks sample some cores were also targeted. Analysis was carried out with a primary O^- beam and secondary ion beam intensities were measured using an ion-counting detector. Calibration was carried out using chips of laboratory zircon standard SL13 mounted together with the samples and the data were processed using SQUID (Ludwig, 2001).

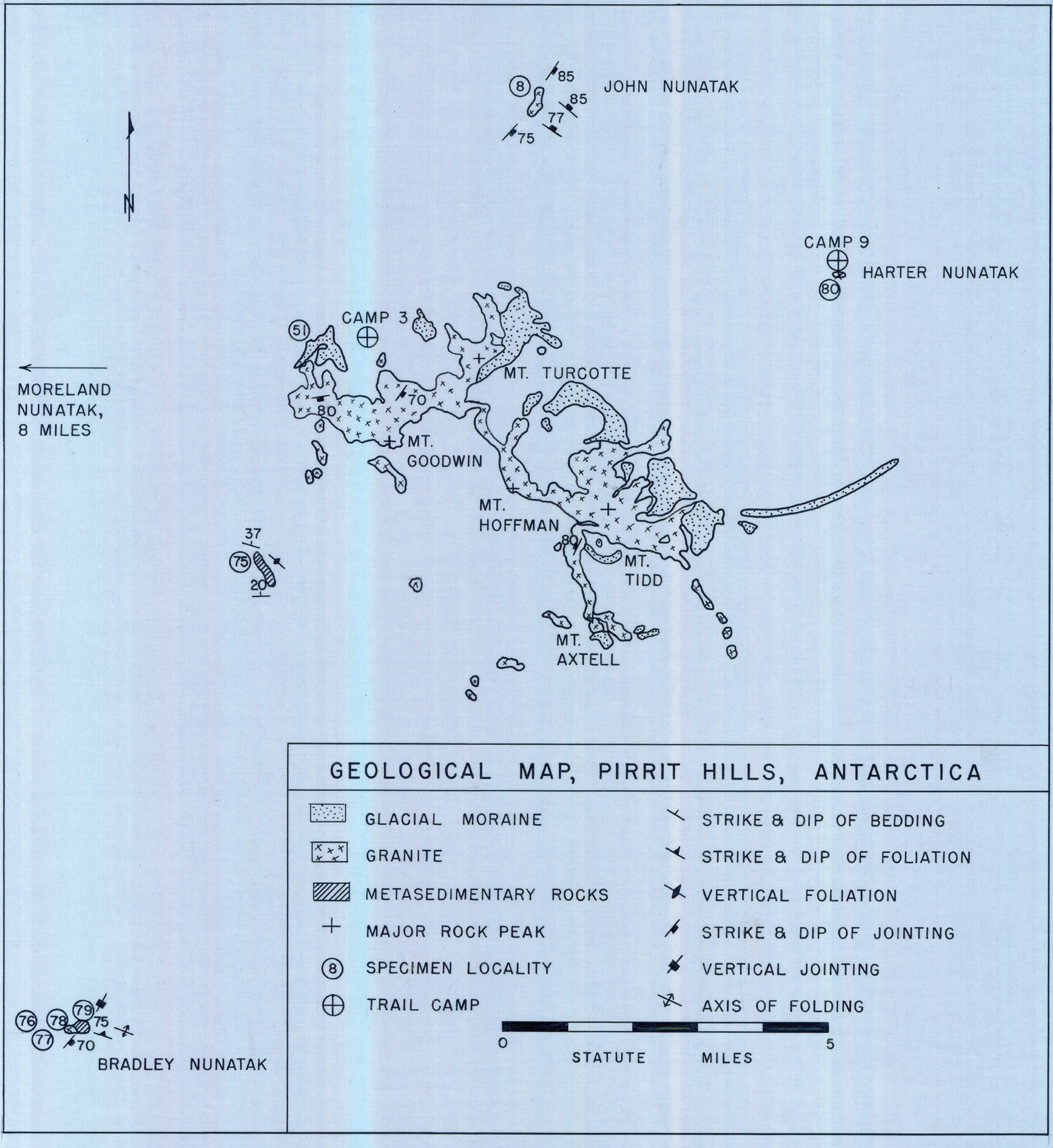

Appendix 2: Geologic map of the Pirrit Hills, central Antarctica.

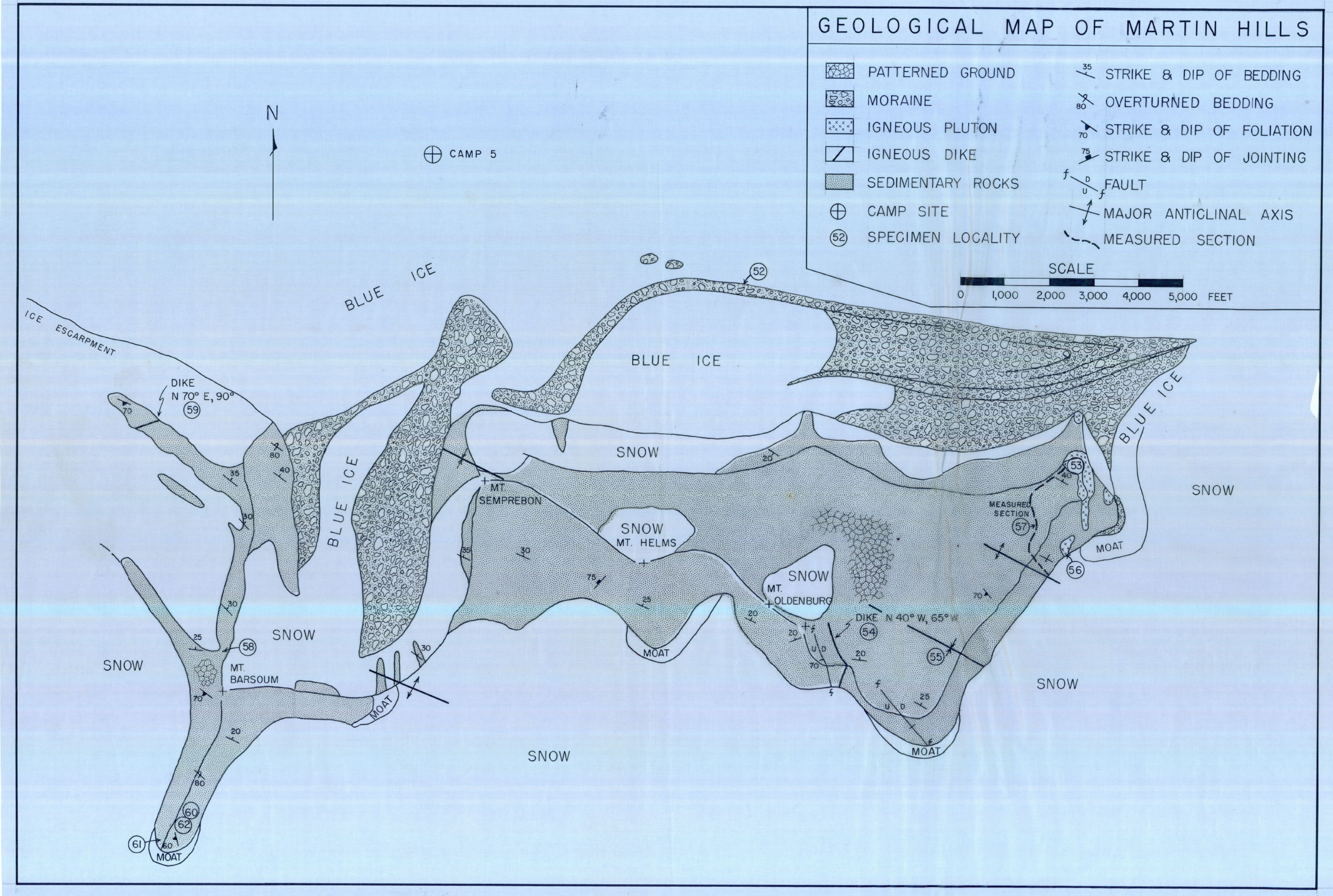

Appendix 3: Geologic map of the Martin Hills, central Antarctica.

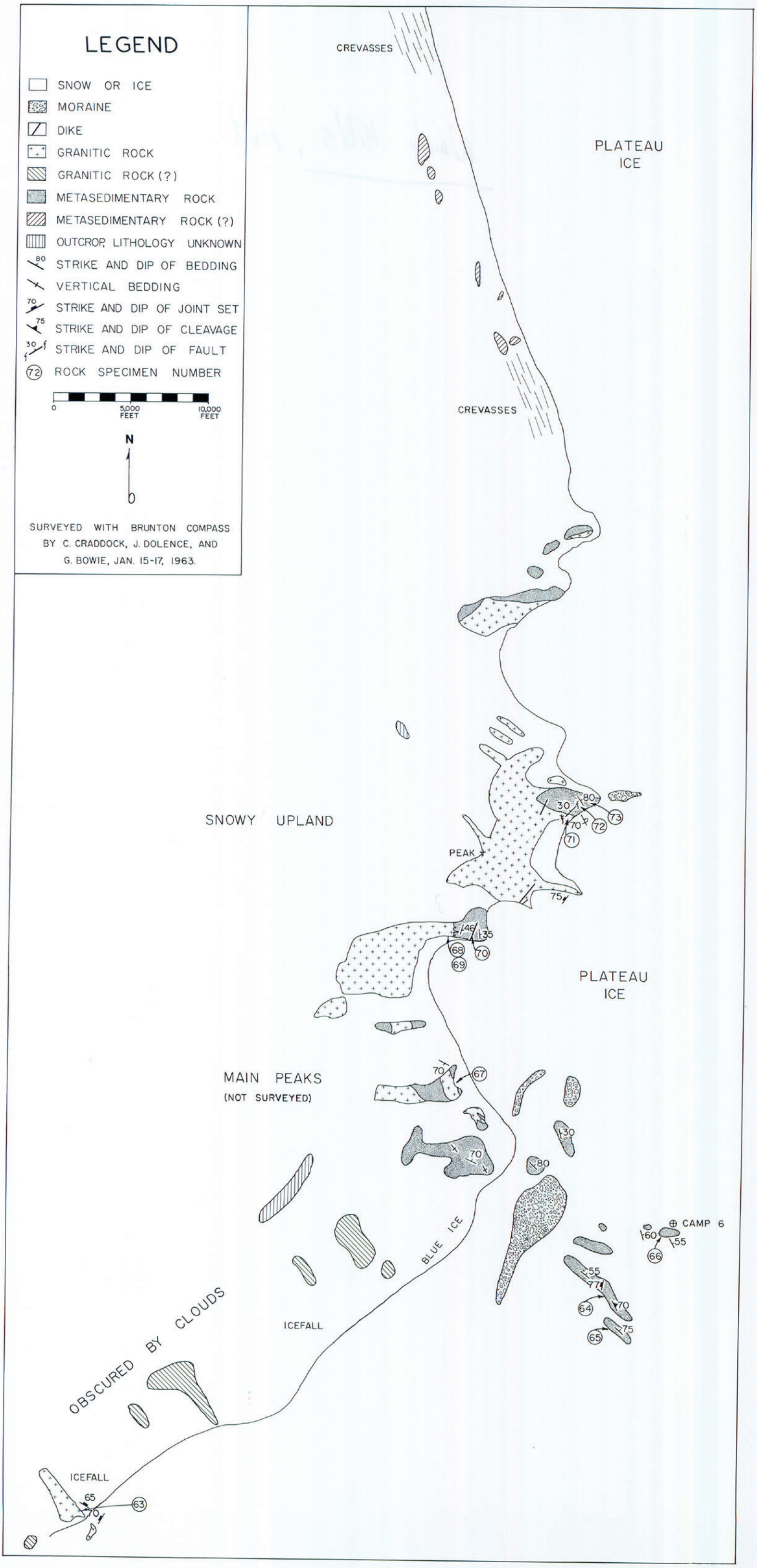

Appendix 4: Geologic map of the Nash Hills, central Antarctica.

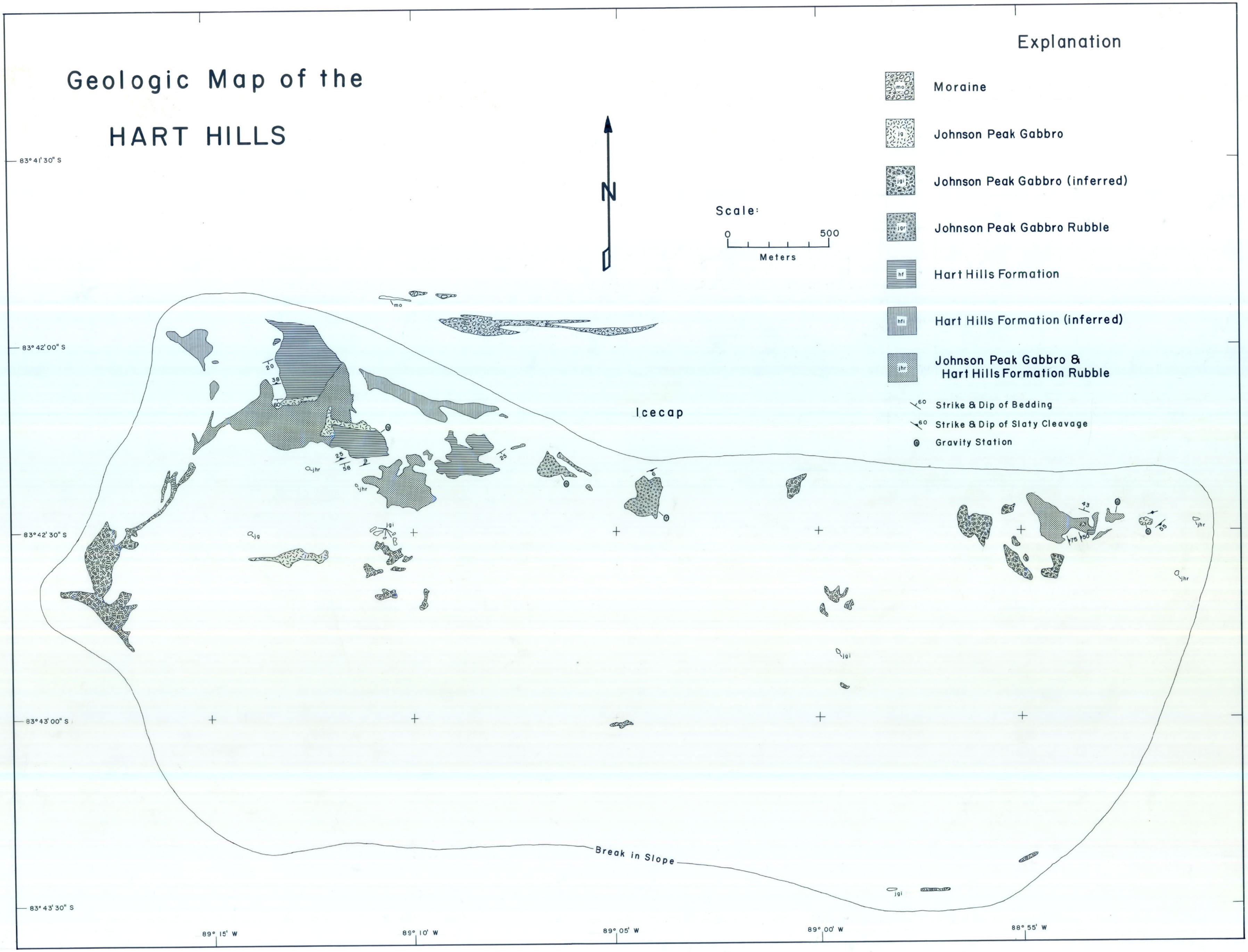

Appendix 5: Geologic map of the Hart Hills, central Antarctica.

Appendix 6 (Supplementary data table): Sr and Nd data from Antarctic Peninsula granitoids.

Sample	Rock type	Locality	Ref.	Age	Rb	Sr	$^{87}Rb/^{86}Sr$	$^{87}Sr/^{86}Sr$	$^{87}Sr/^{86}Sr_i$	Sm	Nd	$^{147}Sm/^{144}Nd$	$^{143}Nd/^{144}Nd$	εNd_i	T_{DM}
Cenozoic (<65 Ma)															
Graham Land															
BR.024.3	DI	Faure Islands	1	48	113	406	0.7999	0.704610	0.704065	7.8	42.8	0.1095	0.512836	4.4	495
BR.024.4	DI	Faure Islands	1	48	36	507	0.2043	0.704210	0.704071	4.0	20.5	0.1186	0.512843	4.5	487
R.008.1	GD	Anchorage Island	1	62	31	443	0.2020	0.704050	0.703872	4.9	21.6	0.1365	0.512866	4.9	453
R.013.4	MD	Anchorage Island	1	62	51	452	0.3273	0.704000	0.703712	5.4	23.7	0.1391	0.512888	5.3	411
North-west Palmer Land															
R.5256.1	GD	Mount Pitman	7	60	103	443	0.6742	0.704968	0.704393	5.5	29.0	0.1147	0.512777	3.3	607
Late Cretaceous (97-65 Ma)															
Graham Land															
R.076.1	DI	Horseshoe Island	1	67	10	778	0.0367	0.704140	0.704105	4.9	20.3	0.1451	0.512807	3.7	574
R.079.1	GA	Horseshoe Island	1	67	11	987	0.0313	0.704180	0.704150	2.9	23.4	0.0746	0.512811	4.4	507
R.080.1	GR	Horseshoe Island	1	67	45	208	0.6196	0.704670	0.704080	7.7	38.4	0.1208	0.512830	4.4	509
BR.138.6	GR	Terra Firma Islands	9	85	85	188	1.3144	0.705960	0.704373	7.6	37.5	0.1230	0.512765	3.3	630
BR.138.13	GA	Terra Firma Islands	9	85	21	654	0.0926	0.704454	0.704342	4.4	19.4	0.1364	0.512752	2.9	668
BR.138.17	DI	Terra Firma Islands	9	85	60	387	0.4444	0.705905	0.705368	5.6	29.1	0.1151	0.512599	0.1	914
R.503.2	GD	Petermann Island	1	93	113	256	1.2776	0.706200	0.704512	7.7	40.4	0.1155	0.512706	2.3	728
BR.132.15	GR	Bourgeois Fjord	9	96	130	113	3.3150	0.710270	0.705748	4.9	26.6	0.1114	0.512545	-0.8	997
R.5860.1	GD	Sellar Glacier	9	96	117	424	0.7953	0.707158	0.706073	2.7	15.9	0.1021	0.512531	-0.9	1010
North-west Palmer Land															
R.5736.1	GD	Scorpio Peaks	7	70	76	570	0.3879	0.704667	0.704281	4.2	24.9	0.1034	0.512821	4.4	511
R.5955.11	GD	Orion Massif	9	70	75	589	0.3694	0.705499	0.705131	4.7	25.2	0.1136	0.512718	2.3	711
R.5501.1	GD	Mount Lepus	9	80	86	150	1.6621	0.707292	0.705403	3.2	22.7	0.0846	0.512660	1.6	784
R.5965.7	GD	Mount Lepus	9	80	80	493	0.4718	0.705913	0.705376	4.9	29.0	0.1030	0.512685	1.9	757
R.5267.1	GD	Goettel Escarpment	9	87	55	496	0.3203	0.706827	0.706431	6.1	30.5	0.1209	0.512531	-1.2	1029
R.2539.2	GD	Taurus Nunataks	9	88	31	935	0.0955	0.706768	0.706648	2.7	14.5	0.1108	0.512479	-2.1	1103
R.5271.1	PO	Goettel Escarpment	9	91	53	691	0.2236	0.705980	0.705691	4.1	21.2	0.1155	0.512605	0.3	903
Early Cretaceous (146-97)															
Graham Land															
BR.125.1	GD	Bourgeois Fjord	9	100	80	469	0.4947	0.706979	0.706276	4.1	23.5	0.1050	0.512452	-2.5	1137
BR.129.1	GR	Bourgeois Fjord	9	100	84	215	1.1323	0.706803	0.705194	3.2	19.7	0.0984	0.512596	0.4	898
R.5552.1	GR	Bristly Peaks	9	98	122	88	4.0131	0.711047	0.705458	5.0	27.0	0.1128	0.512586	0.0	931
R.366.1	GR	Cape Fairweather	1	101	152	61	7.2265	0.715976	0.705605	5.1	26.0	0.1190	0.512566	-0.4	970
R.571.1	GR	Horseshoe Island	1	101	212	12	51.8700	0.779990	0.705508	7.5	37.2	0.1225	0.512548	-0.8	1003
North-west Palmer Land															
R.2414.3	GR	Pegasus Mountains	7	140	84	157	1.5449	0.707309	0.704234	3.9	17.8	0.1329	0.512746	3.2	673
R.2418.4	GD	Pegasus Mountains	7	140	42	287	0.4203	0.705580	0.704743	2.6	12.2	0.1290	0.512625	1.0	880
R.2402.1	GR	Aldebaran Rock	9	140	163	311	1.5216	0.707684	0.704656	7.1	42.6	0.1015	0.512595	0.9	889
R.5902.8	GD	Friedmann Nuns.	7	100	58	638	0.2647	0.706755	0.706379	4.1	21.8	0.1144	0.512449	-2.6	1151
R.2568.2	GD	Sirius Cliffs	9	120	48	753	0.1855	0.707285	0.706968	3.0	19.9	0.0906	0.512431	-2.4	1147
R.5796.4	GD	Cetus Hill	7	120	36	1078	0.0963	0.707003	0.706838	3.2	18.8	0.1023	0.512408	-3.0	1197
R.2556.1	GD	Perseus Crags	7	125	56	642	0.2526	0.707254	0.706805	3.8	18.7	0.1223	0.512437	-2.7	1176
R.5904.7	GD	Puppis Pikes	9	140	76	565	0.3898	0.709361	0.708585	3.6	21.1	0.1034	0.512345	-4.1	1288
R.2585.1	GD	Procyon Peaks	9	140	67	651	0.2994	0.706119	0.705523	6.8	34.2	0.1202	0.512595	0.5	917
R.2784.1	GD	Creswick Gap	8	140	74	287	0.7412	0.706802	0.705327	4.0	23.2	0.1049	0.512547	-0.1	974
R.3204.3	GD	Creswick Gap	8	140	65	569	0.3307	0.706569	0.705911	3.6	19.3	0.1121	0.512510	-1.0	1045
R.3216.2	TO	Burns Bluff	8	140	18	736	0.0712	0.705693	0.705551	2.0	9.4	0.1256	0.512553	-0.4	995
R.3216.3	TO	Burns Bluff	6,8	140	22	612	0.1038	0.705733	0.705526	2.9	14.0	0.1262	0.512539	-0.7	1019
R.5284.1	GD	Renner Peak	9	140	31	910	0.0992	0.706244	0.706046	3.6	20.0	0.1078	0.512509	-0.9	1040
R.5300.3	GA	Auriga Nunataks	9	140	24	452	0.1516	0.707215	0.706913	4.0	11.1	0.2183	0.512536	-2.4	1158
R.5958.1	GD	Wade Point	9	140	30	184	0.4787	0.705202	0.704249	3.8	15.0	0.1523	0.512786	3.7	632

Sample	Rock type	Locality		Age	Rb	Sr	$^{87}Rb/^{86}Sr$	$^{87}Sr/^{86}Sr$	$^{87}Sr/^{86}Sr_i$	Sm	Nd	$^{147}Sm/^{144}Nd$	$^{143}Nd/^{144}Nd$	εNd_i	T_{DM}
R.6314.9	GD	Butler Peaks	7	140	39	573	0.1984	0.706162	0.705767	3.5	19.9	0.1055	0.512479	-1.5	1085
R.6316.4	GD	Butler Peaks	7	140	28	691	0.1166	0.705960	0.705728	3.2	15.3	0.1254	0.512511	-1.2	1063
R.5287.1	DI	Creswick Peaks	7,8	141	77	383	0.5832	0.706879	0.705710	3.3	16.8	0.1170	0.512521	-0.8	1035
R.6057.7	TO	Burns Bluff	6,8	141	31	153	0.5777	0.705836	0.704678	4.3	18.5	0.1394	0.512781	3.8	619
R.6063.5	GD	Burns Bluff	6,7,8	141	18	290	0.1762	0.704916	0.704563	2.9	11.2	0.1563	0.512736	2.6	730
R.6057.16	TO	Burns Bluff	6,8	141	56	489	0.3342	0.707202	0.706532	3.3	21.5	0.0920	0.512454	-1.7	1105
R.6057.20	QDI	Burns Bluff	6,8	141	8	281	0.0816	0.704408	0.704245	1.6	5.5	0.1773	0.512832	4.1	589
R.6057.30	TO	Burns Bluff	6,8	141	36	718	0.1455	0.705706	0.705414	3.0	13.4	0.1373	0.512667	1.6	821
R.2793.1	GA	Moore Point	6,8	140	1	236	0.0130	0.704424	0.704399	0.3	0.9	0.2175	0.512875	4.3	576
R.5259.1	GA	Mount Eissenger	9	140	3	424	0.0188	0.705195	0.705157	1.5	4.5	0.2031	0.512750	2.1	781
R.6057.10	GA	Burns Bluff	6,8	141	29	296	0.2832	0.704958	0.704390	3.5	12.4	0.1727	0.512822	4.0	599
North-east Palmer Land															
E.4021.1	GD	Welch Mountains	4	124	85	415	0.5863	0.707420	0.706387	3.2	16.4	0.1163	0.512432	-2.7	1176
E.4012.1	GD	Black Coast	4	120	81	495	0.4750	0.706540	0.705730	3.7	21.5	0.1054	0.512424	-2.8	1176
R.1906.5	GD	Mount Charity	5	120	233	219	3.0858	0.711129	0.705866	6.7	24.2	0.1666	0.512432	-3.6	1237
R.1906.7	GD	Mount Charity	5	120	114	312	1.0612	0.707736	0.705926	5.2	17.7	0.1778	0.512472	-2.9	1190
R.4278.1	GA	Black Coast	4	120	12	532	0.0669	0.705137	0.705023	5.0	20.7	0.1473	0.512471	-2.5	1154
R.4280.2	GA	Black Coast	4	120	85	524	0.4692	0.705752	0.704952	3.2	13.6	0.1425	0.512515	-1.6	1079
E.4178.1	GD	Mount Jackson	4	114	45	455	0.2890	0.705220	0.704752	2.8	14.4	0.1165	0.512537	-0.8	1012
R.4230.1	GD	Black Coast	4	108	89	316	0.8153	0.707845	0.706594	3.3	17.7	0.1135	0.512346	-4.6	1305
E.4065.1	GD	Giannini Peak	4	105	155	367	1.2210	0.708389	0.706567	3.9	18.9	0.1261	0.512365	-4.4	1290
Late Jurassic (146-157)															
North-west Palmer Land															
R.5260.2	GA	Mount Eissenger	9	150	64	216	0.8605	0.707769	0.705934	1.8	7.6	0.1429	0.512635	1.0	886
R.5260.3	GR	Mount Eissenger	9	150	76	239	0.9216	0.708800	0.706835	7.1	37.6	0.1147	0.512448	-2.1	1146
Middle Jurassic (178-157)															
Graham Land															
R.312.2	GR	Bildad Peak	1	163	144	348	1.1943	0.709060	0.706293	6.4	35.4	0.1098	0.512404	-2.8	1204
R.326.2	GD	Mount Fritsche	1	164	76	311	0.7099	0.708450	0.706795	3.7	20.0	0.1112	0.512361	-3.6	1271
R.302.1	DI	Bildad Peak	1	167	108	744	0.4199	0.707180	0.706183	6.0	24.5	0.1479	0.512425	-3.1	1235
R.310.1	GD	Bildad Peak	1	167	172	291	1.7200	0.710140	0.706056	4.7	25.1	0.1121	0.512396	-2.9	1219
R.2605.1	GA	Scharer Bluff	1	175	18	378	0.1402	0.708330	0.707981	2.1	9.1	0.1407	0.512365	-4.1	1314
R.2605.2	GA	Scharer Bluff	1	175	74	303	0.7067	0.709950	0.708192	4.2	20.3	0.1244	0.512296	-5.1	1388
R.2606.1	GA	Scharer Bluff	1	175	46	366	0.3638	0.709930	0.709025	3.8	16.1	0.1418	0.512263	-6.1	1464
R.2606.6	GR	Scharer Bluff	1	175	243	249	2.8286	0.717200	0.710162	8.3	49.0	0.1025	0.512300	-4.5	1346
R.2607.4	MG	Scharer Bluff	1	175	265	131	5.8885	0.725070	0.710419	10.6	53.5	0.1197	0.512321	-4.5	1344
R.2624.1	GD	Trail Inlet	1	177	141	241	1.6861	0.711900	0.707657	6.2	32.2	0.1157	0.512356	-3.7	1285
R.2625.1	GD	Trail Inlet	1	177	140	276	1.4672	0.711160	0.707468	6.8	35.4	0.1162	0.512359	-3.6	1281
North-west Palmer Land															
R.6308.1	GD	Mount Ward	7	170	173	239	2.0899	0.713930	0.708879	10.0	52.7	0.1149	0.512213	-6.5	1492
R.6309.2	GD	Mount Ward	9	170	38	234	0.4647	0.708407	0.707284	2.9	14.2	0.1216	0.512398	-3.1	1232
R.6315.8	GR	Butler Peaks	7	170	190	27	20.7529	0.757891	0.707733	9.7	34.6	0.1698	0.512358	-4.9	1371
North-east Palmer Land															
R.1906.3	GR	Mount Charity	5	168	190	65	8.5040	0.728482	0.708170	5.7	25.2	0.1364	0.512381	-3.7	1282
R.1907.4	PO	Mount Charity	5	168	231	48	13.9566	0.740769	0.707434	6.9	23.7	0.1759	0.512496	-2.3	1173
R.1914.11	GR	Mount Charity	5	168	110	659	0.4852	0.709057	0.707898	5.2	31.0	0.1022	0.512242	-5.7	1431
Early Jurassic (208-178)															
Graham Land															
R.052.6	OGN	Roman Four	1	200	163	88	5.3428	0.721509	0.706314	10.5	53.4	0.1189	0.512421	-2.2	1189
R.321.3	GD	Target Hill	1	180	120	299	1.1647	0.709310	0.706329	4.5	28.2	0.0958	0.512359	-3.1	1244
R.2619.1	GA	M Pyramid	1	181	24	378	0.1837	0.707900	0.707427	2.7	12.6	0.1309	0.512361	-3.9	1304

Sample	Rock type	Locality		Age	Rb	Sr	$^{87}Rb/^{86}Sr$	$^{87}Sr/^{86}Sr$	$^{87}Sr/^{86}Sr_i$	Sm	Nd	$^{147}Sm/^{144}Nd$	$^{143}Nd/^{144}Nd$	εNd_i	T_{DM}
R.2619.2	GA	M Pyramid	1	181	26	367	0.2059	0.707870	0.707340	2.9	13.3	0.1327	0.512362	-3.9	1305
R.2619.4	GR	M Pyramid	1	181	153	952	0.4638	0.709450	0.708256	4.6	20.0	0.1404	0.512339	-4.5	1353
R.2620.2	GR	M Pyramid	1	181	270	163	4.7929	0.720460	0.708126	10.4	51.6	0.1214	0.512234	-6.1	1472
R.2612.3	GD	Pylon Point	1	204	175	596	0.8495	0.710040	0.707576	5.0	27.9	0.1088	0.512281	-4.7	1379
R.2612.5	GR	Pylon Point	1	204	406	143	8.2413	0.733280	0.709372	7.3	41.0	0.1075	0.512281	-4.6	1377
R.2614.1	GR	Curran Bluff	1	204	398	153	7.5515	0.734980	0.713073	20.9	127.0	0.0997	0.512193	-6.2	1489
R.2614.3	GR	Curran Bluff	1	204	357	173	5.9919	0.731200	0.713817	16.9	101.1	0.1011	0.512191	-6.2	1494
North-west Palmer Land															
R.5254.2	V	Mount Pitman	9	181	184	69	7.7705	0.725311	0.705313	10.8	49.4	0.1320	0.512424	-2.7	1210
R.5254.5	V	Mount Pitman	9	181	104	239	1.2557	0.712287	0.709056	8.3	42.2	0.1193	0.512406	-2.7	1215
R.5270.1	DI	Goettel Escarpment	7	182	46	382	0.3498	0.706802	0.705897	3.9	17.6	0.1331	0.512543	-0.4	1024
R.5271.4	GR	Goettel Escarpment	7	183	87	447	0.5668	0.707919	0.706444	11.8	64.1	0.1110	0.512471	-1.3	1097
R.2549.2	GD	Capella Rocks	9	203	36	990	0.1065	0.707215	0.706907	3.5	19.6	0.1081	0.512461	-1.2	1103
R.5280.2	GD	Campbell Ridges	7	203	131	310	1.2237	0.711610	0.708077	8.5	40.8	0.1261	0.512353	-3.7	1307
R.5280.4	PO	Campbell Ridges	9	203	134	94	4.1231	0.719044	0.707142	6.5	31.8	0.1234	0.512356	-3.6	1297
R.5504.2	GD	Auriga Nunataks	9	203	57	496	0.3324	0.707816	0.706856	2.0	21.1	0.0566	0.512394	-1.1	1101
North-east Palmer Land															
R.4908.11	GRG	Mount van Buren	4	206	360	66	15.7498	0.765920	0.719781	5.4	20.1	0.1630	0.512145	-8.7	1672
R.2109.2	GRG	Mount Jackson	4	199	330	80	11.9488	0.754753	0.720940	6.4	20.7	0.1853	0.512141	-9.4	1714
Triassic (248-206)															
Graham Land															
R.280.4	GR	Cole Peninsula	1	209	120	399	0.8640	0.709250	0.706682	6.4	37.6	0.1035	0.512391	-2.3	1202
R.5506.3	GRG	Elton Hill	9	210	186	39	13.8157	0.747093	0.705833	8.3	30.6	0.1647	0.512464	-2.5	1219
R.6157.1	GRG	Reluctant island	9	200	100	188	1.5359	0.710398	0.706030	9.0	54.0	0.1013	0.512382	-2.6	1214
R.5035.2	AM	N of Werner Peak	9	220	107	210	1.4675	0.713904	0.709312	4.1	16.3	0.1509	0.512197	-7.3	1583
R.5035.6	GR	N of Werner Peak	9	220	474	23	60.9030	0.898134	0.707575	0.7	2.6	0.1687	0.512273	-6.3	1512
North-west Palmer Land															
R.2479.1	GR	Mount Lepus	9	210	82	343	0.6886	0.707860	0.705803	4.2	23.9	0.1069	0.512494	-0.4	1045
R.2480.1	GD	Mount Lepus	7	210	75	555	0.3911	0.707090	0.705922	6.4	31.7	0.1220	0.512520	-0.3	1037
R.3239.4	OGN	Campbell Ridges	9	227	180	482	1.0827	0.712220	0.708724	5.1	24.5	0.1266	0.512254	-5.5	1453
R.5294.1	OGN	Sirius Cliffs	9	227	120	870	0.3986	0.706207	0.704920	9.5	41.0	0.1406	0.512338	-4.2	1361
R.5278.8	OGN	Campbell Ridges	7	227	139	608	0.6636	0.709655	0.707513	5.0	25.1	0.1216	0.512338	-3.7	1319
R.5297.3	PGN	Mount Lepus	7	210	121	316	1.1052	0.715572	0.712256	6.9	34.8	0.1202	0.512347	-3.6	1304
R.2436.2	PGN	Auriga Nunataks	9	227	188	443	1.2270	0.717259	0.713297	8.5	45.5	0.1124	0.512096	-8.1	1645
R.2535.6	OGN	Fomalhaut Nuns.	9	227	114	274	1.2002	0.715872	0.711997	2.6	16.0	0.0965	0.512192	-5.8	1478
R.2535.7	OGN	Fomalhaut Nuns.	9	227	124	271	1.3198	0.716208	0.711947	5.7	35.6	0.0973	0.512207	-5.5	1458
R.5257.1	OGN	Mount Eissenger	7	227	174	189	2.6741	0.724902	0.716268	0.8	3.7	0.1352	0.512543	-0.1	1030
R.5257.2	OGN	Mount Eissenger	9	227	81	190	1.2250	0.720105	0.716150	13.0	62.9	0.1253	0.512548	0.3	997
North-east Palmer Land															
R.1905.1	DI	Mount Charity	5	232	150	770	0.5628	0.708320	0.706463	7.7	35.5	0.1305	0.512361	-3.4	1305
R.1905.4	GR	Mount Charity	5	232	185	489	1.0911	0.710352	0.706752	6.2	49.3	0.0767	0.512278	-3.5	1307
R.1905.5	GR	Mount Charity	5	232	245	117	6.0764	0.726115	0.706064	1.2	3.9	0.1799	0.512550	-1.2	1128
R.1907.2	GR	Mount Charity	5	232	242	113	6.2259	0.726957	0.706413	1.6	4.6	0.2116	0.512503	-3.1	1276
R.4552.2	OGN	Mount Nordhill	4	220	176	150	3.4004	0.726175	0.715536	8.9	43.3	0.1248	0.512143	-7.6	1605
R.4552.9	GGN	Mount Nordhill	4	220	308	109	8.2244	0.742662	0.716929	6.8	34.5	0.1201	0.512126	-7.8	1619
R.4920.5	GR	Mount Nordhill	9	220	201	253	2.3031	0.716426	0.709220	16.3	81.5	0.1208	0.512121	-8.0	1628
R.4920.12	GR	Mount Nordhill	4	220	289	224	3.7368	0.724185	0.712493	8.3	40.2	0.1255	0.512170	-7.1	1570
R.4922.1	MY	Steele Peak	9	220	125	448	0.8060	0.707357	0.704835	2.7	14.4	0.1138	0.512531	0.2	998
R.4942.4	GD	Hall Ridge	4	211	77	477	0.4689	0.706893	0.705486	4.9	22.9	0.1286	0.512453	-1.8	1159
R.5006.7	GD	Pinther Ridge	4	209	95	465	0.5911	0.707586	0.705829	8.6	46.0	0.1128	0.512355	-3.3	1277

Sample	Rock type	Locality		Age	Rb	Sr	^{87}Rb/^{86}Sr	^{87}Sr/^{86}Sr	^{87}Sr/^{86}Sr$_i$	Sm	Nd	^{147}Sm/^{144}Nd	^{143}Nd/^{144}Nd	εNd$_i$	T$_{DM}$
Pre-Triassic															
Graham Land															
BR.041.1	SH	Latille Island	9	250	139	393	1.0244	0.712480	0.708837	5.8	29.5	0.1195	0.512293	-4.3	1380
BR.072.1	SST	Hope Bay	1	250	72	371	0.5581	0.709500	0.707515	6.8	30.8	0.1336	0.512356	-3.5	1320
BR.072.2	SST	Hope Bay	1	250	95	361	0.7574	0.709500	0.706807	5.1	28.7	0.1074	0.512341	-2.9	1278
BR.072.3	SST	Hope Bay	1	250	204	138	4.3041	0.723320	0.708013	7.2	35.8	0.1212	0.512301	-4.2	1372
R.3415.14	PG	Target Hill	2	321	45	211	0.6137	0.708036	0.705232	1.3	2.9	0.2603	0.512703	-1.3	1200
R.3632.1	GR	Marsh Spur	3	325	111	211	1.5168	0.713053	0.706037	9.9	79.5	0.0753	0.512324	-1.1	1183
R.3632.2	GR	Marsh Spur	3	325	136	68	5.7731	0.732655	0.705951	5.7	25.8	0.1336	0.512413	-1.8	1238
R.3632.4	GR	Marsh Spur	3	325	153	36	12.2990	0.763040	0.706149	2.6	7.8	0.2031	0.512602	-1.0	1173
R.3899.18	GR	Mount Lagado	3	325	135	114	3.4434	0.719880	0.703952	1.7	4.9	0.2089	0.512550	-2.2	1274
R.3900.3	GR	Mount Lagado	3	325	62	262	0.6959	0.707110	0.703891	0.6	1.2	0.2994	0.512867	0.2	1076
R.3431.1	GGN	Leppard Glacier	3	392	139	232	1.7426	0.714041	0.704314	3.0	19.9	0.0928	0.512495	2.4	932
R.3431.5	GGN	Leppard Glacier	3	392	74	273	0.7796	0.707910	0.703559	1.5	6.2	0.1444	0.512455	-1.0	1219
R.3431.17	AM	Leppard Glacier	3	392	39	201	0.5606	0.706805	0.703676	2.7	9.0	0.1829	0.512802	3.9	796
R.3434.1	GGN	Leppard Glacier	3	392	118	229	1.4976	0.713111	0.704752	3.2	18.4	0.1043	0.512465	1.3	1034
R.3434.2	GGN	Leppard Glacier	3	392	63	171	1.0656	0.709121	0.703173	1.7	5.8	0.1734	0.512566	-0.2	1161
R.3434.6	GGN	Leppard Glacier	2	392	71	272	0.7551	0.707325	0.703110	4.0	18.6	0.1289	0.512519	1.1	1050
R.3434.7	GGN	Leppard Glacier	3	392	122	183	1.9257	0.715614	0.704865	3.3	19.0	0.1047	0.512478	1.5	1014
R.4016.5	AM	Leppard Glacier	3	392	61	211	0.8382	0.708063	0.703384	7.3	28.9	0.1529	0.512652	2.5	927
R.5511.1	OGN	Target Hill	9	392	39	199	0.5718	0.708604	0.705412	3.0	17.5	0.1031	0.512521	2.4	933
R.348.1A	GN	Adie Inlet	1	246	174	229	2.1962	0.722770	0.715085	8.1	38.8	0.1255	0.512158	-7.1	1588
R.348.1B	GN	Adie Inlet	1	246	148	276	1.5580	0.720930	0.715478	5.4	25.7	0.1270	0.512181	-6.7	1560
R.348.2	GN	Adie Inlet	1	246	151	256	1.7089	0.721100	0.715120	6.0	28.0	0.1283	0.512182	-6.8	1561
R.349.1	GN	Adie Inlet	1	246	125	206	1.7474	0.719760	0.713645	8.4	40.9	0.1236	0.512179	-6.7	1555
R.349.2	GN	Adie Inlet	1	246	129	200	1.8724	0.720190	0.713638	8.2	39.1	0.1268	0.512186	-6.6	1552
R.349.3	AM	Adie Inlet	1	246	99	188	1.5214	0.720560	0.715236	7.1	**33.8**	0.1277	0.512104	-8.3	1667
R.346.5	AM	Adie Inlet	1	246	39	218	0.5170	0.707650	0.705841	2.1	7.2	0.1781	0.512319	-5.6	1481
R.350.1	AM	Adie Inlet	1	246	87	796	0.3274	0.707460	0.706314	8.3	38.7	0.1295	0.512338	-3.7	1338
North-east Palmer Land															
R.4293.2	PGN	Solem Ridge	4	220	257	102	7.3091	0.745647	0.722777	10.4	50.59	0.1240	0.512067	-9.1	1707
R.4294.1	PGN	Mount Nordhill	4	220	144	177	2.3546	0.733153	0.725786	3.4	17.50	0.1161	0.512050	-9.2	1714
R.4920.8	PGN	Mount Nordhill	4	220	140	216	1.8817	0.731113	0.725226	10.9	54.70	0.1200	0.512035	-9.6	1742

Complete Sr and Nd isotope data set for granitoids and country rocks. Published data are reproduced here, in order to correct errors in original papers and theses, and because in some cases revised ages are used for recalculations. Rock types: AM amphibolite; DI diorite; GA gabbro; GD granodiorite; GGN granite gneiss; GR granite; MG metagranite; MY mylonite; OGN orthogneiss; PG pegmatite; PGN paragneiss; PO porphyry; QDI quartz diorite; SST sandstone; TO tonalite; V unclassified volcanic rocks.

References

1. HOLE, M.J. 1986. Time controlled geochemistry of igneous rocks of the Antarctic Peninsula. Unpublished PhD thesis, University of London.
2. MILNE, A.J. & MILLAR, I.L. 1989. The significance of mid-Palaeozoic basement in Graham Land, Antarctic Peninsula. *Journal of the Geological Society, London*, **146**, 207-210.
3. MILNE, A.J. 1990. The pre-Mesozoic geological evolution of Graham Land, Antarctica. Unpublished PhD thesis, Open University.
4. WEVER, H.E., MILLAR, I.L. & PANKHURST, R.J. 1994. Geochronology and radiogenic isotope geology of Mesozoic rocks from eastern Palmer Land, Antarctic Peninsula: crustal anatexis in arc-related granitoid genesis. *Journal of South American Earth Sciences*, **7**, 69-83.
5. SCARROW, J.H., PANKHURST, R.J., LEAT, P.T. & VAUGHAN, A.P.M. 1996. Antarctic Peninsula granitoid petrogenesis: a case study from Mount Charity, north-eastern Palmer Land. *Antarctic Science*, **8(2)**, 193-206.

6. VAUGHAN, A.P.M., WAREHAM, C.D. & MILLAR, I.L., 1997. Granitoid pluton formation by spreading of continental crust: the Wiley Glacier complex, northwest Palmer Land, Antarctica. *Tectonophysics*, **283**, 35-60.
7. WAREHAM, C.D., MILLAR, I.L. & VAUGHAN, A.P.M. 1997a. The generation of sodic granite magmas, western Palmer Land, Antarctic Peninsula. *Contributions to Mineralogy and Petrology,* **128**, 81-96.
8. WAREHAM, C.D., VAUGHAN, A.P.M. & MILLAR, I.L. 1997b. The Wiley Glacier complex, Antarctic Peninsula: pluton growth by pulsing of granitoid magmas. *Chemical Geology*, **143**, 65-80.
9. This paper.

Table 1. Pb isotope data for leached feldspars from Antarctic Peninsula granitoids.

Sample	Rock type	Locality	Mineral	Age (Ma)	$^{206}Pb/^{204}Pb$	$^{207}Pb/^{204}Pb$	$^{208}Pb/^{204}Pb$
Graham Land							
BR.024.4	diorite	Faure Islands	Pl	48	18.729	15.621	38.492
R.080.1	granite	Horseshoe Island	Pl	67	18.796	15.634	38.566
R.312.2	granite	Bildad Peak	Pl	163	18.569	15.658	38.441
R.326.2	granodiorite	Mount Fritsche	Pl	164	18.640	15.649	38.510
R.2614.1	2-mica granite	Curran Bluff	Pl	204	18.735	15.664	38.695
R.349.1	granodiorite gneiss	Adie Inlet	Pl	?550	18.566	15.668	38.460
R.3632.2	metagranite	Marsh Spur	Pl	325	18.468	15.616	38.164
R.5511.1	gneiss	Target Hill	Pl	392	18.985	15.660	38.535
NW Palmer Land							
R.5256.1	granite	Mount Pitman	Pl	60	18.751	15.616	38.504
R.5736.1	granodiorite	Scorpio Peaks	Kfs	70	18.725	15.609	38.452
R.5796.4	granodiorite	Cetus Hill	Pl	120	18.757	15.636	38.522
R.3216.3	tonalite	Burns Bluff	Pl	140	18.701	15.658	38.546
R.5284.1	granodiorite	Renner Peak	Pl	140	18.683	15.633	38.483
R.6057.10	gabbro	Burns Bluff	Pl	141	18.571	15.623	38.370
R.5287.1	diorite	Creswick Peaks	Pl	141	18.681	15.637	38.508
R.5270.1	diorite	Goettel Escarpment	Pl	182	18.644	15.646	38.463
R.5271.4	foliated granite	Goettel Escarpment	Kfs	183	18.641	15.647	38.476
R.5504.2	foliated granodiorite	Auriga Nunataks	Kfs	203	18.741	15.650	38.543
R.5278.8	granite gneiss	Campbell Ridges	Kfs	227	18.707	15.654	38.604
NE Palmer Land							
R.4908.10	leucogranite gneiss	Mount van Buren	Pl	206	18.679	15.655	38.446
R.5006.7	metagranodiorite	Pinther Ridge	Pl	209	18.669	15.657	38.532
R.4942.4	metagranodiorite	Hall Ridge	Pl	211	18.802	15.662	38.626
R.4552.9	leucogranite gneiss	Mount Nordhill	Pl	220	18.715	15.661	38.512
R.4920.12	megacrystic granite	Mount Nordhill	Pl	220	18.694	15.672	38.545

Pl – plagioclase; Kfs – K-Feldspar.

Table 2.
O-isotope composition of granitoids from the Ellsworth-Whitmore Mountains crustal block.

			$\delta^{18}O_{SMOW}$		
Sample	**Rock type**	**Locality**	**Whole-rock**	**Quartz**	**Plagioclase**
R.2243.4	granite	Pirrit Hills	9.1	10.0	9.0
R.2226.4	granite	Linck Nunatak	10.0		
R.2215.4	granite	Pagano Nunatak	10.1	11.7	9.9

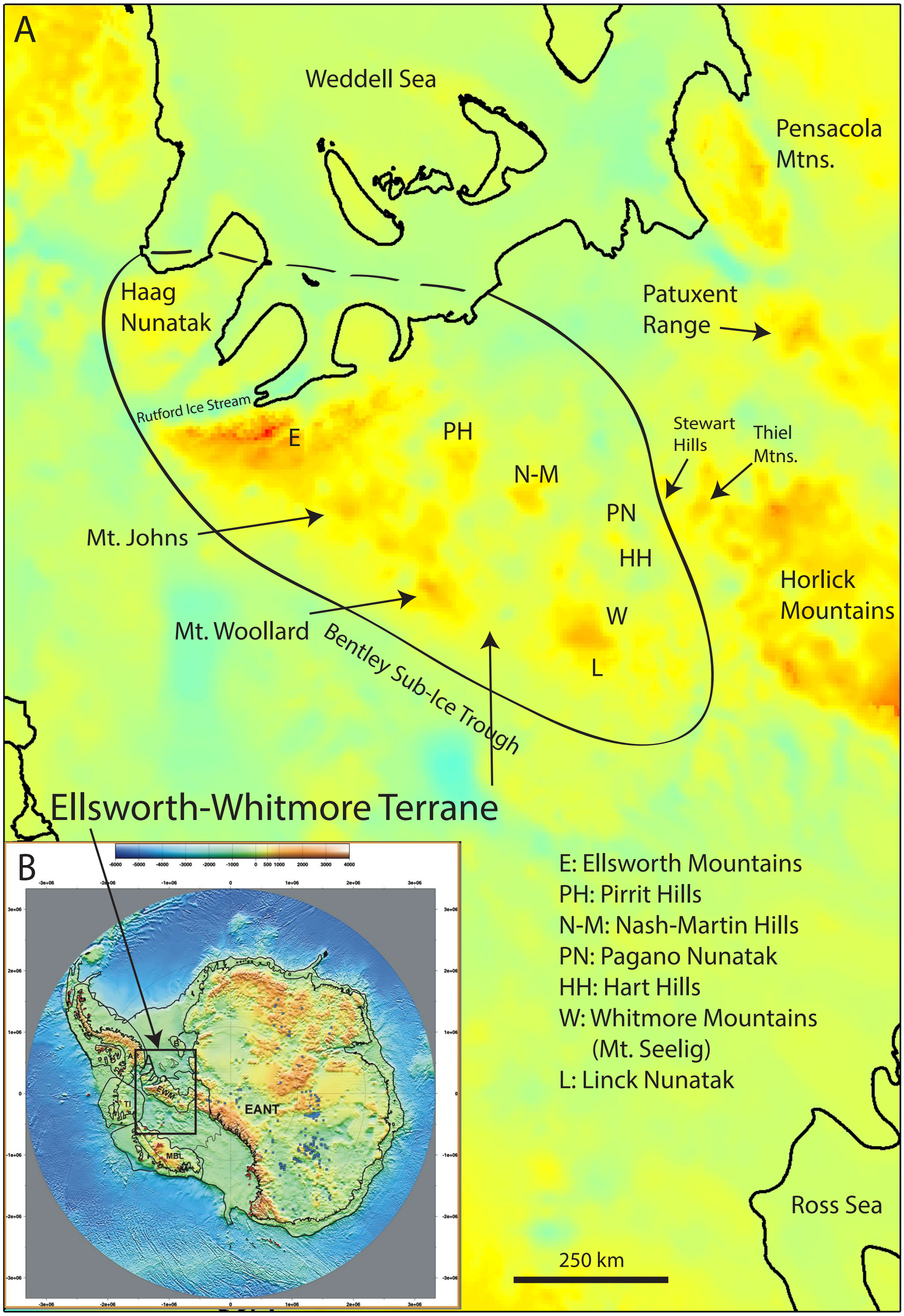

Figure 1: Sub-ice topographic DEM of Antarctica (B) with continental crust terranes identified (EANT: East Antarctic craton; AP: Antarctic Peninsula; TI: Thurston Island; MBL: Marie Byrd Land; EWM: Ellsworth-Whitmore Mountains; from Dalziel, 2008) and in (A), a detailed sub-ice DEM of central west Antarctica. Red-orange area are exposed above ice whereas yellow areas are sub-ice and blue areas are below sea level.

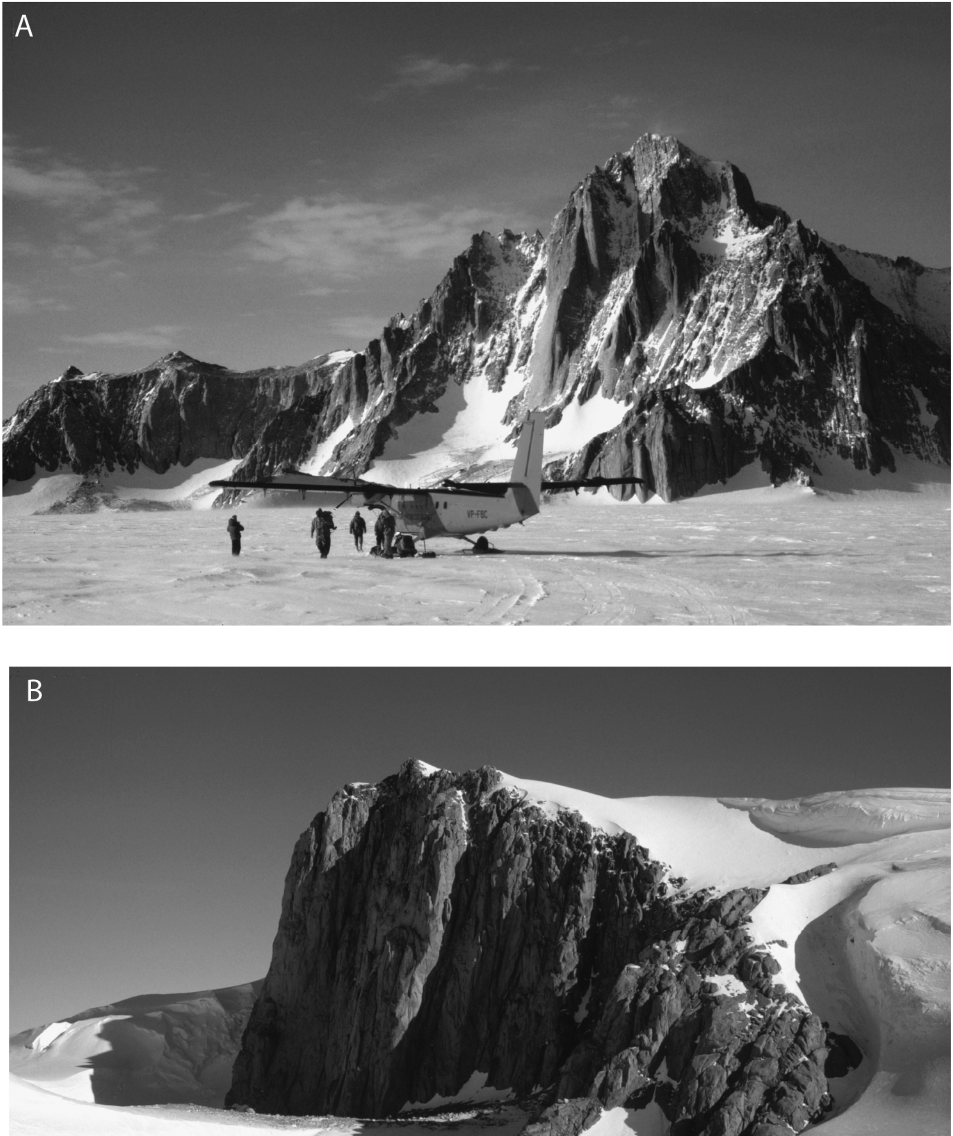

Figure 2: Field photos of the Pirrit Hills (A) and Pagano Nunatak (B; 230 m relief) granites.

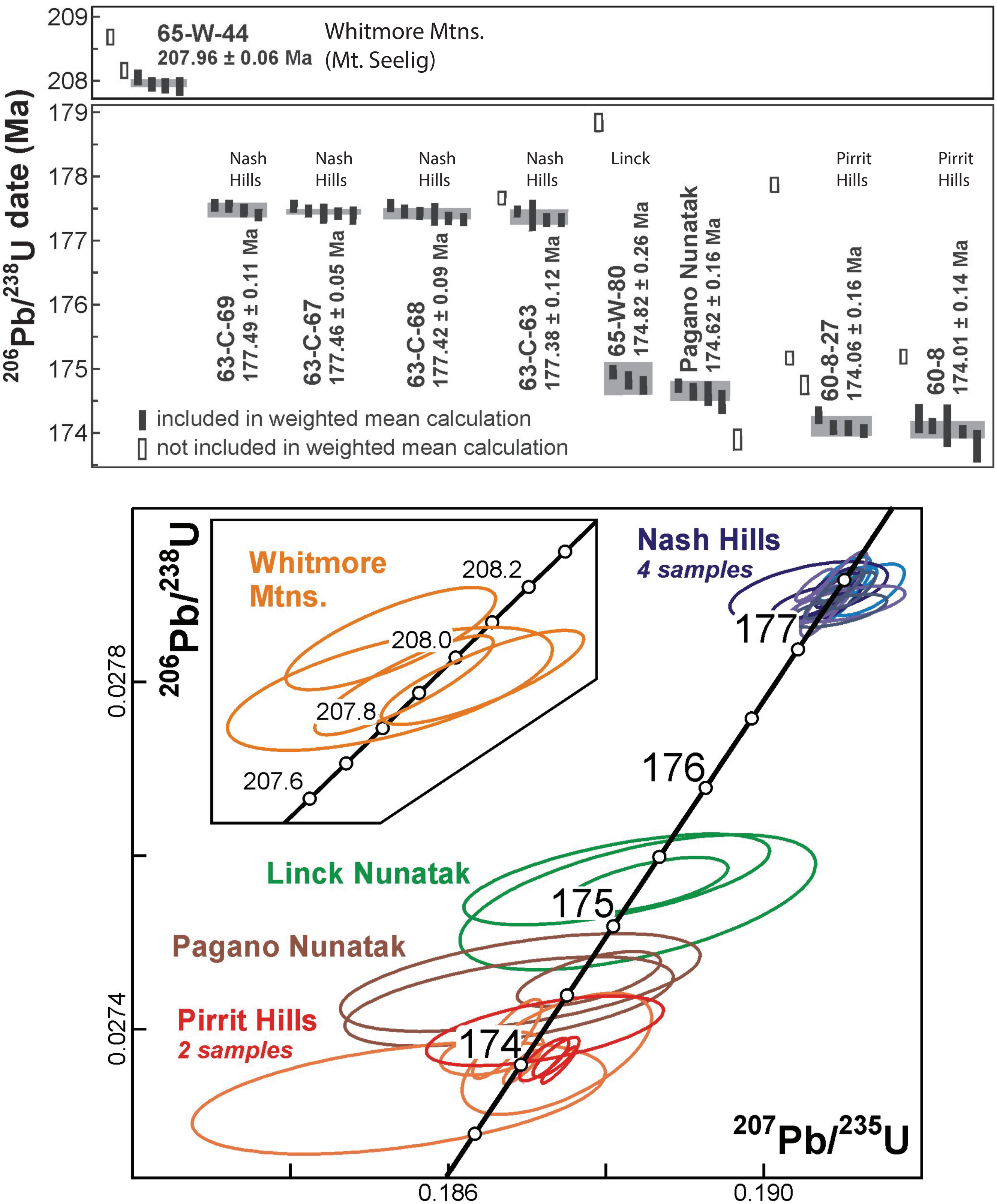

Fig. 3: ID-TIMS plots (Ranked 206Pb/238U age plot) illustrating single crystal zircon analyses from 9 granites of the Ellsworth-Whitmore Mountains. Error bars are plotted at 2σ. Filled bars represent analyses included in weighted mean age (grey horizontal bar); open bars represent analyses interpreted as inheritance or Pb-loss). See Table 2.

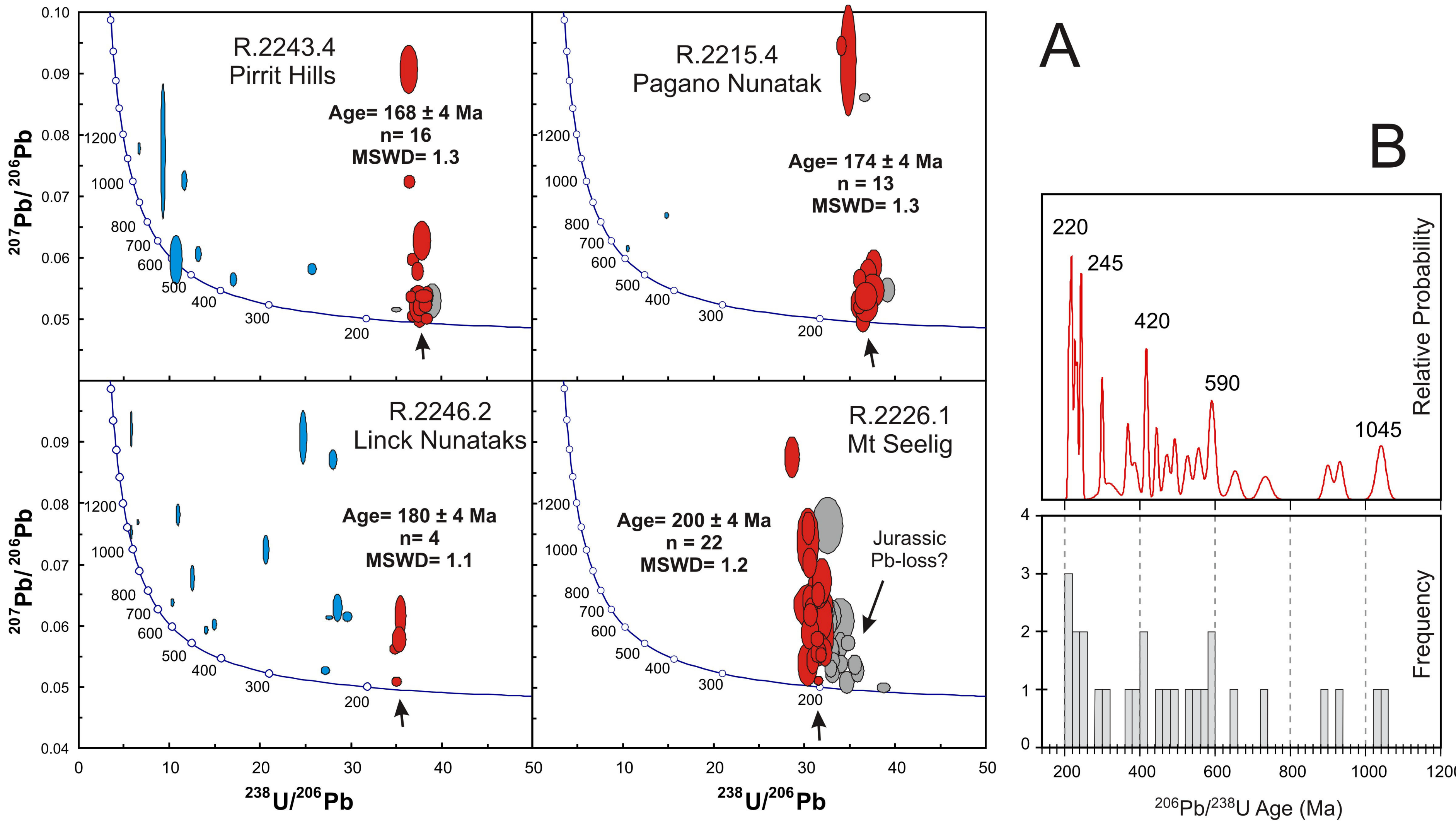

Figure 4: Concordia plots of SHRIMP U-Pb ages from cores and rims of zircons from central Antarctic granites (A) and a relative probablility plot of all ages (B; See Tables 1 and 3).

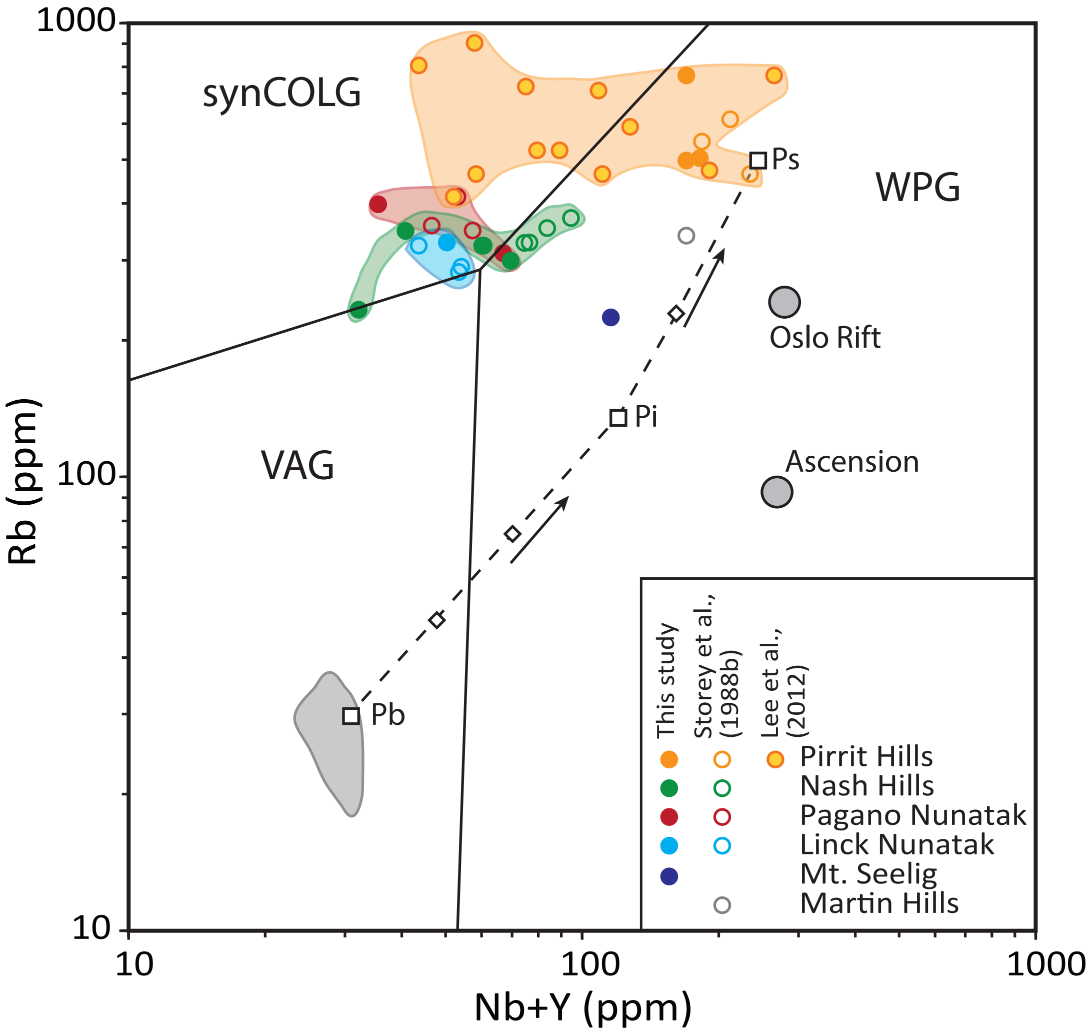

Figure 5. Rb vs (Nb+Y) discrimination diagram for the EWM granitic suite. Fields and data for 'crust-free' WPG from Pearce et al. (1984). Petrogenetic pathway for Ascension Island from Pearce et al., (1984); Long dashes, petrogenetic pathway for the crystallization of Pirrit Hills granite (from Storey et al., 1988b, using parameters therein). Assumed mafic precursor (Pb) to the Pirrit Hills granite (Ps); Pi is the intermediate step. Ancronyms.: WPG, within plate granite; synCOLG, syn-collisional granite; VAG, volcanic arc granite. See Table 4 for data, including Mt. Seelig, Whitmore Mountains (65-W-80; Triassic).

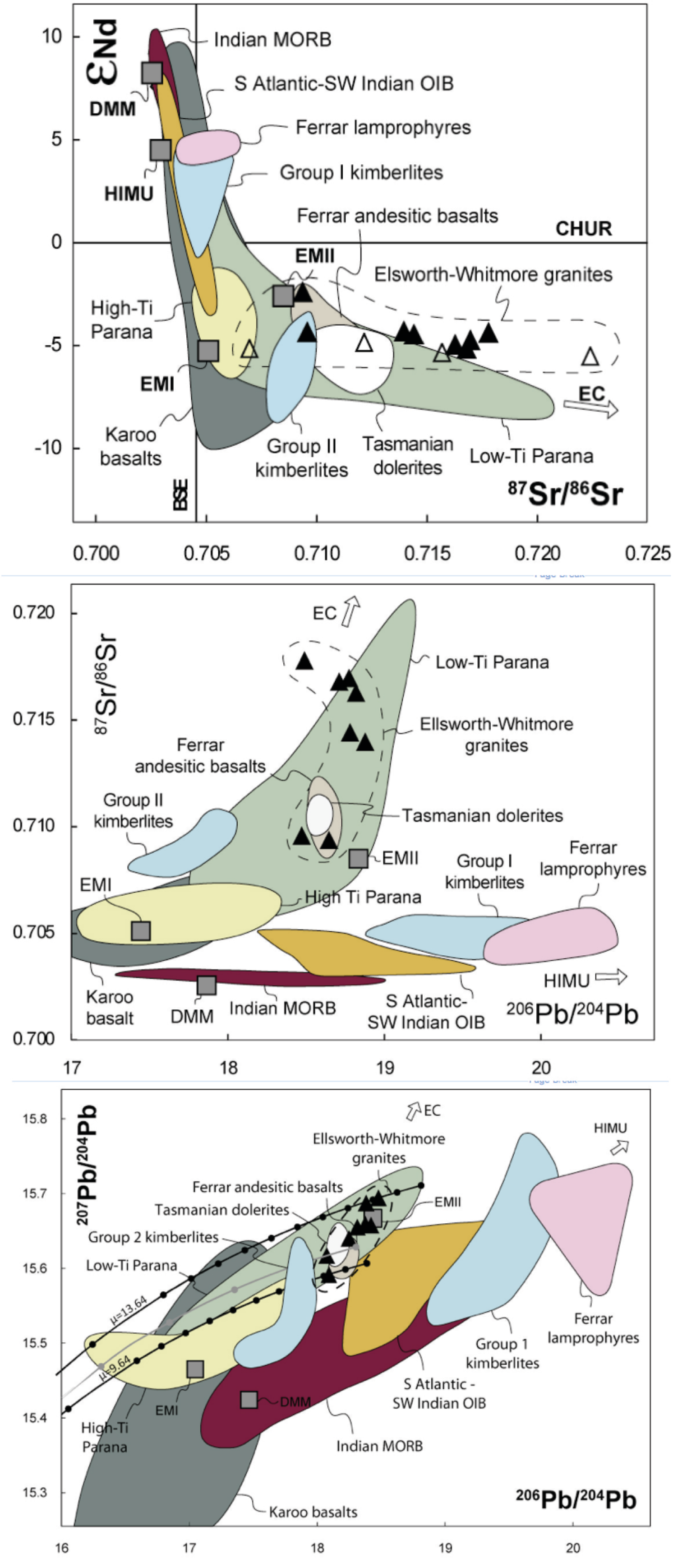

Figure 6: Caption in text. See Table 5 and Appendix 6.

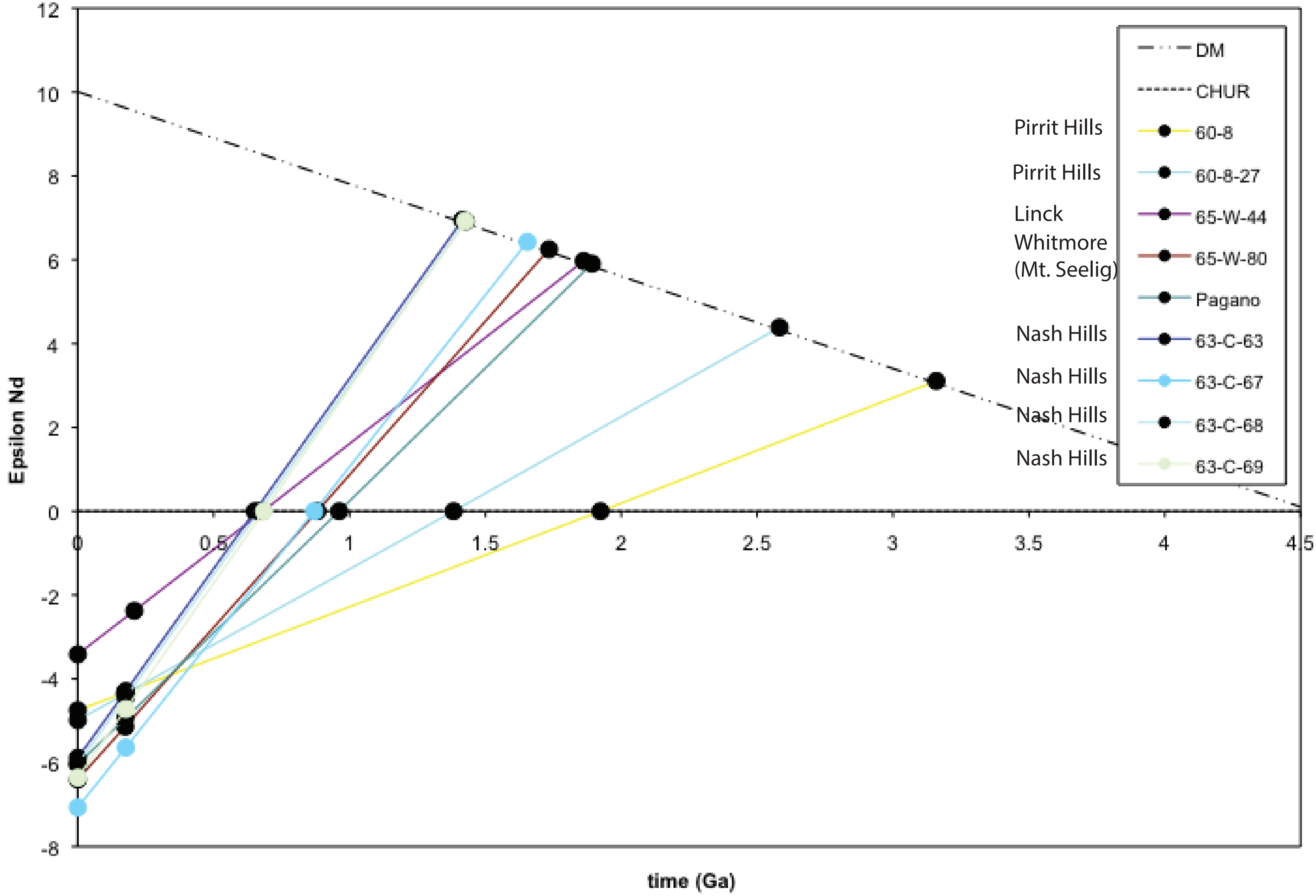

Figure 7: Nd model ages for Ellsworth-Whitmore terrane Jurassic granites. See Table 5.

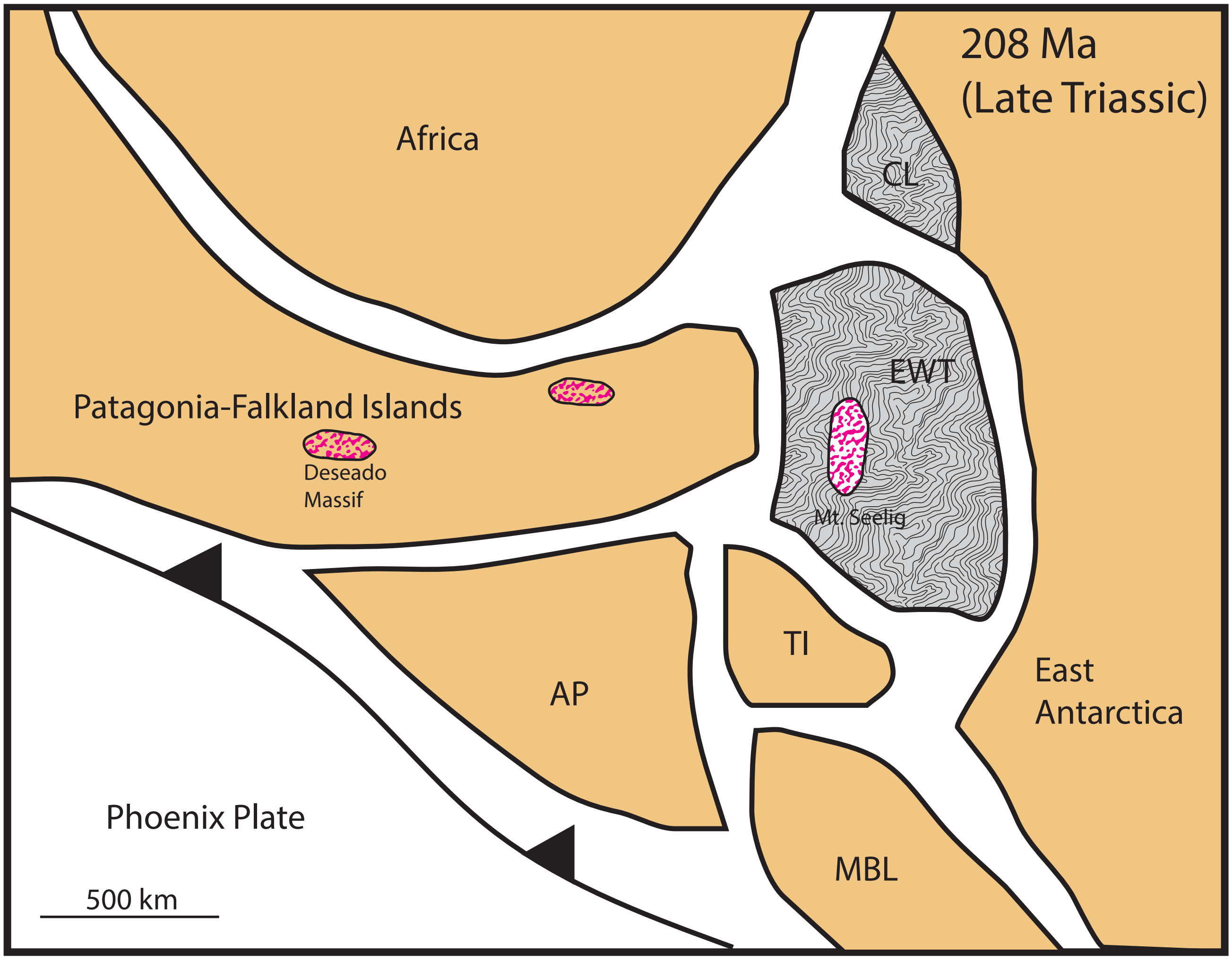

Figure 8a: Schematic tectonic recontruction for Gondwana in the late Triassic when the Mt. Seelig granite (pink) was intruded into the Grenville-aged crust (patterned) of the Ellsworth-Whitmore terrane as a within-plate intrusion. The central Patagonia and Deseado monzonite suites (224-200 Ma; Rb-Sr Pankhurst et al. 1993) are similar intrusions. Symbols: AP: Antarctic Peninsula; TI: Thurston Island; MBL: Marie Byrd Land; CL: Coats Land.

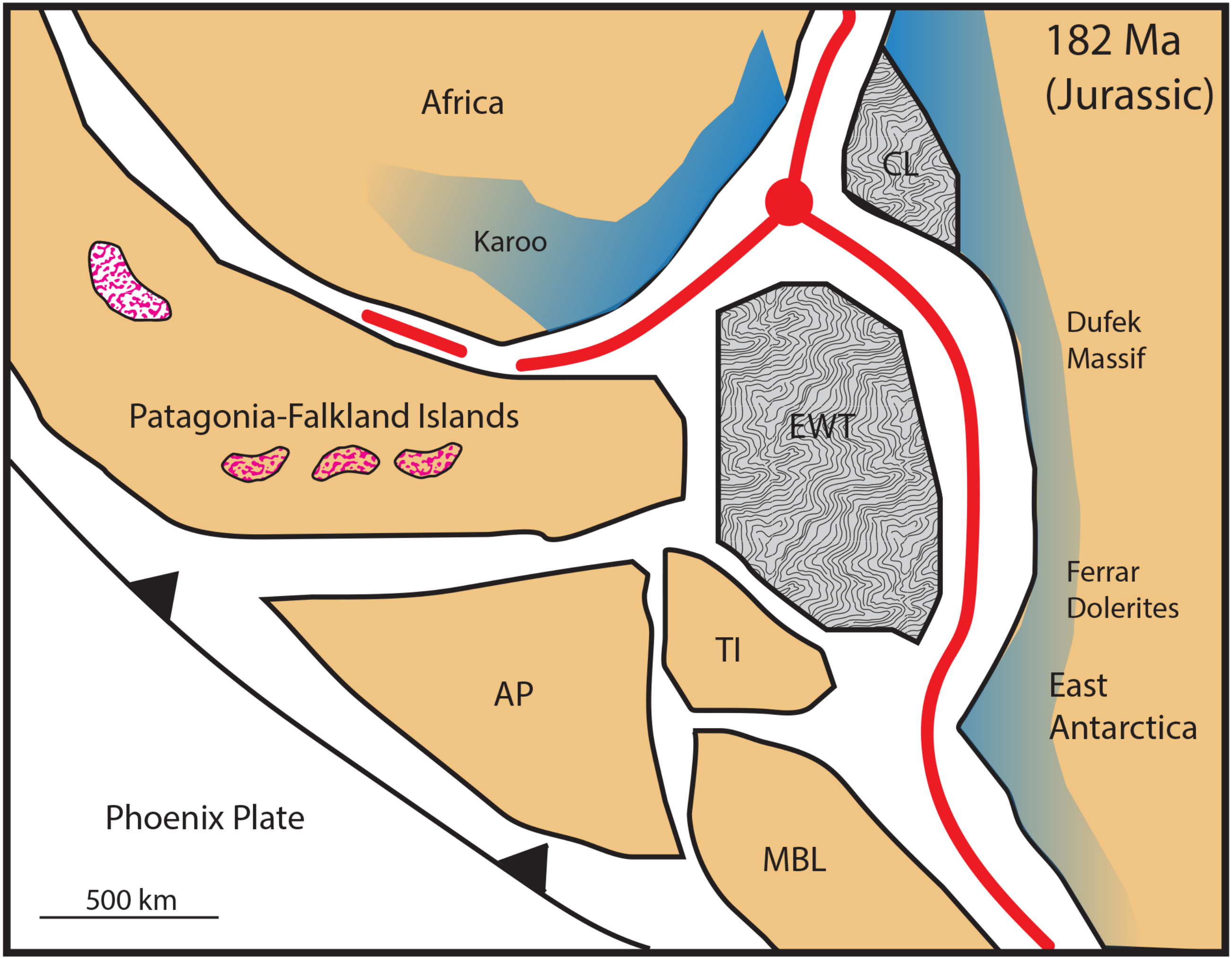

Figure 8b: Schematic tectonic reconstruction for Gondwana in the middle Jurassic when the Weddell triple junction began the divergence of Gondwana coeval with the eruption of Karoo-Ferrar mafic extrusions (182 Ma) and the Marifil Group silicic rocks (188 Ma; see Rapela et al. 2005). These mafic melts are only observed on the east and north side of the rifting margin. Symbols: AP: Antarctic Peninsula; TI: Thurston Island; MBL: Marie Byrd Land; CL: Coats Land.

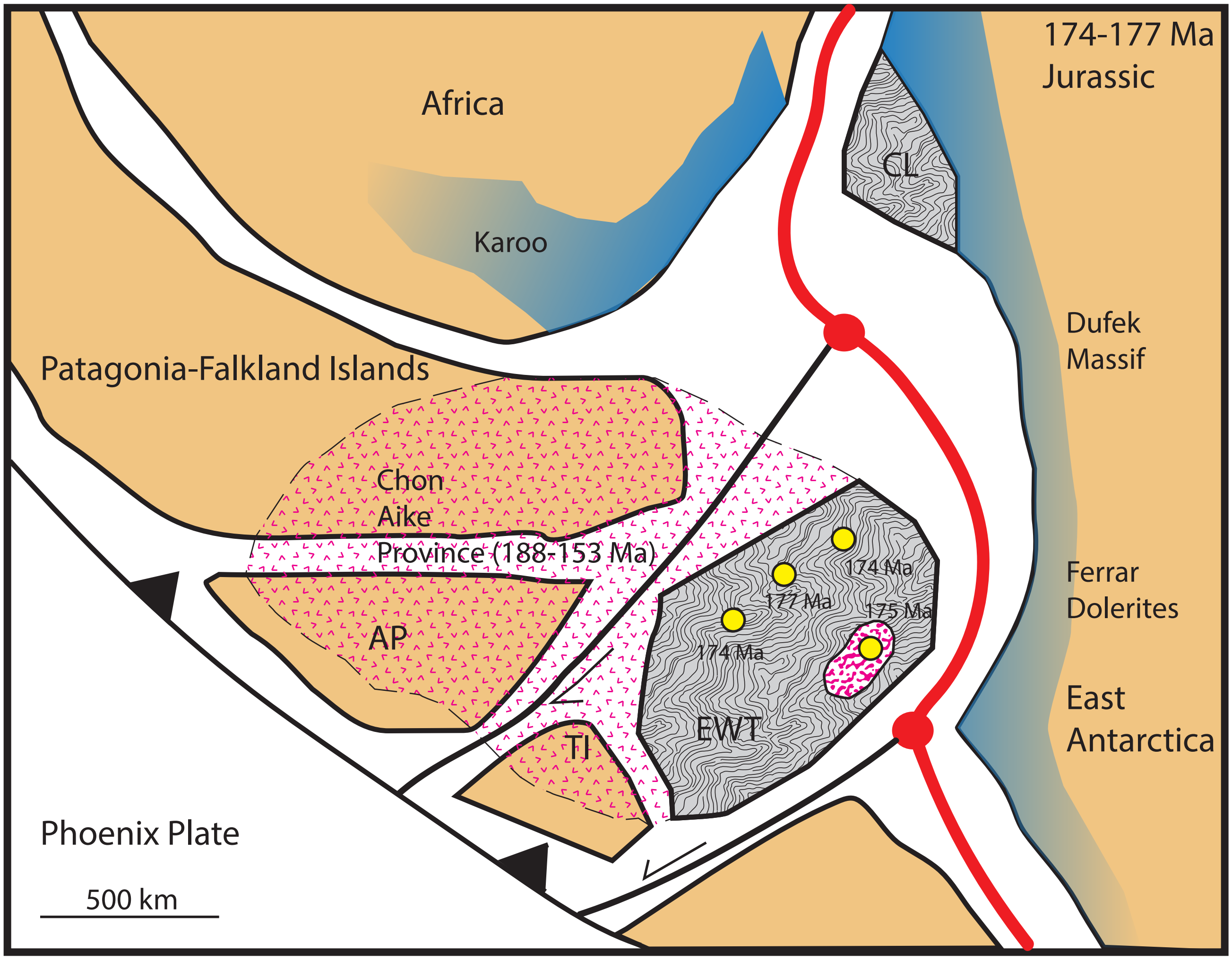

Figure 8c: Schematic tectonic reconstruction for Gondwana in the middle Jurassic when the Weddell triple junction began the opening of the Weddell Sea and the divergence of Gondwana coeval with the intrusion of the granites now exposed in the EWT (174-177 Ma; yellow dots) and the regional extrapolation of the Chon Aike province (Bryan et al. 2002). Symbols: AP: Antarctic Peninsula; TI: Thurston Island; MBL: Marie Byrd Land; CL: Coats Land.